UNIVERSITY OF CAMBRIDGE

Multilayer network methodologies for brain data analysis and modelling

Giovanna Maria Dimitri

Clare Hall College, Computer Laboratory

This thesis is submitted on September 2019 for the degree of Doctor of Philosophy

Declaration

This dissertation is the result of my own work and includes nothing which is the outcome of work done in collaboration except as declared in the Preface and specified in the text. It is not substantially the same as any that I have submitted, or, is being concurrently submitted for a degree or diploma or other qualification at the University of Cambridge or any other University or similar institution except as declared in the Preface and specified in the text. I further state that no substantial part of my dissertation has already been submitted, or, is being concurrently submitted for any such degree, diploma or other qualification at the University of Cambridge or any other University of similar institution except as declared in the Preface and specified in the text. This dissertation does not exceed the prescribed limit of 60,000 words.

Giovanna Maria Dimitri
September 2019

Abstract

Thesis Title: Multilayer network methodologies for brain data analysis and modelling
Author: Giovanna Maria Dimitri

The term neuroscience includes in itself a plethora of research areas devoted to undercover the most fascinating complex organ of our body: the brain. A common denominator of neuroscience areas, is the need for the application of methodologies to integrate different features. In this thesis, we focused on the analysis of two types of brain data: brain data coming from Traumatic Brain Injury (TBI) patients and data collected for the study of neurocognitive healthy ageing. In both cases there was the need of applying computational techniques able to integrate different features. To do so we used multilayer networks. For two groups of TBI patients (adults and paediatrics), time series data were collected from the observations of IntraCranial Pressure (ICP) and Heart Rate (HR). We first detected events of simultaneous increase of HR and ICP, which we called brain-heart crosstalks. Subsequently time series were translated into graphs, and network measures, during brain-heart crosstalks, were obtained. These were then included as predictors in a mortality outcome model, with crosstalks. Causality measures were also investigated, using a Granger causality approach, to understand the dynamics of signals during these events. We further applied multilayer networks to study neurocognitive ageing. To do so, we implemented a pipeline for community detection, which we called **NetRank**, applying it to the Cam-CAN, a large cross-sectional cohort for the study of healthy neurocognitive ageing. Using multilayer networks modelling, we identified subgroups of individuals, with similar lifestyles, and we related them to structural and functional brain features.
We believe that multilayer networks and their extensions represent a powerful tool to be used in integrative and cross modal neuroscience datasets. New insights on cognitive neuroscience and time series analysis, can in fact be gained trough multilayer network, possibly improving patients managements and allowing to develop new predictive tools.

Acknowledgements

This dissertation could have not been completed without the support of many people. First and foremost, I would like to express my deepest gratitude to my supervisor Prof Pietro Lio'. He has been a constant source of inspiration, a continuous guidance, and always ready to support my research with his invaluable advices and ideas. I would also like to thank the Computer Laboratory, and my funding body EPSRC, for offering me the unique opportunity of developing my PhD research in such a wonderful environment. Moreover I would like to express my gratitude to my college Clare Hall, for the support and hospitality, offering a superb context to live and work. I would also like to thank all the people I have met at the University Fencing Club. Being in the First Team for 5 years has been an invaluable honour. Competing in Varsities, winning the British University Fencing Championship and obtaining the Full Blue will always be with me as one of my best memories, together with all the friends I have met while fencing for Cambridge. Last, but not least, I would like to thank with all my heart all of my colleagues, my friends, my family and my parents Isabella and Nicola who made all of this possible. This thesis is dedicated to Nonna Grazia, who will always be with me.

Contents

List of Figures

List of Tables

Glossary

The glossary reports the most used biological and methodological terms used in this thesis.

Biological and Medical Terms

Addenbrookes' Cognitive Examination ACE-R: test that aims at assessing some elements of cognition, such as memory scores, language scores and other cognitive capabilities

Cattell Test: is a test developed with the intent of assessing fluid intelligence, which is independent from the cultural background of a certain individual

Drug Use Abuse Screening Test DAST-20: questionnaire used to assess psychoactive drugs and problems related to drug misuse

Ekman Hex Tests: test which evaluates the capability of recognising emotions

Grey Matter: is a principal component of the central nervous system. It is made of fewer myelinated axons than the white matter

HADS Tests: tests developed for the identification of depression and anxiety in patients and individuals in general

HR: Heart Rate measures heart speed. This is quantified as the number of contractions or beats per minute (bpm)

ICP: IntraCranial Pressure. It is the pressure of brain tissues and the cerebrospinal fluid that cushions and surrounds the brain and spinal cord. It is often used as a measure of potential pathological conditions of the brain

MRI: Magnetic Resonance Imaging. Technique that makes use of a large magnet together with radio waves in order to be able to have an image of the anatomy and physiological aspects of the body

PSQI: Pittsburgh Sleep Quality Index, i.e. hours listed as being asleep by the participant

Story Recall Test: test to assess memory performances. It consists in the capability of recalling a story in the immediate or delayed time

TBI: Traumatic Brain Injury, is used to refer to a severe event which negatively involves the brain. It can be the result of a violent blow, accident or fall

White Matter: areas of the central nervous system, made of the so called tracts, that are myelinated axons

Methodological Terms

Community Detection Methods: methods used for finding clusters of elements most tightly connected in terms of similarity in a graph

Cross-Validation: technique used for validating the results of a statistical model using datasets not previously used for training the model

Elastic Net: is a logistic regression model, in which the penalty term, in the optimization function, linearly combines the L1 and L2 penalties of lasso and ridge

Logistic Regression: is a model used to assess the probability of a binary outcome to happen (pass or fail, win or lose, dead or not)

Multilayer Networks: network composed by multiple layers, in which each layer represents a different feature type

Penalised Regression Models: regression models, in which the likelihood is enriched by a penalty term, and both are part of the optimization procedure. Lasso and Ridge penalty models are examples of such types of penalised models

Ranking Procedure: procedure which replaces to the original vector values, the ranked ordered value of each element

Chapter 1

Introduction

1.1 Motivation

Neuroscience has witnessed an explosion of data availability in the last few years. From genomic datasets to imaging, from transcriptomics to cognitive scores collection, data have become available to the scientific community, with the aim of developing and undercovering the many different aspects involving the brain and its neuropathological dimensions.
The presence of such diverse datasets has therefore implied the need for developing computational and mathematical models, capable of understanding and integrating such heterogeneous data types [33] [148]. As part of this development, a plethora of neuroscience related consortia has been founded, with the primary goal of collecting heterogeneous data types for various cohorts. Additionally, the public availability of such datasets has increased even more the interest of researchers, towards the use and development of mathematical tools suitable to answer such questions. To give an example we could mention the Human Connectome Project (HCP). This study started as a set of smaller consortia, created for different purposes (for example the Young Adults, Life Young Adult HCP or Connectomes). In all of these sub-consortia different types of data have been collected. For instance the HCP consortium includes: structural and functional MRIs, MEG, together with cognitive scores and demographic information, for more than 1200 subjects [146]. As further examples in the field, we could mention studies designed with the aim of investigating neuropathological diseases, such as the Alzheimer Neurodegenerative Initiative (ADNI), or the Parkinson Progressive Markers Initiative (PPMI).

In the thesis we investigate applications of multilayer network modelling for the integration of brain data. More specifically, in Chapter 2, we present an overview of multilayer networks theory fundamentals, which we shall use in the subsequent chapters. In Chapters 3 to 5 we discuss the application of such techniques to cohorts of traumatic brain injured individuals: first paediatrics then adults. When a Traumatic Brain Injury (TBI) case is admitted into hospital, in fact, several different sources of information are collected. A CT scan is usually performed, which leads to the identification of imaging features that are particularly useful towards the treatment and prognosis of the patient. Demographics and blood sample information are also collected with the same goal. Moreover, in some clinical cases, the severity of the situation requires the insertion of an IntraCranial Pressure (ICP) monitoring device. This is an invasive procedure, but needed when the ICP undergoes modifications which can lead to life threatening conditions. Such information can therefore be analysed together with other parameters monitored, such as Heart Rate (HR), in a comprehensive effort of studying the behaviour of complex brain physics dynamics. Furthermore in such cases the application of computational methodologies, integrating different types of data, can lead to extremely important discoveries of underlying brain behaviour mechanisms, in TBI studies. Eventually in Chapter 6 we present a multilayer network approach to integrate and profile neurocognitive ageing. This was developed with data coming from the Cam-CAN project, a study designed with the goal of defining the features of healthy neurocognitive ageing.

1.2 Research problems

In this thesis we present some applications of multilayer network analysis for the integration of brain data. The computational and modelling approach proposed in the work, for the two main projects, can be summarised by the following points:

(a) **Data Integration**: in both projects, the aim was the use of multilayer networks for the integration of different data types. In the case of the TBI cohorts, the integration concerned monitoring data (ICP and HR), and the relationship between mortality with information drawn from the time series, as well as in clinical and demographic features. In the case of the Cam-CAN cohort, the integration was between imaging, demographics and cognitive data.

(b) **Using network theory for analysis and prediction**: for the TBI project, graph

network measures were used in combination with clinical and monitoring information, to predict mortality. In the case of the Cam-CAN cohort, instead, network measures were obtained from the community detection algorithm. This was implemented to look for trajectories of healthy ageing within the clusters identified.

(c) **Development of methodologies towards precision medicine and clinical support systems.** *How can a computer scientist help in a trauma ward?* The models and analysis we present may have an immediate impact in the clinical environment. The work on brain-heart crosstalks and the interaction between ICP and HR will actually be included in one of the leading software for TBI patients monitoring, ICM+ [132]. The new plugin interface will in fact allow, the research we conducted so far, to be directly tested and verified on new patients. Considering the relationship with outcome of this new pattern that we detected, the clinical impact of the new variable monitored could be of great interest and importance for patients management. Research on precision medicine and clinical support systems, could also be performed for the Cam-CAN project. *How can a computer scientist help discovering the features of healthy neurocognitive ageing?* The relationship between the various factors contributing towards neurocognitive ageing could be in fact investigated, and recommendations with respect to lifestyles behaviour could be the future outcome of such research.

The thesis overview is also depicted in Figure 1.1.

1.3 Thesis overview

We hereby describe the structure of the thesis:

- **Chapter 2**: this chapter provides the reader with the methodological background of the modelling and techniques used. We present an introduction to graph theory, focusing on community detection algorithms. This is in fact a central point in the analysis of the Cam-CAN cohort in Chapter 6. We then extend the presentation to multi-layer networks, considering recent developments and applications.

- **Chapter 3**: the chapter exposes a first, exploratory, analysis of the TBI paediatric patients cohort. To gain some early insights of the system, we consider the time

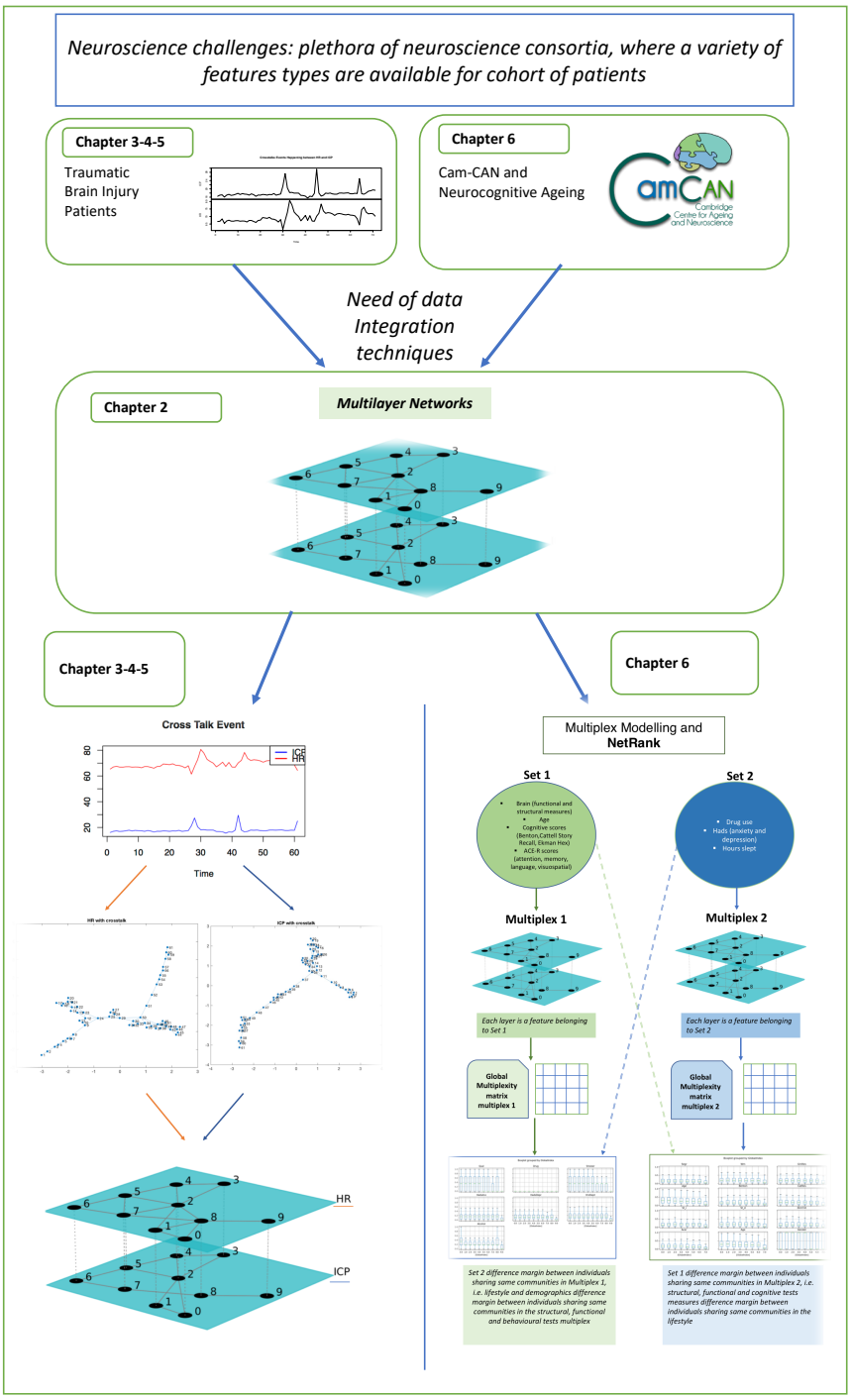

Figure 1.1: Overview of the thesis pipeline. At the top of the figure, we depict the driving research question regarding the need of integration for neuroscience datasets. We then present the two main projects of the dissertation : Cam-CAN and TBI. The pipeline continues showing the model used (multilayer networks), and with a visual description of the analysis performed in the two datasets

series in a comprehensive preliminary statistical analysis. Following a clinical intuition, we then implemented an algorithm for the detection of specific patterns, taking place in the monitored ICP and HR time series, that we named brain-heart crosstalks. This consisted in the identification of a simultaneous increase of both variables of at least 20%, in a 10 minutes time window of observations. We then proceeded presenting a modelling of the ICP and HR time series, using a multiplex network approach. The modelling proposed is a novelty for HR and ICP, and to the best of our knowledge this is the first time that such framework has been discussed in the literature. The two time series, for each patient, are converted from the time domain to the graph domain using a Horizontal Visibility Graph approach, and network measures are derived where the brain-heart crosstalks are detected.

- **Chapter 4-5**: in chapter 4 we discuss a predictive outcome model for the TBI paediatric patients. A dataset of predictor variables composed by demographic, clinical and imaging features are used for mortality outcome prediction. To these more standard dataset of predictive variables, we added the network measures obtained and described in the previous Chapter. The analysis presented in Chapter 4 is repeated for a larger TBI adult cohort of 225 patients in Chapter 5. The novel approach based on the analysis of cross-talks between heart rate and ICP signals, allowed us to show the presence of an interaction between the cerebral dynamics and the autonomic systems, an area that is gaining much interest in the intensive care community. Furthermore the association of the new variable brain-heart crosstalks with outcome, showed in this project, may offer solutions to another piece of the puzzle which TBI presents to the clinician at the bed side.

- **Chapter 6**: in this chapter we present the study conducted on the Cam-CAN cohort. The dataset is initially described, and preliminary statistical analysis is performed. Subsequently, we introduce a multiplex clustering algorithm, allowing us to identify cohort subcommunities, characterized by common neurocognitive ageing traits.

- **Chapter 7**: in this chapter we draw the main conclusions of the thesis. We summarized the principal contributions and also indicated possible future research lines.

1.4 Related publications, presentations and activities

The work of this thesis has been presented in several papers and conferences. The following are the main publications for chapters 3-4-5 and 6:

1. Dimitri, Giovanna Maria, et al. "Simultaneous transients of intracranial pressure and heart rate in traumatic brain injury: Methods of analysis." Intracranial Pressure & Neuromonitoring XVI. Springer, Cham, 2018. 147-151

2. Dimitri, Giovanna Maria, et al. "A multiplex network approach for the analysis of intracranial pressure and heart rate data in traumatic brain injured patients." Applied Network Science 2.1 (2017): 29.

3. Dimitri, Giovanna Maria et al. "Brain-Heart crosstalks: a new variable for outcome prediction in pediatric Traumatic Brain Injury patients", under revision for resubmission at BMC Medical Research and Methodology, 2019

4. Dimitri, Giovanna Maria et al. "Netrank: A Multiplex Community Network approach for profiling Neurocognitive Ageing", accepted for poster presentation at the Organization for Human Brain Mapping 2019 conference, Rome (June 2019)

4. Dimitri, Giovanna Maria et al., " Analyzing cardio-cerebral crosstalks in an adult cohort from CENTER-TBI", accepted for poster presentation at the International Symposium on Neuromonitoring, Leuven September 2019 (Belgium).

The work of this thesis was also presented at several conferences and seminars throughout the PhD. The TBI work was presented at the 2016 Neuroinformatics Conference (University of Reading), 2016 Virtual Phisiology Human (VPH) conference (University of Amsterdam) and at the 5th International Complex Networks Workshop (University of Milan, 2016). Moreover the work has been presented in two Brain Physics Seminar at the Addenbrooke's University Hospital (14th March 2017 and 5th of June 2018). The Cam-CAN work has been presented at the 2019 Human Brain Mapping, OHBM conference in Rome, one of the main conferences in the neuroscience fields.
During my PhD I have also actively participated to the work related to Propag-AGEING, a EU project regarding Parkinson disease and its study at different omics scales. I have participated and presented my relevant work at the following annual meetings: Florence (2016), Sevilla (2017) and Bologna (2018). During the first annual meeting, I presented

the models and the work related to this thesis. Moreover I have organized a workshop on deep learning and data integration for the partners of the project, February 2018, in Cambridge. I participated actively to research activities, and I have been in the local organizing committee of PDP 2018 in Cambridge and of the International Complex Network Workshop in Cambridge 2019. Moreover I have been in the organizing committee of one special session, on neuroimaging and deep learning, at the International Meeting on Computational Intelligence Methods for Bioinformatics and Biostatistics (CIBB 2018) at the Universidade Nova de Lisboa (Lisbon). During the special session I also presented a paper, co-authored with one of the students I supervised for the MPhil dissertation in Advanced Computer Science, on neural connectivity modelling using deep learning approaches. This brought to a forthcoming publication on Lecture Notes in Bioinformatics. We used LSTMs architecture to predict gender given fMRI datasets. During the PhD, I have been very much involved in supervising computer science students (MPhil and undergraduates), allowing me to pursue also other research areas. For example before the beginning of my PhD I conducted research regarding the implementation of machine learning methodologies for the prediction of drugs side effects. This led to the implementation of a machine learning method, coded into an R package, and published in : *Dimitri, Giovanna Maria, and Pietro Lió. "DrugClust: a machine learning approach for drugs side effects prediction." Computational biology and chemistry 68 (2017): 204-210.* Last year, having the opportunity of supervising a master student at Goldsmith University (London), we extended the work to drugs related to psychoactive compounds. Furthermore I have also been interested and worked on other research areas, in particular related to deep neural networks applied to bioinformatics. An example of publications on this in which I have been involved in is: *Maj, C., Azevedo, T., Giansanti, V., Borisov, O.,* ***Dimitri, G. M****, Spasov, S., Lio P., Merelli, I. (2019). Integration of machine learning methods to dissect genetically imputed transcriptomic profiles in Alzheimer's Disease. Frontiers in Genetics, 10, 726.* In this case an approach based on variational autoencoders helped us in discriminating between different genetic tissues.

Chapter 2

Background: multilayer networks and communities detection methods

2.1 Networks: a short introduction

Graph and network theory is a remarkably expanding field, which in the last few decades has seen widespread diffusion. The main key of success for it, lives in the versatility of the methodology, and its possible application in many different fields. Bollobas, the prominent graph and theory scholar and student of the famous and prominent mathematician Paul Erdos, wrote in 2013 [18]:

The time has now come when graph theory should be part of the education of every serious student of mathematics and computer science, both for its own sake and to enhance the appreciation of mathematics as a whole.

As we were mentioning before one of the main important characteristics, of network and graph modelling, consists in its capability of being applied to many different fields: from sociology to biochemistry, from physics to economics. A seminal paper in the field was written by the sociologist Granovetter: *the strength of weak ties*. The work was developed in 1973 as a sociological experiment. It consisted in the evaluation of how many steps on average are needed to send a letter to an unknown person. That meant estimating the average path length separating any two individuals in the whole world, which turned out to be six. According to [108] it is possible to identify four main broad areas in network science: technological networks, networks of information, social networks and biological networks. The first two categories are the ones studying

and modelling network protocols, World Wide Web (WWW) and other networks that characterize today communication protocols. An interesting example [108], for the information category, consists in the citation network. We could in fact consider a network, where each node represents a paper and the connection between two papers exists, in one or the other direction, if there is a citation linking the two. The interest in this area highly developed in the last few years, due to two main reasons.
First of all, a significant corpus of papers databases have become available online and this has allowed the application of machine learning techniques to such freely available datasets [100]. Moreover the interest in computing impact factors and other similar parameters, towards an evaluation of research, has attracted much attention. The third area, as previously mentioned, consists of social networks studies [108]. This is composed by those contributions which analyse social behaviour, interactions and effects. The original inspiration for this area of research has been the work by Granovetter [62]. His research techniques have in fact been translated to our age, for the understanding of new communication behaviour through current media such as Facebook, Twitter or Whatsapp. Such communication protocols have, in fact, highly modified the interaction across individuals, and this is an important aspect that needs to be taken into account [89]. The last, and fourth, area is the one dedicated to modelling biological and natural networks, that appear in medicine, biology and chemistry. Also in this case, several papers have been devoted to their analysis and applications: from protein protein interaction [107], to metabolic [4] and brain networks [23]. Research interest in brain networks, have been particularly developed in recent years. Interactions between different brain areas can, in fact, be investigated nowadays through the use of multiple imaging techniques such as structural MRI, functional MRI, MEG and diffusion. Such approaches can reveal insightful information driving neurological degenerative processes, ageing and other yet less understood brain mechanisms [135]. Networks analysis can also describe irregular systems structures, together with their complex and dynamic evolution, and therefore is suitable for the analysis of large heterogeneous types of systems [17]. Quite recently the science of complex networks has been applied to time series analysis. An example of construction of complex networks from pseudoperiodic time series is [154]. In the paper the authors show how noisy time series correspond to random networks, while chaotic time series exhibit small world and scale free properties [154]. An interesting application of such approach was made in terms of comparison between healthy and coronary care patients [154]. Therefore the underlying nature of the two time series could be detected by looking

at their network representation. Another interesting approach has been proposed by [99]. In the paper the authors compute the recurrence matrix of the time series, and use it as the adjacency matrix of the network. Then they analyse it, using standard network metrics. In the coming sections we will proceed as follows. First we will formally define the structure of a network and its components. We will then introduce the definition of multilayer and multiplex networks. Subsequently we will thoroughly describe methods for multiplex and multilayer networks clustering.

2.1.1 Graphs and networks: a formal definition

Graphs and networks are two words often used in literature in an interchangeable way [8]. However a few technical differences exist between the two terms. First of all there are semantic differences in the way in which the main components of graphs and networks are called. In the case of networks, in fact, they are defined as nodes and links. On the other hand, in graphs, they are defined as vertices and edges. This is due to the distinction between real life systems components and their mathematical description. Therefore different networks can correspond to the same graph. An interesting example in this sense is shown in [8].
A graph G is defined as a mathematical structure, composed by a set of vertices V and a set of edges E. For convenience, in what follows, the terms edges and links, as well as the terms vertices and nodes, will be used interchangeably. Edges between vertices can be of two types: $directed$ or $undirected$. In the first case there is a "direction" in the relationship connecting the two nodes, linked by an edge (not necessarily a causal relationship between the two). If, for example, we are modelling as a network a set of web pages, there could be a link redirecting the user from page 1 to page 2, without necessarily having a link from page 2 to page 1. Some networks could have the presence of both directed and undirected links. For example, metabolic networks [8] could have both reversible and irreversible reactions, modelled as directed and undirected edges. This would therefore imply the coexistence of both types of links. Moreover networks can be defined as weighted or unweighted, according to the presence of a value (i.e. a weight) assigned to the edges. There are many important elements allowing to analyse and describe a network.
Its structure can be fully summarised using the so called adjacency matrix. Such matrix describes the presence of a link between two given nodes. It can therefore be binary or non-binary, according to the presence of an unweighted or weighted network

model. The adjacency matrix of an undirected network will be therefore symmetric, and the presence of a non-zero value will mean the presence of a non zero weight edge connecting two given nodes. More formally we can say that, if A is the adjacency matrix of a network, having N number of nodes, then the matrix will be of dimension $N \times N$. Moreover the generic element $A_{i,j}$ [8] will be such that:

- $A_{i,j} = 1$ if there exists an edge connecting nodes i and j in the case of an unweighted matrix. Otherwise $A_{i,j} = w_{i,j}$ where $w_{i,j}$ is the weight associated to the edge connecting the two nodes i and j
- $A_{i,j} = 0$ if the connection between nodes i and j does not exist

Among the various measures, important for assessing and analysing networks, one of the most widely used is the node degree. For a generic node i, this is defined with the symbol k_i. The node degree represents the number of connections that a node holds, i.e. the number of edges that are incident to a certain node. For example, given node i we can define its node degree, according to the two cases of undirected or directed networks, [8] as:

- For an undirected network $k_i = \sum_{j=1}^{N} A_{i,j}$: that is the degree of node i can be defined as the sum over the i-th row or column of the adjacency matrix [8]
- For a directed network we need to define two types of node degree. This is because for each node, there is a degree corresponding to the number of links entering the node and a degree representing the number of links exiting the node. In particular: $k_i^{in} = \sum_{j=1}^{N} A_{i,j}$ and $k_i^{out} = \sum_{j=1}^{N} A_{j,i}$. The total sum of undirected and directed node degrees in the graph is $2L$, where L is the number of edges.

The number of total links L in a network, can vary from 0 to a maximum value, that we can define as L_{max} [8]. This is:

$$L_{max} = \frac{N(N-1)}{2} \tag{2.1}$$

where N is the number of nodes. If a network has a number of links equal to L_{max} is said to be a complete graph. Another important and widely used measure in graph and network analysis is the so called clustering coefficient. The clustering coefficient is used to understand how much a given node i is linked to its neighbour nodes. For

example if we consider node i, with a degree k_i, we can define the clustering coefficient as [8]:

$$C_i = \frac{2L_i}{k_i(k_i - 1)} \tag{2.2}$$

where L_i represents the number of links between the k_i neighbours of node i. C_i can be interpreted as the probability that two neighbouring nodes of i are linked [8]. The value of C_i is between 0 and 1, with 1 being the case of a complete graph.

2.1.2 Community detection methods

In this section we cover another important topic for network analysis, that is communities structure and network communities detection algorithms. The topic is particularly relevant also for what we will present in the rest of the thesis and this is why, among many other important aspects of networks, we have decided to dedicate a complete subsection to it.
Identifying *tight* groups of nodes in a network has a remarkable importance in several applications. If we are, for example, in the context of a biological protein-protein interaction network, identifying the most tightly connected communities is a fundamental task [76] [31]. This is where graph theory, together with machine learning algorithms, can best perform its tasks in undercovering biological mechanisms behind. Other important bio inspired applications of community detection and network modelling are metabolic or gene networks analysis. For example in [119] the authors suggest a method to find groups of molecules in metabolic networks [8]. Starting from these early attempts, a very large amount of literature in this field has been developed [59] [111] [66]. Brain network analysis, as mentioned earlier, is also another topic in which community detection algorithms play an important role. The availability of a large number of different types of imaging information (fMRI, MRI, MEG and diffusion imaging) has led to the spread and application of networks methodologies to this field [135]. For example network measures could help in undercovering different mechanisms between healthy and neurodegenerated brains, or events taking place in other processes such as brain ageing [23] [122]. In [8] the definition of a community is given according to two fundamental hypotheses that have to be satisfied:

- Hypothesis 1: *"A network's community structure is uniquely econded in its wiring diagram" [8]*

- Hypothesis 2: *"Connectedness and density hypothesis: a community is a locally dense connected subgraph in a network" [8]*

Paraphrasing these two hypotheses, in a community nodes members have a higher probability to be connected with each other rather than to members outside the community. The reachability is also another key point in the definition of community: each community member, must be able to be reached by another member belonging to the same community. The importance of finding such groups inside a network is manifold. First of all it can reveal fundamental and unknown functionalities of the network itself. If we are modelling a social network, for example Facebook, then we can efficiently find and identify subgroups in friendships networks, that could correspond to interesting sub social networks to analyse separately from the rest of the individuals in the community [143] [108]. In gene interaction networks, discovering and analysing a community could provide us with new insights on molecular interactions and uncovered pathways describing the system [85]. To solve the problem of community detection, many different approaches have been proposed, due to the inherent difficulty and computational expensive procedures that need to be implemented to solve the task [109]. These rely on the stronger or weaker definition of community and clique and on how the problem can be treated as a relaxed, or a more strong, assumption optimization problem to be solved [8].

Graph partitioning

To introduce different ways for detecting communities in a network, we can start thinking on how to solve the easiest version of this problem. This consists in the problem of dividing the original graph into two parts: the so called graph partitioning problem [109] [8]. Heuristic approach algorithms need to be implemented to solve such problem. If for example the task is to divide into two subgroups of dimension X and Y, then the total number of ways in which this can be done is:

$$\frac{N!}{X!Y!} \tag{2.3}$$

with N as the number of nodes. To understand the implications of this, suppose we want to compute the number of possible bisections of the graph in Figure 2.1. The number of nodes in this case is $N = 8$. That means that if the task is to divide the graph into two subnetworks of dimensions 4, the possible number of combinations, according

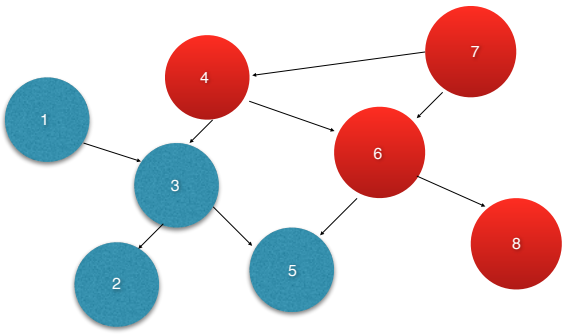

Figure 2.1: Example of a graph bisection. In this case the graph has a number of nodes $N = 8$ and the task consists in bisecting it in two subgraphs of dimension 4. The number of possible combinations in which such division can be made is $\frac{8!}{4!4!}$, that is 70 possible combinations

to Equation 2.3 is $\frac{8!}{4!4!}$, i.e. 70 possible combinations.
We can easily therefore grasp, how the number of possible combinations for graph of bigger dimensions, become exponentially large. Brute force approaches are bound to fail, and computationally and more heuristic approaches are needed.
The development of graph partitioning algorithms, can be considered the prodrome of the development of communities detection algorithms. One of the probably best known and mostly used ones, was published and proposed in 1970 [79] by Kernighan-Lin. The algorithm relies on a heuristic approach. The initial network is randomly divided into two subgroups. Subsequently two random nodes a and b belonging to the two different groups are swapped. The objective is to minimize the cut-size, i.e. the number of edges cutting through one set to the other. If the swap improved the cut-size (i.e. the number of connections going from one set to the other diminishes) then the new configuration is accepted. The procedure continues until convergence, i.e. no possible improvements in cut-size are possible.

Hierarchical community detection approaches

In the graph partitioning problem, the desired number of communities is known a-priori, i.e. 2. In the case of community detection algorithms, instead, the number of communities needs to be identified directly by the algorithm, and the methodologies proposed must rely on optimization procedures. The mathematical law that regulates the number of k possible partitions, given a network with N nodes, can be expressed

using the Bell number [8] [12] as:

$$B_N = \frac{1}{e} \sum_{j=0}^{\infty} \frac{j^N}{j!} \tag{2.4}$$

Studying Equation 2.4 we can see how the number of possible partitions follow a behaviour which leads to a growth faster than the network size N [8]. Heuristic approaches to overcome the NP completeness of the problem, need therefore to be applied to the field. Many different types of approaches have been proposed for the goal.
Hierarchical clustering is a common solution used to overcome the NP completeness issue. Clustering is, in fact, commonly used for partitioning elements into subgroups, according to their features similarities. Hierarchical clustering methods have been originally developed regardless of their application to networks. The basic idea of clustering algorithms, can be summarized in the following steps[87]:

- Consider an initial set of size N. In the first iteration, N sub-clusters are obtained, each one containing one element.
- A measure of similarity between the two clusters can be therefore defined as the distance between the two elements they contain.
- Computing the similarity between all the pair of clusters, we can therefore find the two most similar ones, and merge them into a single cluster. Definition of distance can change from method to method, and different approaches can be applied.
- At this point the distance between the new clusters can be computed again, and the operation of merging them together again can be iterated until one single cluster of size N is obtained.

Going back to the networks and graphs, a similar approach can be applied. As a starting point, the definition of a similarity matrix S for a graph is necessary. The element $S_{i,j}$ indicates the similarity strength between two nodes i and j, i.e. the distance between two nodes within the network. Hierarchical clustering can be of two types: agglomerative and divisive. In the first case, nodes with the highest similarity are merged into the same community. In the second case, communities are isolated according to the similarity, and this is performed removing weak links among the communities identified [8]. The

outcome of these two types of approaches is a so called dendrogram, which predicts the possible communities partitions.
An example of agglomerative approaches is the so called Ravasz algorithm, that was originally developed to identify groups in metabolic networks and details can be found in [119]. On the other hand a famous example of the divisive procedure is the Girvan Newman Algorithm, which is based on the *centrality* concept [112].

Modularity

As suggested by [8] we could define communities detection algorithms based on three main hypotheses. The first one is fundamental for networks community, i.e. the fact that the wiring diagram of a community is its characteristic. The second hypothesis is based on the two important concepts of *connectedness* and *density*. The first property implies that a community in a network, can be represented by a connected subgraph. In line with this, the density hypothesis states how nodes that are part of a community tend to connect to each other with a higher probability than with nodes outside the community. The third and last hypothesis, that drives the description of communities [8], is the random hypothesis. If a network is randomly wired, i.e. if edges connections do not follow a clear pattern, then a community structure will not emerge. Building up on these three fundamental hypotheses, it is possible to define the concept of modularity. The intuition behind such concept can, in fact, immediately follow hypothesis 3. Comparing edges density in a community with edges density in a random graph, having the same nodes, it is possible to understand which of the two is the community. The quality of the detected community structure, can therefore be assessed looking at the so called modularity indicator.
Given a graph with E edges, V nodes and n_c communities, then the modularity value for a subnetwork graph G_c, with $c = 1, .., n_c$, can be defined as:

$$M_{G_c} = \frac{1}{2E} \sum_{i,j \in G_c} A_{i,j} - p_{i,j} \tag{2.5}$$

where $A_{i,j}$ is the value of the adjacency matrix restricted to the subgraph G_c, while $p_{i,j}$ represents the probability of having a link between the two edges i, j of the randomized subnetwork graph. Using the null model definition [8], we can define $p_{i,j}$ as:

$$p_{i,j} = \gamma \frac{k_i k_j}{2E} \tag{2.6}$$

where k_i and k_j represent the node degree of the two nodes i and j and γ is a resolution parameter ad hoc. As γ varies the desired scale of the communities changes. Usually by default the value of γ is set to 1. A first straightforward consideration can be made looking at Equation 2.5. If M_{G_c} is positive, it means that the number of real connections in the subgraph considered are higher than chance, and therefore it means that higher is the probability of having identified a community. On the other hand if M_{G_c} tends to 0, then it means that the distribution of edges in the subgraph identified is indistinguishable from a random distribution. When M_{G_c} is negative then the nodes identified do not form a community, as the probability of having them randomly wired is higher than the actual wiring conformation. The concept of modularity can be therefore generalized to the case of a full network and rewritten as shown in Equation 2.7 (from now on we set $\gamma = 1$).

$$M = \frac{1}{2E} \sum_{i,j=1}^{N} (A_{i,j} - \frac{k_i k_j}{2E}) \delta_{C_i,C_j} \tag{2.7}$$

The δ_{C_i,C_j} will be 1 only when two nodes belong to the same community. Therefore we can rewrite the first part of Equation 2.7 as follows:

$$\frac{1}{2E} \sum_{i,j=1}^{N} A_{i,j} \delta_{c_i,c_j} = \sum_{i,j=1}^{N} \frac{1}{2E} \sum_{i,j \in C_c} A_{i,j} = \sum_{c=1}^{n_c} \frac{E_c}{E} \tag{2.8}$$

where E_c is the number of edges in the identified subgraph. Similarly the second part of Equation 2.7 can be rewritten as:

$$\frac{1}{2E} \sum_{i,j=1}^{N} \frac{k_i k_j}{2E} \delta_{c_i,c_j} = \sum_{c=1}^{n_c} \frac{1}{(2E)^2} \sum_{i,j \in C_c} k_i k_j = \sum_{c=1}^{n_c} \frac{k_c^2}{4E^2} \tag{2.9}$$

where k_c represents the total node degree of a subnetwork c, i.e. the sum of all nodes degrees. Therefore the modularity of a whole network can be defined as:

$$M = \sum_{c=1}^{n_c} (\frac{E_c}{E} - (\frac{k_c}{2E})^2) \tag{2.10}$$

Modularity values are included in the range [-1,1]. A high modularity value indicates a good communities configuration, while a low modularity value implies a poorer configuration. We can consider as an example the network shown in Figure 2.2. To summarize we can therefore add to the communities hypothesis, also a last one [8],

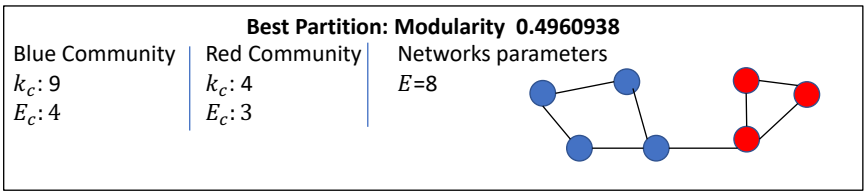

Figure 2.2: Consider the network, and the two communities identified (blue and red). In this case the blue community, has a total node degree k_c of 9, number of edges E_c of 4. The red community instead has k_c of 4 and E_c of 3. The total number of edges of the network is 8. Therefore according to Eq. 2.10 $M = [\frac{4}{8} - (\frac{9}{16})^2] + [\frac{3}{8} - (\frac{4}{16})^2] = 0.4960938$

called the Maximal Modularity hypothesis. Such hypothesis states how the division of the original network, which has the highest modularity value, can be considered the best partition of the original network. This one is used as the initial hypothesis of several detection algorithms. Following a brute force approach, that consists in obtaining all the possible community structures, and validating the value of modularity in all these cases, is computationally intractable. One example of this is the Greedy algorithm, proposed by Newman in [110]. This algorithm follows a hierarchical approach, with an agglomerative procedure. Each node is initially assigned to a distinct community. Then the differential modularity ΔM is computed, considering the communities that share at least one edge. Pair of subgraphs with the highest value for ΔM are merged together. The procedure continues until convergence to only 1 community. The number of communities in the hierarchial procedure will be chose where M is maximal. The best optimized implementation of the algorithm has a complexity of $O(Nlog^2N)$ and $O(N^2)$ in the case of a sparse graph.

Louvain community detection method

The Louvain algorithm was developed in 2008. The authors Vincent Blondel, Jean-Loup Guillaume, Renaud Lambiotte and Etienne Lefebvre proposed it while they were all at the Universite' Catholique de Louvain in Belgium, and the algorithm was named after the town [15] [87]. The method was designed to deal with large scale networks, and using an optimization approach, it was the first one proved to be time and space computationally efficient. In particular it was shown to overcome the difficulties in solving a $O(N^2)$ computationally complex problem in the case of sparse graphs. The algorithm is composed of multiple iterations called *pass*. In particular is made of two iterative steps. These multiple iterations of passes lead to an optimal solution in a

divisive fashion, following an approach similar to what is described in Section 2.1.2. In Step 1 each node is assigned to a different cluster. The algorithm then considers the gain in modularity if one node i is moved to one of its neighbour nodes j community. The node's neighbours community which brings maximum positive gain in modularity is chosen. If this is not possible, then the node remains in its original community. In the original formulation the Louvain method considers weighted networks, but the methodology can easily be extended to unweighted cases. If, following [8] [15], we define:

- Σ_{in} the total sum of the the edges part of a given community C (which in Equation 2.7 corresponds to E_c for unweighted graphs)
- Σ_{tot} as the sum of all the weights of the links which are incident to nodes inside the community C
- W as the overall sum of the weights inside the whole network
- $k_{i,in}$ as the sum of the weights from node i to other nodes which are part of C
- k_i sum of the weights of the edges which are incidents to node i

then it is possible to compute the modularity change ΔM as:

$$\Delta M = \left[\frac{\sum_{in}+2k_{i,in}}{2W} - \left(\frac{\sum_{tot}+k_i}{2W}\right)^2\right] - \left[\frac{\sum_{in}}{2W} - \left(\frac{\sum_{tot}}{2W}\right)^2 - \left(\frac{k_i}{2W}\right)^2\right] \quad (2.11)$$

We can then proceed to Step 2. In this step a new network is built. In this case the vertices of the graph become the communities identified by the previous step. Weights in the edges among communities are calculated as the sum of the weights of the edges among the nodes that are in the respective communities. The *pass*, composed of steps 1 and 2, is repeated until convergence, i.e. until there are no more changes and the maximum modularity value is obtained. Louvain algorithm is more constrained by space complexity rather than time complexity. The maximum space complexity obtained by the algorithm is $O(E)$ where E is the number of edges of the original network.

2.2 Multilayer and multiplex networks

In recent years the field of multilayer networks has found fertile ground and application in many different areas. Ranging from economics to politics, medicine to literature, to

social interaction, most of these areas present an intrinsic multi-level structure, to be taken into account in the analysis. The need to integrate different feature types is, in fact, a common trait of many of such disciplines. A multilayer network [16] can be imagined as a framework in which different channels of the same overall modelled structure are included. In such framework each channel is represented by a layer, and each node can maintain different neighbours and characteristics across different domains. For example consider the first ever whole genome sequenced organism: the *Caenorhabditis elegans* or *C elegans*. The *C Elegans* studies were originally initiated by the Nobel Prize and south-african biologist Sydney Brenner (recently passed away on the 5th of April 2019) [22]. In 1986 then, the almost full neuronal wiridng diagram of the organism was completed by the Nobel Prize and his collaborators, and the results published in an article in 1986 [149]. More recently in 2011, an even more complete wiring diagram of the organism was proposed [147]. The overall identified structure consists of 302 neurons, with thousands of links, depending on different types of biological and molecular characteristics. If we model the neurons identified as a node in a graph, then we can have different types of edges to be considered in the overall description of the organism. Molecular, chemical, or ionic channels, can in fact be the links connecting two nodes. It is natural therefore to think of such type of structure as a multilayer network: neurons are represented by nodes, and edges in different layers represent the various types of molecular or chemical links, that can exist between such two neurons. Consequently the study and comparison across different layers can bring and induce important conclusions on the organism.

2.2.1 Multilayer networks: a formal definition

A multilayer network can be formally defined as a pair $M = (G, C)$, where $G = G_\alpha : \alpha = 1, ..., M$ is composed by a set of graphs and C represents a set of interlayer connections existing between the graphs across different layers. In the case of a multilayer network structure, two types of connections can be defined: the interlayer and the intra-layer edges.

The intra-layer represents the wiring diagram of a graph, and the adjacency matrix representation is the most straightforward way of summarizing it. In the interlayer case, on the other hand, edges are defined across different layers, i.e. between two graphs G_α and G_β with $\alpha \neq \beta$.

A multiplex network is a special type of multilayer. In a multiplex network, in fact, each layer of the architecture has the same set nodes and each node in any layer is connected to its corresponding node in another layer. Each graph layer can be directed or undirected, weighted or not. Each layer G_α can be defined by the pair (X_α, E_α). As for graph theory, mathematical concepts such as degree nodes, and centrality can be extended to the case of multilayer networks. One of the most used centrality measures in a network is the node degree. In the case of a multiplex network, such concept can be easily generalized. If we consider a multiplex network $M = (G, C)$ then we can define the degree of a node as the vector:

$$k_i = (k_i^{[1]}, k_i^{[2]}, ...k_i^{[M]}). \tag{2.12}$$

Each element of the vector $k_i^{[j]}$ is the degree of a node in a given layer α, in other words we can say that $k_i^\alpha = \sum_j A_{ij}^{[\alpha]}$ [16]. To create a node ordering, considering the vector notation given for nodes degree in case of multiplex networks, we can aggregate the node degrees together, in an overlapping degree measure o_i, defined as:

$$o_i = \sum_{\alpha=1}^{M} k_i^\alpha \tag{2.13}$$

Centrality measures are of different types and can be easily extended to multilayer and multiplex networks. Other several important metrics and descriptors of single layer networks have been generalized to the case of multilayers. For example, in [43], the authors present a tensorial framework to study multi-layer networks and introduce many different topological metrics, generalized for the case of a multilayer approach. Other important works concentrate on the generalization of concepts, such as community detection, to the multilayer case. An example is [103]. Here the authors focus on the extension of the community detection approach to a multilayer network, in a time dependent and multiscale environment. In [37] for example the authors generalize the concept of clustering coefficient for multilayer networks, showing drawbacks and difficulties of the generalization procedure. In [41] the authors provide a deep and extended description of processes on multilayer networks, highlighting some of the physical phenomena related to spreading processes. A specific example of a multilayer network is the multiplex network in which each layer has the same nodes. Therefore each node is connected to itself in the other layers. Structural measures for multiplex

networks have been formalized as [11] shows. A comprehensive review of the extension, of more standard graphs measures to multilayer and multiplex structures, is presented in [16].

2.2.2 Communities detection methods

In the last few years, an increasing number of community detection algorithms have been developed and extended to the case of multilayer and multiplex frameworks. In 2010 Mucha et al [102] presented an approach for clustering multi-slice and time dependent multiplex networks. In particular the authors concentrated on the development of a quality function, targeted to time-dependent networks, showing results across different types of networks. In [75] an interesting algorithm for multilayer networks local community detection is presented, called ML-LCD. In such framework the authors provided an optimization network function which allows to use both across-layers, and intra-layer topological features. However the authors focused on the identification of local communities. Local communities identification is a special case of communities network analysis, where the goal is to identify a specific type of community network, which is proper to a few specific users. There are, in fact, some cases in which a global community network identification is neither required nor necessary, according to the research problem at hand.
This means that we can effectively improve time and space occupied in such analysis, reducing the attention to local communities structures. An increasing number of papers regarding such topics, have been written in the last few years, and many examples in such sense can be found in the literature [32] [21] [90].
For what concerns multiplex networks, slightly different approaches need to be taken into account [91]. In a multiplex network, the general idea is to use algorithms which extract features from multiplexes. There are various strategies that can be adopted to solve this problem. A first widely used and implemented technique is the so called *projection*. Such technique relies on the projection of the various layers into one, and then on the application of clustering and communities detection techniques, on the resulting collapsed network [91]. Other commonly used approaches include data mining techniques,generalized canonical correlations or tensor decomposition. These frameworks allow to identify the auxiliary partitions present in the multiplex structure and are therefore able to identify the potential local communities in the network.

2.3 Visibility graphs

The idea of applying graph analysis to the time series domain has led to the identification of algorithms and methods capable to produce the conversion, from time series to networks. In a paper by Lacasa et al [82] authors present an interesting approach for defining a graph associated to a certain time series, according to what is defined a visibility criterion. Let's first formally define edges and nodes for a graph, deriving from a time series. Each time stamp will be a node, labelled with the corresponding value and an edge will exist with another node, if the visibility criterion is satisfied.
Two variants of the visibility graph mapping exist: the Natural Visibility Graph (NVG) and the Horizontal Visibility Graph (HVG). The former is based on the following criterium: each node in the graph corresponds to a time stamp and two nodes share an edge if the two time stamps *can see* each other [82] through a line. This means that given a time series of N data points, and given two points z and t with their corresponding values y_z and y_t, these two will be connected by an edge if for a given value y_l, between y_z and y_t, the following holds [82] :

$$y_l < y_t + (y_z - y_t)\frac{t-l}{t-z}. \tag{2.14}$$

The second criterion works as follows: two nodes t and z share an edge connection in the HVG if given any other time values y_l the following holds:

$$y_l < inf(y_t, y_z), \forall l : t < l < z \tag{2.15}$$

The latter version of the visibility graph is computationally more tractable. Complexity of both algorithms is low, with a $O(NlogN)$ for both NVG and HVG. Intuitively HVG allows for the presence of an edge between two nodes if and only if the two values considered are higher than any value between the two [82].
A few important properties of the graph so obtained, can therefore be derived. First of all the graph will be connected. This is due to the fact, that in the worst case scenario at least each point in the time series will see his neighbour, i.e. each node in the graph will be able to be linked to his neighbour. Secondly the graph will be *undirected*. In fact, the way in which an edge is defined does not imply a direction. Moreover a third important property of a visibility graph is the invariancy against affine transformations of the time series data. Such visibility criterion has in fact proven to be invariant with

respect to horizontal, or vertical, axes rescaling and translation [82]. Extension of the visibility graph defintion has been developed, for example for what concerns the identification of *motifs* in graph structures [74] or for the analysis of random time series [93]. In recent years, an interesting application of these techniques to neuroscience has been developed. In [155] the authors present a classification of sleep stages, from an EEG single channel, using features in the graph domain, in particular the mean degrees and degrees distribution. The translation of EEG channel signal into a graph domain is made using the graph visibility approach and a final machine learning classifier is used to determine the sleep class to which certain EEG signals belong to. Another example of visibility graphs applications to EEG is [1]. In this paper the application is based on EEG, and differences in sub-bands of the signals are found when comparing a group of controls to a group of Alzheimers' patients. With the increasing interest in the connectomics and connectivity features of the brain, the field of visibility graphs found example of applications also in the case of the connectivity studies in large-scale brain networks. In [152], for example, the authors propose a new Horizontal Visibility Graph measure defined as Horizontal Visibility Graph Transfer Entropy (HVG-TE), which is used to estimate the information flow considering pairs of time series.

2.3.1 Extension of visibility graphs to the case of multilayer networks

In [83] Lacasa et al. introduce an interesting extension of the visibility graph approach to the case of multivariate time series. The natural extension of this approach is in fact the case in which from a mono layer we shift to a multilayer architecture, as described in previous paragraphs. Transitioning from a multivariate time series, to a multilayer Horizontal Visibility Graph, can be done simply converting each time series into a graph and then considering such graph as one of the layers in a multilayer architecture. Authors then show how descriptors and measures associated with the new multi-layer structures, can be used as a network descriptor and entail non-trivial properties of the time series which can effectively be used in network analysis [83]. The natural translation of a multivariate time series is a multiplex kind of network. Nodes represent the same time stamps across layers and multiplex measures can be obtained in order to identify features and characteristics of the multivariate time series. An example of such modelling in neuroscience is [123]. Here the authors apply the method to a large open dataset, analysing the differences and the characteristics of resting state fMRI networks.

The patterns and clusters of activities identified in the resulting network, can then be considered as a measure of activity and related to psychiatric and pathological patients clinical characteristics.

Chapter 3

Crosstalks and brain trauma: a multilayer network approach

3.1 Brain-heart crosstalks: problem definition

Intracranial pressure (ICP), which represents the pressure measurement of the brain tissue and the cerebrospinal fluid, can be continuously monitored after severe traumatic brain injuries (TBI) or similar life threatening conditions [72] [38]. ICP behaviour can in fact be highly affected and altered, due to TBI events and other neurocritical conditions of the central system. Its normal behaviour can dramatically and pathologically change [38] leading to dangerous patients conditions.
ICP monitoring can be performed through the application of an ICP transducer, inserted by mean of an invasive procedure. In this way the ICP signal and its variations can be continuously checked [38] [72]. The information contained in the ICP signal is in fact of vital importance, and can be used to predict critical medical issues, such as intracranial hypertension. This requires immediate clinical intervention. ICP pathological and sudden increase can in fact lead, in the worst cases, to patient's death.
Therefore the analysis of elements that could possibly alert in advance the clinician, regarding the presence of such conditions, is essential.
To the best of our knowledge only a few works focus on the identification of a model describing the intracranial system behaviour. In [5] the authors use a Hidden Markov Model approach to perform an unsupervised clustering of recorded information. Such compressed representation of the signals is then linked to patients outcome, showing how such identified states can still retain important patients prognostic information.

Moreover in [70] a hidden state algorithm is used for the estimation of unobserved measurements, such as ICP and cerebral blood flow velocity (CBFV). This is a two steps procedure, in which parameters of a modified nonlinear intracranial mathematical model are first identified in an offline stage. Subsequently a nonlinear Kalman filter estimator is applied to evaluate unobserved variables. Such estimator is derived given some patients measurements, such as ICP and cerebral blood flow velocity (CBFV). The relationship of ICP with respect to other monitored parameters, is in fact a key aspect to study. An example of this is [69]. In this work the authors present ApEN, an algorithm based on the adaptive calculation of approximate entropy, integrated with a causal coherence analysis. Through such modelling the authors are able to analyse and exploit the potential interaction between ICP and R wave intervals [69]. Moreover, in [71], the authors also extract indices of causal coherence and generalized synchronization. This is done considering beat to beat mean ICP pressure measurements and intervals between consecutive normal sinus heartbeats (ICP and RR intervals). In [55] ApEN is also used to investigate the correlation between heart rate, mean arterial pressure, ICP and the combination of the three considering outcome after TBI .

Our study started from the visual observation of simultaneous increases taking place in HR and ICP, in a cohort of paediatric patients. These clinical observations, led to the formulation of our initial research question: *can we quantify the number of these events?* And consequently: *are these events related in some ways to the clinical state of the patients, and how?* We therefore introduced a new variable that we called brain-heart crosstalks. This was defined as a simultaneous increase of at least 20% of both ICP and HR, in a 10 minutes window frame of observations. The 10 minutes was suggested by clinicians, as a reasonable amount of time, to observe such behaviour of the two signals. The robustness of the model to the window length was not the goal of this study, but could be investigated in future work. This is the reason why, in the implemented code, we left the 10 minutes as a parameter, changeable by the clinician. The focus on HR and ICP simultaneous increases, as well as the choice of the sampling rate, and the definition of crosstalk all come from a specific clinical research question that we investigated in the present work. This was a way of creating a "proxy" of interaction between brain and heart to be related to patients outcome.

The interest in the interaction and the behaviour intercurring between heart and brain, is in fact part of a wide field of research that has been developed in the last few years [145] [144] [48] [101]. The physiological coupling between the two systems, has been shown to be an important signal and biomarker for pathological and traumatic events

[129].
We therefore derived an algorithmic approach for detecting and quantifying the number of brain-heart crosstalks between ICP and HR. This allowed us to compute the number of brain-heart crosstalks events happening per patient as we can see in table (see Table 3.1) [45]. An example of a brain-heart crosstalk event identified by the algorithm is shown in Figure 3.1.

In the following sections we will thoroughly describe the algorithmic procedure

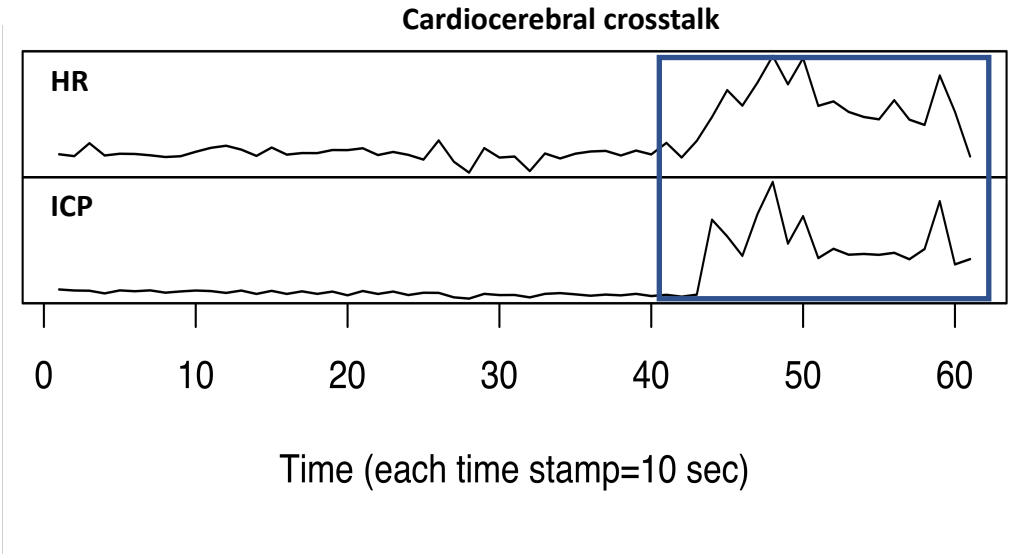

Figure 3.1: The figure shows the presence of one brain-heart crosstalks (highlighted with the blue square) for a 10 minutes observations of HR and ICP in one patient of our cohort. Each time stamp in the x axis corresponds to 10 seconds of observations.

implemented, and we will go through its results and application to the paediatric dataset we used in our analysis. Subsequently to that, we proceeded with a multilayer network modelling of the two time series. We then computed some relevant network measures, derived from the time series, as we will discuss later in the present Chapter.

3.2 The dataset

The dataset for this study was collected prospectively from 27 paediatric TBI patients admitted to Addenbrooke's Hospital, Cambridge, Paediatric Intensive Care Unit (PICU). The data collection took place between August 2012 and December 2014. TBI patients with a clinical need for ICP monitoring were included for the current analysis. The

insertion of an intracranial monitoring device is part of standard clinical practice and as such did not require ethical approval. Data are routinely collected for clinical purposes and guide the management of patients. The analysis of data within this study, for the purposes of service evaluation, was approved by the Cambridge University Hospital NHS Trust, Audit and Service Evaluation Department (Ref:2143) and did not require ethical approval or patient consent. ABP mean arterial pressure (mmHg), HR heart (Hz), ICP intracranial pressure (mmHg) were all collected during the study. Inclusions criteria were the presence of TBI cases confirmed by Computer Tomography (CT) scan, severe injury with a Glasgow Coma Scale (GCS)$<$8 and the need of continuous monitoring of ICP [151]. Data management and TBI recruitment process is described in [151]. The monitoring variable sampling rate was 100 Hz and data was collected using ICM+. This is clinical research software [132], pioneering in the sector. Real time data, and analysis are performed bedside, allowing the development of personalized treatments and analysis of TBI patients. High resolution waveforms were cleaned manually. Moreover they were down-sampled to 0.1 Hz by coarse graining using 10 seconds a mean filter. The whole monitored period was considered for each patient. Data cleaning and handling was performed exclusively by the clinical team, and I was given the dataset ready to be analysed. The choice of the sampling rate was made by the clinical team involved in the study, since it was considered a good rate to be used for the current exploratory analysis of brain-heart crosstalks interaction. Future studies could also investigate the impact of different rate choices in the final brain-heart crosstalks analysis.

3.3 Methods

3.3.1 Algorithm for crosstalks detection

As a first step we proceeded with the implementation of the brain-heart crosstalks detection algorithm. A challenging aspect in research, which is still an open and unsolved question, concerns the implementation of automatic algorithms to perform peak detection in the presence of noise. This in fact finds a very wide range of applications, from bioinformatics [6] to medicine, from computer science (for example CPU data [124]) to economics [65]. The definition of peak is based on two main properties of a given time time series, according to [116]. First a peak needs to be defined as a local maximum within a time window of interest. This implies that a peak,

in general, is not the *global maximum* of the whole time series. Secondly it has to satisfy the property of *isolation*. Considering the window frame of interest, a limited number of points in it needs to have similar values, so that it can be identified as a peak [116]. As described in [116] mainly two approaches have been followed in the literature. On the one hand, the time series can be smoothed and then a known function fitted. In this way we can obtain an identification of the peaks, looking at the function that has been fitted. The second strategy, instead, consists in defining in advance the shape of the peak or burst that we are looking for, in the time series. In this way we can accordingly write the algorithm able to detect the desired pattern. Given the shape of brain-heart crosstalks that we needed to identify, we followed the second strategy, also because the dataset was provided already cleaned for the analysis. Our proposed algorithm is based on a sliding window approach. In particular it works as follows.

1 Consider two time series $X = x_1, x_2, x_3, ..., x_T$ and $Y = y_1, y_2, y_3, ..., y_T$ which in our case are the HR and ICP time series

2 Take a window of observations of length L. In our experiments L= 10 minutes. This was experimentally motivated by clinical observations.

3 We then consider all the simultaneous windows of length L, in the two time series X and Y, and their respective maximum values in the time window. If in both time series the maximum value is reached by at least an increase of 20%, with respect to the minimum value in the window, and followed by a similar decrease, then a brain-heart crosstalk is detected.

4 To avoid counting twice the same crosstalk event we also proceeded with a filtering of the windows detected by the sliding window approach, in which we filtered out events which were detected within the same temporal frame.

The application of the brain-heart crosstalks detection algorithm enabled us to identify several events taking place in the HR and ICP time series. We found an average number of crosstalks of 38.37 (S.D. 57.20). The number of events detected varied across patients, from 1 to more than 150. The number of brain-heart crosstalks and the number of observations are summarized in Table 3.1. Each observation corresponds to 10 seconds.

3.3.2 The multiplex horizontal visibility graph

There is a variety of approaches that could be undertaken when studying time series and dynamical systems. For example Takens's theorem is a powerful way for reconstructing the main features of a coupled dynamical system, by looking at one of the two time series [139]. To the best of our knowledge network theory and graph analysis have never been applied to the study of ICP, which was the motivation behind our approach. In our experiments we decided to use HVG. One of the motivation behind this is the proven capability of HVGs to work well with local analysis and short correlations, due to the typical exponentially decaying degree distribution, for more details please refer to [123]. An example of construction of the HVG for a patient, given the ICP time series, is shown in Figure 3.2. Each time stamp t of the x axis will be a node in the graph. Connection will exist between the nodes that "can see" each other, i.e. between two nodes who have no higher values between them. Edges in the graph are represented by the arrows displayed in the figure between the time points. Since we were interested in analysing the behaviour of the multivariate time series system, formed by ICP and HR, we adopted the multiplex visibility graph approach of [83]. Suppose in fact to have M time series. Then following the visibility graph approach, each time series can be mapped as a layer in the multilayer representation. Since every graph in each layer presents the same set of nodes (the temporal time stamps t), this is the so called multiplex visibility graph [11] [16] [82] [84] [93]. We therefore proceeded as follows:

1 We used the sliding window brain-heart crosstalk detection algorithm to obtain non overlapping windows, in which crosstalks were detected

2 We mapped each time series window, in which a crosstalk was detected, into a graph following the HVG approach

3 We computed graphs and network statistics as described in the results Section

We used two metrics for the analysis of the multilayer graph. The reason why we chose this is because such metrics are widely adopted in the literature to model the interaction between layers [83]. Moreover one is focusing on the node distribution, while the other on the degree distribution, reporting a complete picture of the system behaviour. The first indicator is the average edge overlap. Such metric is defined in [11] [14] [43] as:

$$\omega = \frac{1}{2K} \sum_{i,j} o_{ij} \tag{3.1}$$

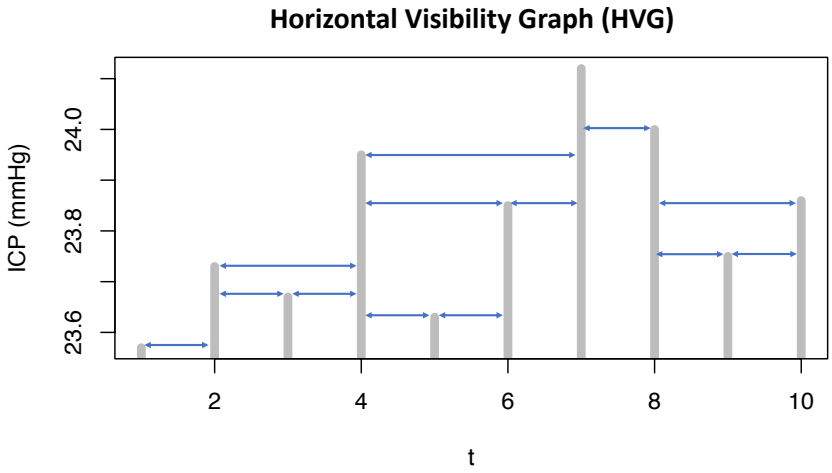

Figure 3.2: Example of the horizontal visibility graph. The time series is plotted. Each time stamp will be a node in the HVG graph, and edges will exist between two time stamps which can see each other, and that are represented in blue in the graph.The example is shown on a portion of the ICP time series for a patient.

where $o_{ij} = \frac{1}{M} \sum_{\alpha} A_{ij}^{[\alpha]}$ and $A_{i,j}^{[\alpha]}$ is the value of the adjacency matrix of layer α for the pair (i,j). In Equation (3.1) K is the number of pairs of nodes having at least one link across layers. The average edge overlap quantifies the coherence of the overall graph and the higher it is, the higher the coherence of the graph layers. The second metric is the interlayer mutual information; this is defined as [83]:

$$Mi = \sum_{k^{[\alpha]}k^{[\beta]}} P(k^{[\alpha]}, k^{[\beta]}) log \frac{P(k^{[\alpha]}, k^{[\beta]})}{P(k^{\alpha})P(k^{\beta})} \tag{3.2}$$

and in this case $P(k^{[\alpha]}, k^{[\beta]})$ is the joint probability of having a node with degree $k^{[\alpha]}$ at layer α and of degree $k^{[\beta]}$ at layer β. Such measure is in part limited by the fact that only the degree distribution of the network is considered. More sophisticated and complete measures exist, as shown in [42]. Applications are in different areas from climate dynamics [46], to the analysis of the gold price time series [92], to the detection of sequential motifs in visibility graphs [74]. An extensive review of the applications of such methodology is done in [113].

3.4 Results

As described in the previous section, we first identified non overlapping windows in which a brain-heart crosstalk was detected by our algorithm. Once obtained the window, we transformed it into a HVG. Figure 3.3 shows an example of the pipeline that leads from the time domain to the construction of the multiplex graph with the ICP and HR observations. At the beginning we can see the two time series during a brain-heart crosstalk event. Then we can see how through the conversion into the HVG, we transform them into two different graphs. These graphs will then become layers of the multiplex ICP-HR structure where we can study the dynamics of the coupled system. In the example shown in Figure 3.3 we obtain the following average edge overlap ω and interlayer mutual information: $\omega = 0.7920$, Mi=0.7285. For a summary measure regarding the ω and the Mi we proceeded as follows: for each patient we considered 10 windows in which a crosstalk was detected and 10 windows with no brain-heart crosstalks. Then we computed the average value of ω and Mi for the 10 windows with brain-heart crosstalks and the 10 windows without. From now on we will refer to:

- ω_{ct} for the omega values during crosstalks
- ω_{nct} for the omega values when no crosstalks are detected
- Mi_{ct} for interlayer mutual information values during crosstalks
- Mi_{nct} for the interlayer mutual information when no crosstalks are detected

The results are shown in Table 3.2. We chose 10 windows because it seemed a reasonable number, given the high variability of cross talks events across patients. For this reason we discarded only a few patients. Considering Table 3.2, we can see how there seems to be a trend in the way the ω and Mi behave with respect to brain-heart crosstalks and non crosstalks events. In particular it seems that ω is more stable in the two cases than Mi. More specifically, Mi, has a clearer increasing trend on average with brain-heart crosstalks than without. This is shown in the last row of Table 3.2, where the average values of each column are presented. This would suggest that with cross-talks the two time series are more similar than without. The trend is confirmed by the paired Welch two sample t test performed between the ω and the Mi in the case of the crosstalks and non crosstalks cases. In the case of ω in fact the p value is 0.99, so no significant difference exists between the two cases. On the other hand in the

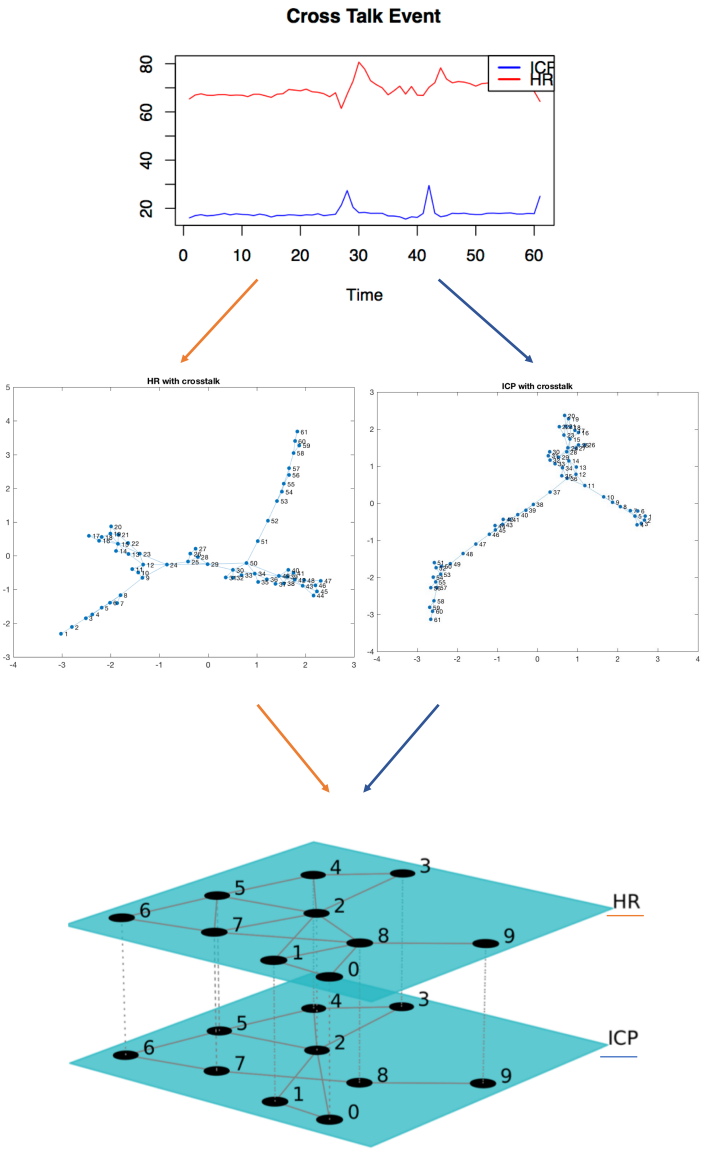

Figure 3.3: The pipeline that leads to the construction of the ICP-HR. Top of the figure and example of a window in which a brain-heart crosstalk takes place. From this we can obtain the two graphs of ICP and HR, which will become part of the multiplex.

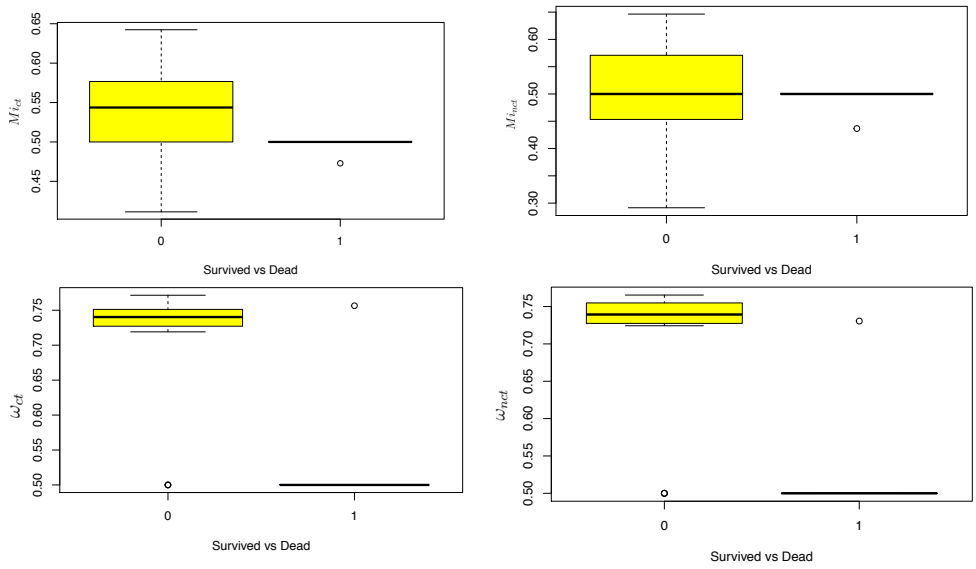

Figure 3.4: Figure showing the distribution of the network measures with respect to mortality for the paediatric cohort. On the top row the mutual information for the cases of crosstalks and non-crosstalks, and bottom row the average edge overlap.

case of Mi the p value = 0.02144, i.e. highly significant difference exists between the two vectors. The boxplot of the distribution of Mi in the cases of crosstalks and non crosstalks is shown in Figure 3.5. Moreover in Figure 3.4 is shown the distribution of average edge overlap and mutual information with respect to mortality for the paediatric cohort analysed.

Such preliminary findings could imply that the network topology metrics considered so far, might be important for further analysis of the system. In the next chapter, we will discuss how network metrics could be included in an outcome prediction model for mortality.

3.5 Summary

This analysis was performed with no a priori assumptions for a possible relationship between HR and ICP. The 27 records of monitored data are samples of paediatric patients admitted to Addenbrooke's Hospital, Cambridge. We implemented a sliding window peaks detection algorithm. With such algorithm we were able to detect the cross-talk events happening in the two time series of HR and ICP for each patient. We found an average number of cross-talks events of 38.37 (S.D. 57.20). We then presented

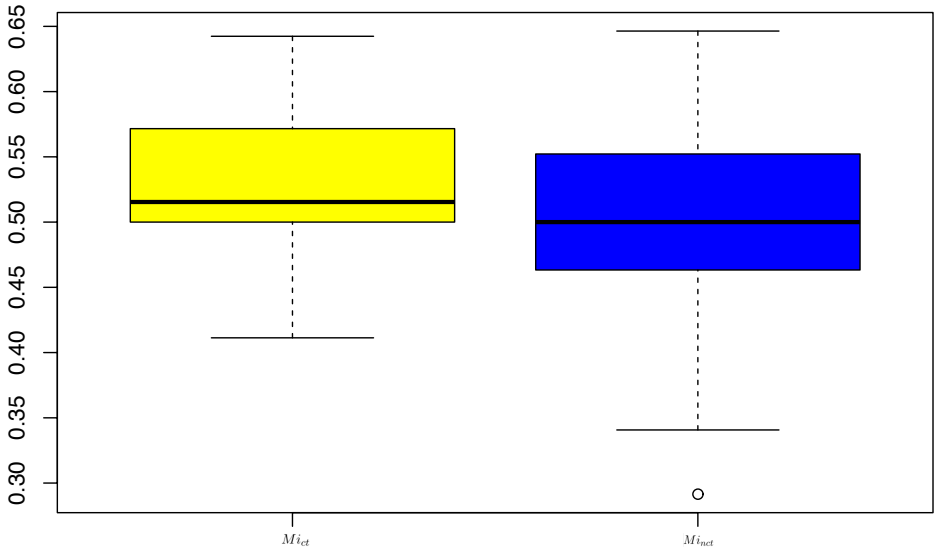

Figure 3.5: Boxplot showing the mutual information values between the case of crosstalks and non crosstalks in the cohort analysed. In the figure Mi_{ct} represents the value of mutual information with crosstalks, and Mi_{nct} the case in which the mutual information is computed in non-crosstalks windows. The Welch two sample paired t-test returns a significant p value of 0.03

a multiplex network model for the analysis of multivariate time series. We modelled our system using the horizontal visibility graph approach as described in [83]. In particular we analysed the behaviour of the system considering two multilayer network metrics: the average edge overlap and the interlayer mutual information. We decided to use these two measures, as classical indicators adopted in the literature, for a first investigation of the system. We evaluated the average trend of these two metrics on 10 brain-heart cross-talks and non cross-talks windows for each patient. Findings suggest that while the average edge overlap seems to have a more stable behaviour between the two situations, the mutual information on the other hand shows a clear trend. In particular the average value increases when cross talks events are detected, meaning that the two time series behave more similarly in the second case. Future directions of research include the integration of further parameters that are monitored in this cohort of patients, and that could help the analysis and understanding of the cross talks behaviour. We therefore plan to extend our multiplex model, also considering further multiplex network properties and measures, integrating the biological knowledge regarding the system into its network representation. For example we could consider characterizing the two layers in terms of their connectivity. The findings presented in this thesis could,

in fact, possibly help also in understanding the dynamics of ICP and HR signals to further develop the modelling of the coupled system.

3.6 Related publications

1. Dimitri, Giovanna Maria, et al. "Simultaneous transients of intracranial pressure and heart rate in traumatic brain injury: Methods of analysis." Intracranial Pressure & Neuromonitoring XVI. Springer, Cham, 2018. 147-151

2. Dimitri, Giovanna Maria, et al. "A multiplex network approach for the analysis of intracranial pressure and heart rate data in traumatic brain injured patients." Applied Network Science 2.1 (2017): 29.

Patient	Number of brain-heart crosstalks	Number of observations
1	15	64717
2	35	24683
3	66	173040
4	21	25706
5	1	705
6	24	70576
7	22	8836
8	47	34559
9	59	24459
10	69	65881
11	20	47095
12	142	84427
13	31	63089
14	29	11914
15	7	16286
16	36	45035
17	2	27213
18	1	15276
19	1	43425
20	19	25406
21	281	99175
22	57	37159
23	2	52718
24	15	38229
25	1	25782
26	15	53200
27	18	30214

Table 3.1: Table presenting the number of crosstalks and observations for each patient. Each time stamp corresponds to 10 seconds. For example patient 1, has approximately 180 hours overall monitoring time.

Table 3.2: Mean values of the average edge overlap and mutual information for brain-heart crosstalks and non cross talks events windows. Each row is a patient. Every value presented is averaged over 10 windows. Patients 5,15,18,19,23,25 had less than 10 cross talks detected. CT and non CT stands for crosstalk or non crosstalk event.

Patient	ω_{ct}	Mi_{ct}	ω_{nct}	Mi_{nct}
1	0.7535	0.5690	0.7513	0.4721
2	0.7334	0.4913	0.7306	0.4633
3	0.7444	0.5782	0.7388	0.4155
4	0.7424	0.6424	0.7298	0.5522
6	0.7505	0.5752	0.7544	0.6037
7	0.7715	0.4113	0.7630	0.2915
8	0.7431	0.5370	0.7277	0.5831
9	0.7382	0.6013	0.7552	0.6202
10	0.7301	0.5516	0.7399	0.4434
11	0.7473	0.5233	0.7633	0.3407
12	0.7346	0.6232	0.7243	0.5017
13	0.7635	0.4901	0.7622	0.3662
14	0.7420	0.6017	0.7540	0.6219
16	0.7611	0.5504	0.7495	0.6464
20	0.7260	0.5716	0.7321	0.5587
21	0.7283	0.4647	0.7272	0.4721
22	0.7191	0.5154	0.7545	0.5996
24	0.7520	0.6271	0.7654	0.4976
26	0.7565	0.4729	0.7306	0.4367
27	0.7818	0.7818	0.7764	0.3088
Average values	0.7460	0.5590	0.7465	0.4898

Chapter 4

Brain-heart crosstalks, network multiplex measures and mortality in paediatric TBI patients

4.1 Introduction

Treatment and management of Traumatic Brain Injury (TBI) remains a leading research priority in clinical practice, being a worldwide cause of death and disabilities. Particular attention should be devoted to paediatric and young adults cohorts, given that TBI is their leading factor of mortality, as well as representing a critical issue in adults [94] [60] [86]. Towards a better understanding on how to best manage TBI cases, identifying factors that could help towards outcome prediction, is a central research question nowadays. A few examples of adults outcome prognostic models can be found in the literature [105] [117] [153] [73]. Such models are usually based on a combination of clinical, imaging and monitoring information, and some of them have been accepted and currently used in clinical practice [137].

In the case of paediatric patients, however, much less has been developed, and the models proposed concentrate mainly on certain types of parameters for outcome prediction. For example, [53] and [128] show how features extracted from Diffusion-Weighted Imaging can be used to obtain prognostic outcomes in paediatric TBI patients. In [78] Computer Tomography (CT) information is, instead, used for identifying a threshold in pathological ICP in a paediatric cohort. An interesting example is [34], where the authors apply machine learning techniques to predict outcome, but with the use of CT

features only. In [57] a wider retrospective analysis of mortality with respect to clinical, CT and demographics, is performed and a few factors (clinical data, low Glasgow Coma Score, initial hypotension, presence of coagulopathy and age) were found to be significant in predicting mortality. In our analysis we included an ensemble of these features as predictors: clinical, demographics and CT. In addition to this initial features set, we added three new variables to the predictors set: the brain-heart crosstalks variable and the two multiplex network measures of average edge overlap and mutual information (described in the previous chapter). We then related all such variables to patients outcome, using an elastic net regression modelling [51]. To the best of our knowledge this is the first time that such relation of mortality with brain-heart crosstalks, and network measures, has been formalized and studied in a comprehensive way. The results show promising and interesting relationships between the new derived variables and patients outcome, and the biological and clinical implications lay the ground to further research.

4.2 The dataset

The cohort used for the current study is the same as in Section 3.2. Monitoring data, introduced in that section, were in fact collected together with clinical records as part of a routine standard during the hospitalization of patients. Data management and TBI recruitment process is described in [151]. Not for all of the 27 patients clinical information was however available, but only for 25. Patient 14 and 27 of the previously described cohort were therefore removed from the analysis. Moreover we considered a combination of CT and clinical variables for our study. CT features considered for the study were the following: Diffuse Axonal Injury or Space Occupying lesion (DAI vs SOL) as discussed in [44], presence of petechial haemorrhage, width of basal cisterns (mm), shift of the midline structures (mm), width-depth of the space occupying lesion and the presence of subarachnoid haemorrhage. Clinical variables considered for the study were instead the motor component of the Glasgow Coma Scale at hospital admission [141], presence of pupils dilation (binary variable with 1 meaning at least one pupil dilated), hypoxia and hypotension. The modified Marshall score for the CT scan was included in a range between 2-6 with a median of 3 [96] [151]. The Marshall score is a measure of the severity of injury given CT features, widely used in clinical practice nowadays. There are also other severity scores such as Helsinki, Stockholm

and Rotterdam which however were not available for this cohort. Moreover we also considered in the predictor set an additional variable, the so called theatre variable. This is is defined as the time between the traumatic event and when the monitoring device is inserted (expressed as a fraction of a day).

4.3 Methods

4.3.1 Modelling brain-heart crosstalks and mortality

We derived the absolute number of brain-heart crosstalks variables as described in Chapter 3. However the number of observations for each patient was different. This is, in fact, obviously dependent on the time length of the hospitalization required. Therefore there was the need of using a normalized version of the raw brain-heart crosstalk variable. We call such a measure ct_{np}. Let $p = 1, .., N$ be the generic patient in our cohort. Each patient p is characterized by a pair (ct_p, l_p), where ct_p is the absolute number of brain-heart crosstalks for patient p and l_p is the number of the time series observations. The normalized measure can therefore be defined as:

$$ct_{np} = \frac{ct_p}{l_p}. \tag{4.1}$$

In other words ct_{np} expresses the number of brain-heart crosstalks per observation (in our case 10 seconds, which is the sampling rate of the time series in our analysis).
We then proceeded relating mortality to the set of predictors. In a first preliminary phase we proceeded computing some descriptive statistics, for example the Pearson correlation coefficient. We then investigated the possibility of introducing the three new variables in a prediction model.
A lack of outcome prediction modelling characterizes studies on TBI paediatric cohorts. There are various explanations for this absence. In most cases paediatric TBI datasets are small, and this makes it difficult for machine learning methodologies to be applied in a reliable way [26]. In particular, this could always bring the risk of overfitting, that is the construction of statistical models that do not generalize properly. However, being the small sample datasets a widespread characteristic of many machine learning applications, further techniques have been developed in recent research, that could be applied and partly overcome this issue [50]. In particular, an application of methodologies requiring a lower number of parameters to be fitted, such as regression methodologies,

could help in these cases. For our small paediatric cohort study, we made use of a binary outcome prediction method, widely employed in biomedical research, that is logistic regression. Suppose we have a response variable y that can take two possible values $1 = dead, 0 = survived$. Using a logistic regression approach we can predict the probability of death, given a predictors dataset x as:

$$\Pr(y = 1|X = x) = \frac{e^{\beta_0+\beta^T x}}{1 + e^{\beta_0+\beta^T x}} \tag{4.2}$$

which can be rewritten using the log notation as:

$$z = \log \frac{\Pr(y = 1|X = x)}{\Pr(y = 0|X = x)} = \beta_0 + \beta^T x \tag{4.3}$$

In our case we applied a variation of the more standard logistic regression approach, named elastic net model. This logistic regression framework can be combined with the properties of Lasso and Ridge regression [142] [67], adding two penalty terms and making use of a penalized log-likelihood maximization approach [64] [51] [130]. This model was mainly developed to overcome overfitting issues. Given the small sample size, before fitting the regression model, we first proceeded with a features selection step. The task of features selection, has been widely addressed in bioinformatics nowadays [120]. A common and largely used technique is based on thresholding the original matrix, discarding elements that, for example, do not satisfy a minimum threshold value of correlation. In our case, the interest was to understand the importance of brain-heart crosstalks and network measures for outcome mortality prediction.
To do so, we built a subset including them as well as a number of predictors, which were not *too* correlated. We proposed, therefore, a slight modification of the thresholding method, that we called Pivoting Method. The intuitive idea behind it is to build the set of features least correlated among themselves, considering a given threshold and a certain $pivot$ variable of interest. If we call $VarSelect$ the vector where we store the selected variables and $Pivot$, the pivot variable of interest, we can describe our procedure as described in Algorithm 4.1.

After this preliminary features selection step, we could therefore proceed to fitting the logistic regression model, using the selected variables. In our experiments we set the correlation threshold to 0.5.

Algorithm 4.1 Pivot Algorithm

$VarSelect = [Pivot,]$
for $i \quad in \quad 1 : numfeatures$ **do**
  if $|cor(X_i, Pivot)| < 0.5$ **then**
    if $i = 1$ **then**
      $Add \quad X_i \quad to \quad VarSelect$
    else
      for $j = 1 \quad to \quad i$ **do**
        $add \quad to \quad VarSelect \quad the$
        $element \quad minimally$
        $correlated \quad to \quad Pivot$
        $and \quad to \quad all \quad the$
        $other \quad elements \quad already$
        $in \quad VarSelect$

4.3.2 Causality and Brain-Heart Crosstalks

A natural extension of our analysis was the investigation of causality between the two signals, i.e. ICP and HR, inside identified brain-heart crosstalks windows. To do so we applied a Granger Causality approach [61]. Previous research in the field has shown the presence of a bidirectional causality existing between ICP, Mean Arterial Pressure (MAP) and Heart Rate, studying 24 hours of observations and linking this to the mortality rate post TBI [56]. In this case, though, the study was based on a longitudinal adult cohort of 171 TBI patients. Death was shown to have a relationship with lower Granger Causality for ICP causing MAP, and HR causing ICP. These findings are in line, therefore, with the idea of information exchange happening between the cerebrovascular, autonomic and cardiovascular systems in severe TBI [56]. There are of course a few important differences with respect to our study. First adults versus paediatric cohorts used for the analysis. Secondly, we concentrated on understanding the role of causality in the brain-heart crosstalks windows and not on the entire time series. To proceed with causality analysis, the time series in the brain-heart crosstalks windows were preliminary checked for stationarity, using a Box-Ljung [20] test and an augmented Dickey Fuller test [121] [7]. Subsequently we performed a Granger causality test in the crosstalks windows, to detect if there existed a causality between the two signals. The Granger test performed was based on the autoregressive model approach [61] with an order lag of 4. As in the previous case of brain-heart crosstalks, there was the need of normalizing the causality measure with respect to the length of the time series observations. We then defined ct_{gr1} as the number of brain-heart crosstalks

windows in which the signal goes in the direction *ICP causes HR*. Similarly ct_{gr2} we defined as the number of brain-heart crosstalks windows in which the signal goes in the direction *HR causes ICP*. If we consider a patient p, with $p = 1, ..., N$, as well as for Equation 4.1 we can say that a patient is characterized by the pair of values (ct_{gr1}, l_p) where l_p is the number of observations of the time series. Therefore the normalized value can be defined as:

$$ct_{n_{gr1}} = \frac{ct_{gr1}}{l_p} \tag{4.4}$$

Same reasoning applies for $ct_{n_{gr2}}$.

4.4 Results

4.4.1 Statistical analysis

Demographics, Clinical and CT features

In Table 4.1 we summarize demographics, clinical and CT variables statistics, for the TBI paediatric cohort of our analysis.

Mean age at admission time was 12.08 years, ranging between 6 months and 16 years

Table 4.1: Table showing the statistics of demographics, clinical and CT characteristics at admission for the paediatric cohort.

Features	Survived (n=20)	Non-survivors (n=5)	p value
Age, mean ± SD	12.675 ± 5.74	9.7 ± 4.43	0.32
Female (%)	7(35)	1(20)	0.53
Diffuse Axonal Injury (DAI vs SOL) (%)	12(60)	3(60)	1
Petech (%)	3(15)	2(40)	0.17
Cistern	3.9 ± 1.78	1.64 ± 0.98	0.002628
Midline Shift	0.895 ± 1.52	1.49 ± 2.07	0.5726
Soldepth	1.05 ± 1.65	1.78 ± 2.49	0.5635
Sah (%)	6(30)	3(60)	1
Modified Marshall Score **(median)**	3.45	3.8	0.56
Theatre *(fraction of a day)*	0.16 ± 0.028	0.19 ± 0.02	0.018
Motor Score, median (range)	4 (1-5)	3 (3-4)	0.048
Pupils			
Fixed Unilaterally (%)	19(95)	3(60)	0.42
Fixed Bilaterally (%)	1(5)	2(40)	0.72
Hypoxia(%)	5(25)	3(60)	0.23
Hypotension (%)	3(15)	3(60)	1

old, with 17 male and 8 female patients. On average the observation time was 12 hours (S.D. ± 9 hours).

4.4.2 Brain-heart crosstalks and mortality

In Table 3.1 we showed the absolute number of brain-heart crosstalks per patient. Mean value is 38.37 with a very high standard deviation (57.20). The intuition behind such a high variability was the different patients clinical conditions. We then computed initial descriptive statics. In Figure 4.1 we show the Pearson correlation coefficient; interestingly it emerges a negative correlation between brain-heart crosstalks and mortality, equal to -0.30. We double checked with the point biserial correlation coefficient, showing the presence of a -0.30 coefficient also in this case between Ct_{np} and mortality. For the correlation analysis we used the standardized brain-heart crosstalks variable ct_{np}. In the correlation matrix we included all the network measures (with and without crosstalks) as well as the outcome and other clinical predictors. We can also observe a negative correlation between network measures and mortality. As we will see, this is in line with the negative correlation existing between ct_{np} and mortality. We also included in the correlation plot the causality measures ct_{ngr1} and ct_{ngr2} obtained as described in Section 4.3.2: the two measures exhibit high correlation. The more meaningfull negative correlations concerning mortality is with ω_{ct}, ω_{nct}, cistern and ct_{ngr2} while the more meaningfull positive correlations are with theatre, pupils and hypotension. Notice that the Marshall score is highly positively correlated with DAI vs SOL, soldepth and midlineshift. This is because the score is derived from CT scan features, as well as the three listed above. We then proceeded plotting the distribution of brain-heart crosstalks considering survivors and non survivors. This is shown in Figure 4.2. Here we can clearly see a distinction between the distributions of the two groups, with a significant p value of 0.005 using a Welch two sample t-test.

4.4.3 Brain-heart crosstalks and network measures

The next step we performed was to consider a model in which all the three newly introduced measures, were present. We first proceeded running the pivoting procedure using ct_{np} as the pivot variable and including the two network measures in the list of candidate set of predictors. The resulting list of selected features is the following: ct_{np}, ω_{ct}, Mi_{ct}, DAI vs SOL, petech, cistern, sex, age, theatre, pupils, hypoxia and sah. The estimated coefficients of the selected model, with $\alpha = 0.5$ and $\lambda = 0.000045$, are shown in Table 4.2. It is important to point out that the significance of the estimated coefficients in the elastic net is embodied in the selection process. As a matter of

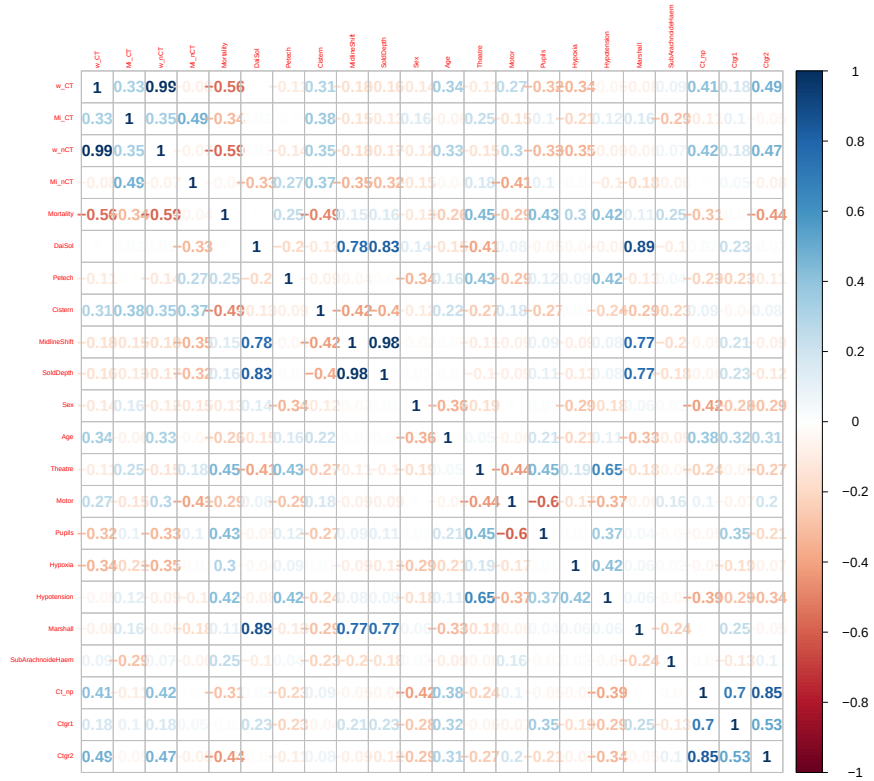

Figure 4.1: Pearson correlation coefficient symmetric matrix for the features considered in the logistic regression model. The matrix includes all the clinical, CT, network measures and outcome. Each element reports the value of the correlation coefficient, in the range (-1,1)

fact, only recently have been proposed procedures to estimate the significance of the coefficients, but only for the Lasso and not for the elasticnet estimation [88]. This will be true for all the tables 4.2, 4.4, 4.5 and for figure 5.6.

In the model the percentage of deviance ratio explained is very high 99%. We performed a robustness check for what concerns the deviance ratio explained with and without the presence of the new measures. The robustness check was verifying the deviance ratio explained, when considering the model with or without the 3 new measures of Ct_{np}, ω_{ct} and ω_{nct}. For several different values of the parameter λ, the model was implemented and consistently showed higher values of the deviance ratio when the 3 new measures were included in the model. A leave one out approach was used to fit the lambda parameter. This model is particularly interesting. It shows the significance of all of the three new measures in predicting mortality, and it also highlights how their contribution is in the same direction (negative for all of them). This therefore seems to confirm the presence of a negative correlation between brain-heart

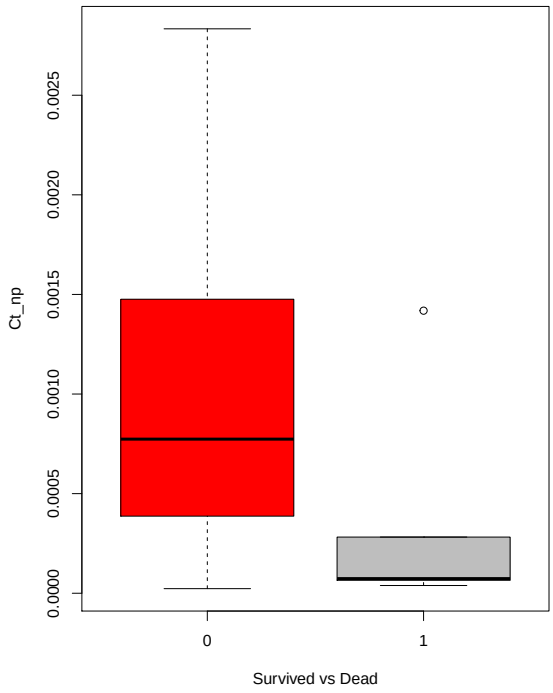

Figure 4.2: Box plot showing mortality versus ct_{np} in patients. As we can appreciate immediately from the figure the survivors have a higher number of crosstalks, with respect to those who did not survive. The survived distribution is shown in red, and the dead ones are shown in grey. The p value resulting from Welch two sample t-test is significant and equal to 0.005

crosstalks and patients mortality outcome.

4.4.4 Brain-heart crosstalks and causality

For the causality analysis as a first step we counted the number of significant HR causing ICP and ICP causing HR events, in the brain-heart crosstalks windows, that is ct_{gr1} and ct_{gr2}. This is reported in Table 4.3. We then normalized them according to the number of observations for each patient, obtaining the two normalized variables $ct_{n_{gr1}}$ and $ct_{n_{gr2}}$. As we can see from Table 4.3 the number of causal events in one or the other direction is similar, and the Welch two sample t test confirms the hypothesis with a non significant p value. We then proceeded with the preliminary statistical analysis and we show the Pearson correlation matrix in Figure 4.1. The two causality measures ct_{ngr1} and the ct_{ngr2} appear very much correlated. However their correlation with the mortality variable is different. This is in line with the results obtained in the

Table 4.2: Coefficients of the logistic regression model for predicting mortality. In the model $\lambda = 0.000045$ and $\alpha = 0.5$. The variables shown here are those selected from the pivoting procedure. Moreover here we show the resulting coefficient of the elastic net (the variables with no significant coefficients show the presence of . in the table)

Variable	Coefficient Value
(Intercept)	-10.7533486
ct_{np}	-2.1587280
ω_{ct}	-4.5054153
Mi_{ct}	-3.8018932
DAI vs SOL	-0.7591782
Petech	3.0374139
Cistern	-3.7099515
Sex	.
Age	.
Theatre	3.4666346
Pupils	3.5871005
Hypoxia	0.5567095
SubArachnoideHaem	4.4925538

previous paper, and the possible physiological intuition behind such behaviour are sketched at [56]. We checked the point biserial correlation coefficients [19] between ct_{ngr1} and mortality which is in fact low, equal to -0.013. On the other hand the biserial correlation coefficient between ct_{ngr2} and mortality is much higher, i.e. -0.44. This is an interesting aspect. Measure ct_{ngr1} are the events in which the causality goes in the direction from ICP to HR, while ct_{ngr2} is the opposite way. So even if there is not a significant difference between their numbers, their relationship with mortality shows a different behaviour. The next step implemented was therefore the pivoting selection to identify the variables to be included in the predictors set (correlation threshold 0.5). Since ct_{ngr1} and ct_{ngr2} are highly correlated we derived two distinct models. In the case of $ct_{n_{gr1}}$ the variables selected were: midline shift, petechial haemorrhage, cistern, sex, age, theatre, motor, hypoxia and subarachnoid haemorrhage. On the other hand in the case of ct_{ngr2} we obtained: DAI vs SOL, petechial haemorrhage, cistern, sex, age, theatre, motor, hypoxia and subarachnoid haemorrhage. Estimated coefficients of the logistic regression models are reported in Table 4.4 and Table 4.5. Both models show a strong similarity with the ct_{np} model. This was expected since the correlation among ct_{np}, ct_{ngr1} and ct_{ngr2} is quite high. From this first analysis a clear causality

during brain-heart crosstalks, between HR and ICP, does not emerge. However the two variables ct_{ngr1} and ct_{ngr2} are both significant in the respective models, suggesting the possibility of further studies of the mechanism underlying the brain-heart crosstalks behaviour.

Table 4.3: Causality information for the paediatric cohort. In the table we can see the number of brain-heart crosstalks going in the direction ICP causes HR and the opposite case.

Patient	ICP causes HR	HR causes ICP
1	6	8
2	3	7
3	22	10
4	14	8
5	1	0
6	12	8
7	7	9
8	13	13
9	21	15
10	39	27
11	9	3
12	56	57
13	11	12
15	3	3
16	19	21
17	1	1
18	0	0
19	0	1
20	11	10
21	58	93
22	7	4
23	1	1
24	10	5
25	0	0
26	10	1

Table 4.4: Coefficient of the logistic regression model, where the causality measure $ct_{n_{gr1}}$ is taken into consideration and mortality is predicted. In this model $\lambda = 0.01146018$,$\alpha = 0.5$, dev.ratio= 76%. The variables shown here are those selected from the pivoting procedure. Moreover here we show the resulting coefficient of the elastic net (the variables with no significant coefficients show the presence of . in the table)

Variable	Coefficient Value
(Intercept)	-3.5801914
ct_{ngr1}	1.1542801
MidlineShift	0.3414623
Petech	1.0147905
Cistern	-1.6085804
Sex	.
Age	-1.4228719
Theatre	1.0934077
Motor	-0.4671977
Hypoxia	1.2594210
SubArachnoideHaem	0.5582012

4.5 Summary

Prognostic models have been widely and mainly developed for adult TBI cohorts [35]. For what concerns TBI paediatric cohorts not so many examples exist in the literature. Clinical decision rules were developed for the need of having a CT scan or not, at the time of admission of paediatric patients. This was mainly due to the high risks of exposing children to unnecessary radiations to perform such investigations. However, for severe cases, CT scans are performed also on paediatrics regardless of this consideration. Clinical paediatric rules recently developed include: the Paediatric Emergency Care Applied Research Networks (PECARN), Canadian Assessment of Tomography for Childhood Head Injury (CATCH), and the Children's Head Injury Algorithm for the Prediction of Important Clinical Events (CHALICE) [47]. Less, however, has been developed in term of prognostic models predicting long/medium term outcome or mortality [34]. In our analysis we introduced multiple novelties. The first and most important one is the introduction of a new variable, expressing events of interaction between brain and heart, that we term brain-heart crosstalks. Even if neurocardiology and the interaction between brain and heart have been under investigation in the last few years, not much has been done on the relation between brain-heart and TBI. As

Table 4.5: Coefficient of the logistic regression model, where the causality $ct_{n_{gr2}}$ is taken into consideration and mortality is predicted. In this model $\lambda = 0.02412259$ and $\alpha = 0.5$. The variables shown here are the ones selected from the pivoting procedure. Moreover here we show the resulting coefficient of the elastic net (the variables with no significant coefficients show the presence of . in the table)

Variable	Coefficient Value
(Intercept)	-2.58662744
ct_{ngr2}	-1.58266238
DAI vs SOL	.
Petech	0.03136925
Cistern	-1.09886958
Sex	-0.38616545
Age	-0.24518131
Theatre	0.63984033
Motor	-0.31405632
Hypoxia	0.38387678
SubArachnoideHaem	0.52975342

a further novelty, we related this new cardiocerebral measure to mortality, together with the network measures derived. We believe that our findings open the possibility for looking deeper into the correlation between brain-cardiovascular parameters and mortality, in paediatric TBI patients. Indeed our results suggest a positive correlation between survival probability and the number of brain-heart crosstalks. This is true also for the two network variables added to the model. To the best of our knowledge this is the first time that network measures are used in such context. In addition to this we analysed possible causality interaction between ICP and HR during crosstalks events. Such analysis was developed using the Granger Causality approach and the measures of causality derived were also included in the set of predictors. Results do not show a clear direction for the causality between the two observed variables. A limitation of our study is the small dataset sample size, and results would need to be validated in a bigger sample, before entering clinical practice. This in particular could also affect the presence of no direction in the causality approach that we investigated. Small sample sizes studies are, however, common in paediatric TBI research, due to the invasive procedure required for ICP monitoring. However, similar small sample sizes, have being shown to be significant and important towards making progress in this research area as [151], [78] and [150] show. We are currently investigating how

cross talk events relate to other physiological variables (eg autonomic nervous activity), or clinical variables, (treatments patient receives, respiratory suctioning, presence of intracranial hypertension (high ICP) or impaired autoregulation) and how this could be transposed in the adults domain.

4.6 Related publications

Dimitri, Giovanna Maria et al. "Brain-Heart crosstalks: a new variable for outcome prediction in paediatric Traumatic Brain Injury patients", under revision for resubmission at BMC Medical Research and Methodology, 2019. The work has been presented at the Brain Physics seminar, June 2018.

Chapter 5

Brain-heart crosstalks, network multiplex measures and mortality in adult traumatic brain injury patients

5.1 Introduction

As briefly introduced in Chapter 4 it has been widely shown in research, and therefore clinical practice, how adults and paediatric TBI patients need to be treated differently. The famous article in the field, by Giza et al. [60], clearly gives this message directly in the title stating: *"Paediatric traumatic brain injury: not just little adults"*. The main goal of the article is, in fact, to establish different clinical guidelines between adults and paediatric patients [60]. Indeed there is a consensus on the fact that younger brains may rearrange and be able to behave differently when they undergo TBI events. For example the authors point out the effectiveness of therapeutic interventions, such as decompressive craniectomy or hypothermia in younger brains as compared to adult brains. Such behaviour is of course due mainly to physiological and anatomical differences. As extensively explained in [49] brain physics and dynamics concerning adults cannot be automatically transferred to paediatric patients and the contrary, and a stratification inside paediatric cohorts would also be needed. Newborn, infants, and children (between 8 and 16 years old) differ greatly anatomically, and this is a key aspect that needs to be taken into account when analysing data. This further emphasizes how different adults and children could be.
Based on these considerations, we extended our brain-heart crosstalks and network

modelling also to an adult TBI cohort. To the best of our knowledge, as for paediatric patients, the brain-heart crosstalks was a complete new variable for mortality prediction. The analysis proceeded in analogy, with what we did with the paediatric cohort in Chapters 3-4. First we computed some preliminary statistics on the dataset of predictors. We then proceeded with the identification of the number of brain-heart crosstalks per individual, applying our detection algorithm. Subsequently we modelled the system, using the multiplex approach as in Chapter 3, and we derived the two measures of average edge overlap and mutual information between ICP and HR layers. We then concluded adding the three newly derived variables (i.e. brain-heart crosstalk, average edge overlap and mutual information) to the predictors dataset, and we applied an elastic net logistic regression model for the prediction of mortality probability. This allowed us to understand the impact of the new variables towards mortality prediction also in the adult case.

5.2 The dataset

The data used for the present study is a subset cohort from the CENTER-TBI project. CENTER-TBI is a consortium founded in 2011 with the goal of improving classification and treatment of TBI patients [95]. The project started with the idea of integrating, in the TBI patients management, a whole source of different information that could help towards the application of new discoveries and techniques, in a precision medicine perspective. The study was geographically spread across 22 countries (Europe and Israel) and is composed by a collection of monitoring, imaging, clinical and demographic data. Overall the data came from more than 5400 patients admitted to hospitals with a TBI diagnosis [95]. The project represents a unique longitudinal study. Later temporal information, regarding patients cognitive scores, will also be added to the dataset, to effectively follow the course of the patients once dismissed from the hospital (up to 24 months) [95]. Patients initial recruitment time was originally made in the period between October and December 2014 [95]. For the present study we were given access to a subset cohort of 226 patients. For each patient we had the availability of a similar set of features (monitored, clinical and demographics) as the ones used in the experiments with the paediatric cohort. For the monitoring features, we had available heart rate together with the ICP (mmHg) signal, both sampled at a frequency of 100 Hz. In addition to this we had a dataset where CT, clinical and outcome information

measures were added. The variables used for the analysis are the following:

- **Demographics**: similarly to the paediatric study we had the availability of the demographic variables such as age and sex
- **TBI scores**: together with mortality a few more TBI scores were available for the present cohort. In particular:
  - Injury Severity Score (ISS), i.e. a score for assessing the severity of the TBI injury as defined in [36]
  - Best total Glasgow Coma Score (GCS). This score was first proposed in 1974 and it has become a standard in clinical practice. The total score includes partial assessments and is composed by subscores assessing three different areas i.e. eyes movements, motor and cognitive skills [141].
  - Abbreviated Injury Score (AIS): this is another widely spread clinical practice injury score, that was introduced since 1971 [114]. The subscores assess the following components of injuries: brain, face, head and neck, thorax, abdomen and pelvis, upper and lower extremities, cervical, thoracic and lumbar spine.
  - CT classification scores: the dataset included scores for assessing the trauma given imaging information (similarly to the paediatric case). In particular there was the availability of the following: Fisher, Rotterdam, Marshall and Helsinki CT scores.
- **Lab variables**: unlike the paediatric dataset, for the adult cohort we also had available lab information. These data were collected through a blood sample, at the time of hospitalization. The data available were the following: sodium, potassium, glucose, haemoglobin, white blood cell counts, lymphocytes, neutrophils, platelet, CRP (C Reactive Protein) and albumin. These values have received an increasing attention in TBI research nowadays. It has been shown, for example, a strong link between glycemia and outcome in patients, as studies like [150] show. This was also in the original IMPACT score paper [137].
- **CT Variables**: as for the paediatric case CT variables were available for the adult cohort. In particular, the presence of a DAI vs SOL lesion, subarachnoid haemorrhage, midline shift, contusion, basal cistern absent compressed and extradural haemorrhage.

- **Emergency Department data (ED)**: emergency data information were available for adults. In particular: arrival PH, arrival lactate, hypoxia, hypothension, hypothermia, seizures, cardiac arrest, arrival arterial CO_2 (mmHg). Moreover the pupil response variable was available, similarly to the paediatric cohort.

- **Theatre variable**: the theatre variable was not originally present in the predictors set. However we were able to derive it from the following four variables: time $TimeInj$ and date $DateInj$ of injury together with time $TimeInsICP$ and date $DateInsICP$ of insertion of the ICP device. The theatre variable is in fact computable through the formula: ($TimeInsICP$ + $DateInsICP$) - ($TimeInj$+ $DateInj$)

Besides these variables we also considered brain-heart crosstalks and the network measures, of average edge overlap and mutual information, derived as in Chapter 3. Among the original patients from the CENTER-TBI cohort, only 226 were selected and screened. These corresponded to non external ventricular drains (EVD) patients with good quality of data and outcome available at the time of the analysis. ICP and HR waveforms were processed with ICM+ software [132] sampled at 100 Hz. Demographic data as per version 2.0 of CENTER-TBI were retrieved.

5.2.1 Comparison with the paediatric cohort

Only some of the adult variables were available for the paediatric patients. In Table 5.1 we describe those variables which were used in both studies. We can see that almost all the variables are present in the two cases, except for the following:

- **Petechial haemorrhage**: this is available for the paediatric cohort. In the adult case, we have the contusion variable, which brings similar clinical information and which we will use with adults.

- **Cistern**: with paediatrics the information regarding the basal cistern concerns its width. With adults, instead, we have a binary variable, which describes the presence of a basal cistern compressed or not.

- **Midline Shift**: for paediatrics is the quantification of shift of the midline structure. In the adult case is instead a binary variable, expressing the presence or not of a midline shift in the CT scan.

- **Theatre**: was not directly available in the adult case, but was derived as described in Section 5.2. The unit of measurement is a fraction of a day.

Table 5.1: Table reporting the corresponding variables in the adult and paediatric cohorts

Paediatrics Variable	Adult Variable	Variable Type
DAI vs SOL	CT Lesion DAI	Binary
Petech	CT contusion	Paediatric:0,1;Adults:0,1,2
Cistern	CT BasalCisterns Absent Compressed	Width paediatric, binary adults
Midline Shift	CT MidlineShift	Width paediatric, binary adults
Soldepth	Absent	(Width and depth space occupying lesion)
Sah	CT Subarachnoid Haem	(1=yes,0=no)
Sex	Sex	Present in both
Theatre	Derived	Present in both
Pupil	Pupil Response IMPACT	Pupil reactivity
Hypoxia	ED Hypoxia	Prehospital low oxygen
Hypotension	ED Hypotension	Prehospital low blood pressure
Age	Age	Present in both

5.3 Methods

The pipeline of the analysis for the adults cohort was similar to the paediatrics. We first performed some preliminary statistical analysis of the data. Subsequently we applied our sliding window peaks detection algorithm, to obtain the number of brain-heart crosstalks per patient. Afterwards we modelled the system using a multiplex approach. In this way we could obtain the two network measures: average edge overlap and mutual information to use in the set of mortality predictors, together with the brain-heart crosstalk measure.

5.4 Results

5.4.1 Statistical analysis

In Table 5.2 and Table 5.3 we present summary statistics for the variables described in Section 5.2. In the two tables, the minimum, maximum and mean values of the various features are computed.

Table 5.2: Descriptive statistics for the adult cohort dataset, except for the TBI scores, which are in Table 5.3

Statistic	Mean	St. Dev.	Min	Max
Mortality	0.221	0.416	0	1
Age	46.624	18.387	16	85
Pupil	0.584	0.851	0	2
ED Arrival pH	4.642	3.545	0	8
ED Arrival Lactate	2.612	6.403	0	57
ED Arrival Art CO2 (mmhg)	25.816	21.421	0	76
Hypoxia	0.204	0.536	0	2
Hypotension	0.133	0.411	0	2
Hypothermia	0.124	0.380	0	2
ED Seizures	0.142	0.497	0	2
ED CardArr	0.018	0.132	0	1
DL Sodium_1	121.082	47.615	0	151
DL Potassiumm _1	3.235	1.511	0.000	7.070
DL Glucose_1	6.521	4.502	0	22
DL Hemoglobin_1	11.535	4.366	0.000	17.900
DL White Blood Cell _1	11.503	7.671	0.000	34.140
DL Lymphocytes_1	7.422	10.500	0	53
DL Neutrophils_1	44.809	39.832	0	95
DL Platelet_5L_1	180.531	93.696	0	440
DL CRP (mgL)_1	3.396	15.525	0	218
DL Albuming _1	13.403	17.702	0	50
CTIC LesionDAI_1	0.177	0.383	0	1
CT AcuteSubdurHema_1	0.708	0.768	0	2
CT MidlineShift_1	0.403	0.492	0	1
CT SubarachnoidHem_1	1.115	1.137	0	3
CT Contusion_1	0.695	0.653	0	2
CT DeprSkullFract_1	0.199	0.533	0	2
CT BasalCisternsAbsentCompressed_1	0.204	0.404	0	1
CT ExtraduralHema_1	0.177	0.503	0	2
DecompressiveCran	0.235	0.425	0	1
ct_{np}	0.160	0.183	0.003	1.000
Theatre	0.998	0.694	0.062	3.522

Table 5.3: Descriptive statistics for the TBI scores of the adult cohort

Statistic	Mean	St. Dev.	Min	Max
BEST_GCSTot	7.872	4.220	0	15
Total ISS	35.566	14.462	1	75
BrainInjury AIS	4.810	0.545	1	6
Face AIS	1.027	1.644	0	5
Head Neck AIS	2.438	2.249	0	5
Thorax Chest AIS	1.350	1.823	0	5
Abdomen Pelvic Contents AIS	0.345	1.090	0	5
Pelvic Girdle AIS	0.199	0.811	0	5
Upper Extremities AIS	0.367	0.972	0	4
Lower Extremities AIS	0.376	1.026	0	5
Cervical Spine AIS	0.279	0.965	0	5
Thoracic Spine AIS	0.274	0.945	0	5
Lumbar Spine AIS	0.137	0.662	0	4
Fisher Classification_1	1.965	1.336	0	4
Rotterdam CT Score_1	2.850	1.787	0	6
Marshall CT Classification_1	3.137	2.281	0	6
Helsinki CT Score_1	3.544	3.445	−3	14

As a further visual inspection we present the correlation matrix of the predictor variables and of the TBI scores, as shown in Figure 5.1.

At a first glance of the correlation plot, we can see some *"squared"* patterns of the more highly correlated variables in the matrix. Starting from the left upper corner of the correlation matrix, we can see that the *"squared"* patterns mainly correspond to similar features: AIS score, lab blood samples analysis, CT features and network measures. Such subgroups appear to be naturally correlated although other correlations, even if milder, appear in the rest of the plot.

5.4.2 Brain-heart crosstalks in adults

Following the work pipeline adopted for paediatrics, the next step consisted in the computation of the number of brain-heart crosstalks events. This was performed using the algorithm, described in Chapter 3. Also in this cohort, the number of observations varied across patients, due to the different time length of their hospitalization. Therefore we normalized the absolute number of brain-heart crosstalks per patient, by the number of observations. By analogy with the paediatric group in Chapter 3, we called such variable ct_{np}. The distribution of ct_{np} is illustrated in Figure 5.2. The table with the complete results of the number of brain-heart crosstalks per patient is presented in Appendix 1, Table 7.1. As in Chapter 4 we evaluated the relationship between brain-heart crosstalks and mortality. The point biserial correlation coefficient between the two variables is -0.13, showing two interesting points. The correlation is less pronounced than for the for the paediatrics, where it was -0.30, although is still exhibiting the same negative sign. In Figure 5.3 we can see the boxplot of the mortality with respect to the ct_{np} variable, where this trend is confirmed. The Welch Two Sample t-test performed in this case, confirmed the difference between the two distribution, with a significant p value of 0.03.

5.4.3 Multilayer network modelling

Subsequently we proceeded with modelling the ICP-HR system using a multiplex network approach. The steps followed were exactly the same as for the paediatrics cohort. From time series to horizontal visibility graph, from single graph to multiplex to obtain the two network measures average edge overlap and mutual information. Then we extracted 10 time windows in which a brain-heart crosstalk was identified for each

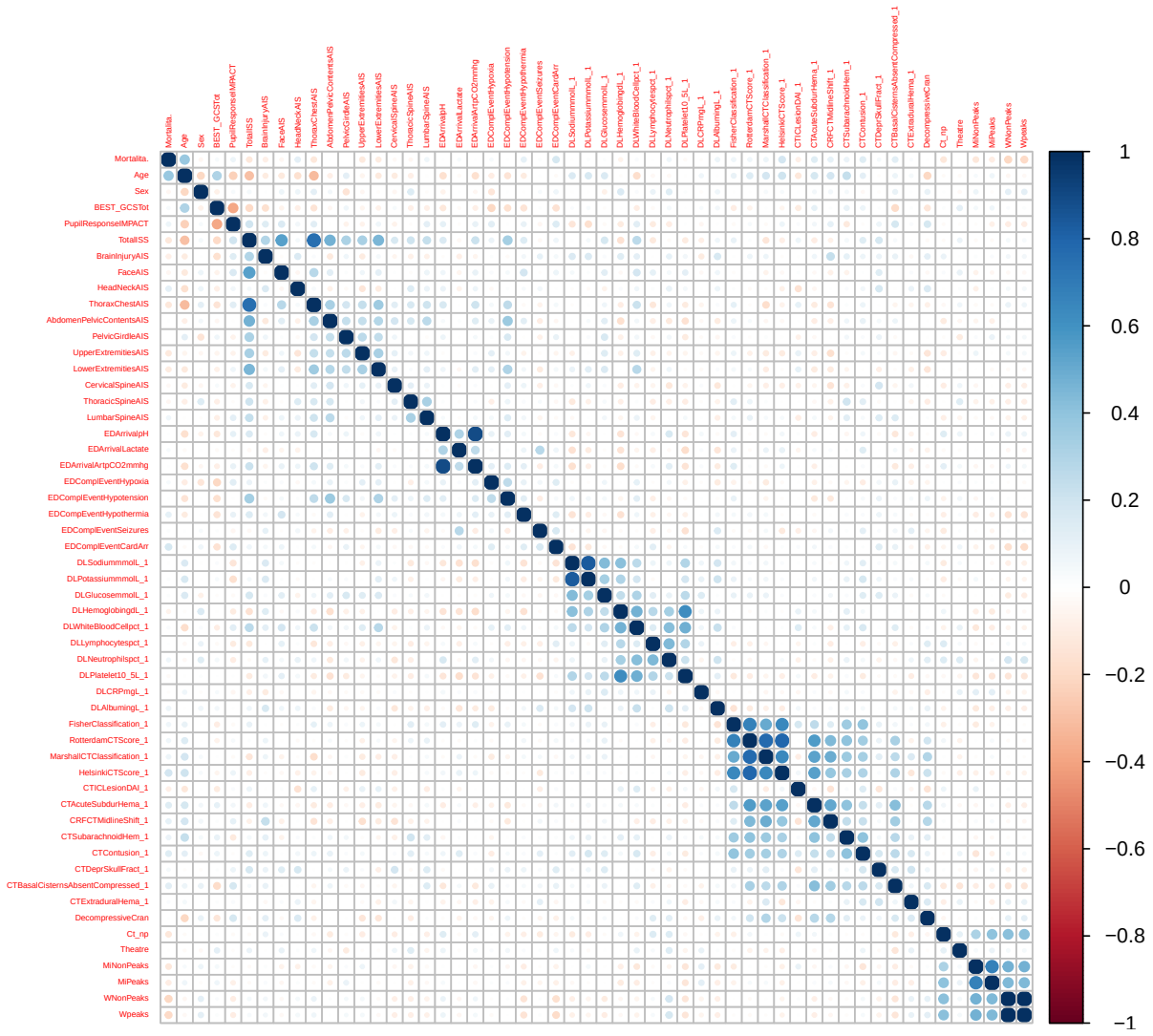

Figure 5.1: Plot showing the Pearson correlation coefficient between the variables used in our adult study cohort. The matrix is symmetric, and we included here all the clinical, lab, as well as outcome variables described in the previous section.

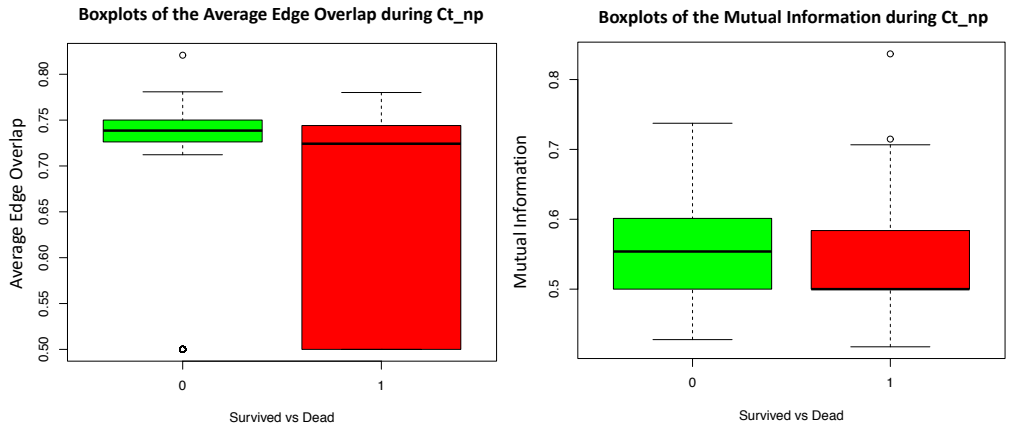

Figure 5.2: Distribution of the normalized brain-heart crosstalks measure ct_{np} for the adult cohort. The distribution shows how a large number of patients, have a low number of crosstalks. (Ct_np=ct_{np})

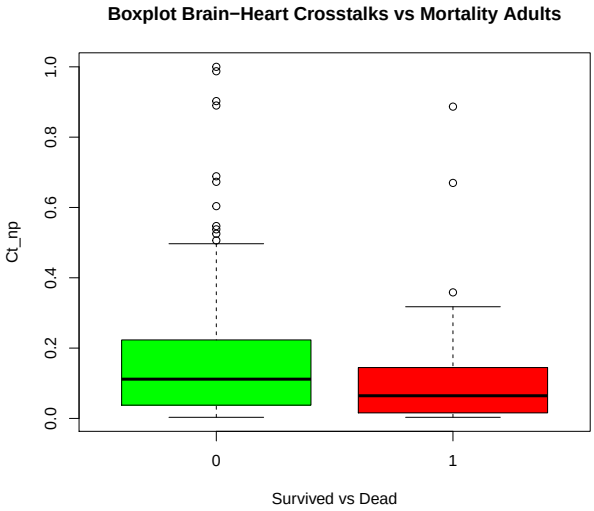

Figure 5.3: Boxplot showing the distribution of crosstalks with respect to the survived (green) and dead (red) patients in the adults cohort. It shows a higher number of crosstalks for the surviving patients, with respect to those who died. The Welch Two sample t-test on these distribution show a significant p-value of 0.03

patient, and 10 in which it was not.
Hence, for each of those, we computed the values of ω and of the Mi, and considered the mean of such values per patient. We present these results in Table 7.2 of the Appendix 2. To those patients who had less than 10 brain-heart crosstalks, we assigned 0.5 as the value of ω and Mi. We report in Table 5.4 the descriptive statistics for the network measures .

Table 5.4: Descriptive statistics of the network measures for adults

Statistic	Mean	St. Dev.	Min	Max
Mi_{nct}	0.562	0.071	0.339	0.897
Mi_{ct}	0.555	0.070	0.417	0.837
ω_{nct}	0.692	0.101	0.500	0.823
ω_{ct}	0.691	0.101	0.500	0.821

The same type of behaviour observed in the case of paediatrics cohort is also seen with adults. In particular the average edge overlap does not seem to change between the crosstalks and non crosstalks case, while, on the other hand, the mutual information is higher with crosstalks than without crosstalks. Performing a paired t test between the two samples, the result is far from being significant in the case of the average edge overlap. On the other hand, when considering mutual information, the t test shows a p value of 0.06, with a confidence interval of (-0.01453, 0.00036) much closer to the significance threshold of 0.05. In Figure 5.4 we present the boxplot for the two network measures with respect to patient mortality.

5.5 Outcome mortality model

In analogy with the paediatric case, we built an outcome predictor model based on the features described in Section 5.2. As well as for the paediatrics, the logistic regression, was based on the elastic net model. As a first step we considered the whole dataset, with no segmentation according to age. The estimated model showed a low deviance ratio (approximately 20%), meaning that the model is not a good fit to predict in a reliable way patients outcome. Therefore, as a second step, we decided to split the dataset in four subpopulations according to age. The age range is included between 16 and 85

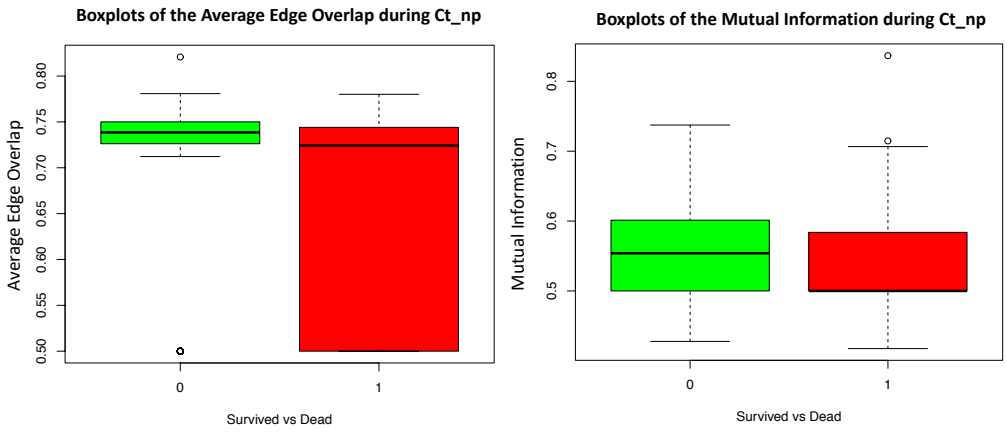

Figure 5.4: Boxplot showing the relationship between mortality and network measures, of average edge overlap and mutual information, in the case of the survived (green) and dead (red) patients. Welch two sample t-test is not significant for the average edge overlap, but is close to the significant threshold for the mutual information ($p = 0.06$)

years old and the distribution is shown in Figure 5.5. We decided to do that, rather than pooling all the subjects in a single dataset to keep age homogeneity in the analysis.

Dividing it into four subpopulations, we obtained the sets as described in Table 5.5.

Table 5.5: Demographics and composition of the adults cohorts subpopulations

Age range	Number of patients
16-29	56
30-49	63
50-64	61
65-85	45

Then we implemented the logistic regression model for each subpopulation. We present the results using the pivoting feature selection as described in Chapter 4, with the ct_{np} variable considered as pivot and with a correlation threshold of 0.5. The α value of the elastic net model was fixed to 0.5 also in this case. In Figure 5.6 we present the results of the selected model for each of the four subpopulations.

The findings in Figure 5.6 are interesting. The best fitting model appears to be for the population range aged 16-29. Indeed the deviance ratio is almost 1 which means that the predictors included in the model explain with a very high reliability the

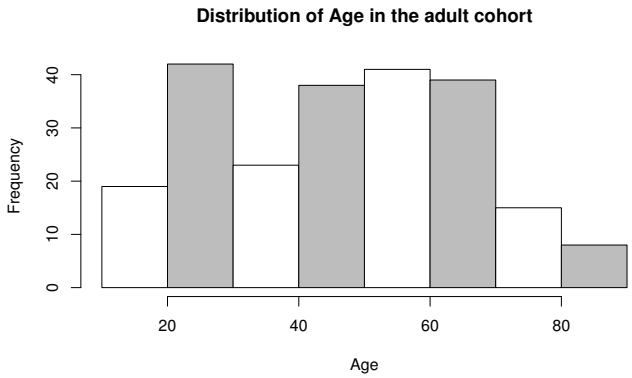

Figure 5.5: Distribution of age in the adult cohort.

mortality outcome. Interestingly the negative relationship between mortality and ct_{np} is confirmed, as well as the one between mortality and the mutual information during crosstalks. In so far as the other populations are concerned, the best fit of the model appears to be for the age range 65-85. Here the deviance ratio is also very high, although not as for the age range 16-29. Finally for the two intermediate populations of 30-49 and 50-64 the fitting of the model is much lower (respectively 48% and 63% deviance ratio), which suggests that mortality may not be well predicted by the available predictors. Future research should be devoted to improve the understanding of the behaviour of the coefficients, across the various age subpopulations. As a further discussion over this difference in Table 5.6 we can see the Pearson Correlation coefficients between mortality and number of brain-heart crosstalks per patients, and per age category.

Table 5.6: Point biserial correlation coefficients between mortality, ct_{np}, and network measures

Age Group	ct_{np}	ω	Mi
16-29	-0.114344	-0.1648246	-0.3340289
30-49	-0.03290012	-0.3275235	-0.06849099
50-64	-0.1627141	-0.1377024	-0.1437248
65-85	-0.2293428	-0.1634196	-0.02666362

5.6 Summary

In this chapter we presented an extension of the work of Chapter 4. The computational pipeline implemented for detecting brain-heart crosstalks, and then relating them to

16-29

Lambda	Dev.ratio
0.0002943866	99%

Variable	Selected Coefficients
Intercept	-12.24
Ct_np	-0.07
Age	0.64
Sex	.
Pupils	0.16
EdArtpCO2	0.71
Lactate	1.51
Haemoglo	-1.26
Neutroph	-0.45
CRP	1.6
Albumin	3.62
CT_DAI	-0.62
MidShift	-0.32
Sah	3.40
Contusion	-60
DeprSkull	-0.22
BasalCistern	-0.11
ExDurHaem	-0.60
MiPeaks	-4.06

30-49

Lambda	Dev.ratio
0.03768093	48%

Variable	Selected Coefficients
Intercept	-2.58
Ct_np	.
Age	.
Sex	0.07
Pupils	0.16
PH	0.67
Lactate	0.05
Haemoglo	.
Neutroph	.
CRP	0.06
Albumin	.
CT_DAI	.
MidShift	0.04
Sah	.
Contusion	0.08
DeprSkull	0.7299
BasalCistern	.
ExDurHaem	-0.30
Mi_Ct	.
Theatre	0.49
Omega_Ct	-0.44
Glucose	.
WhiteBldCel	.
Lymph	.
Platelet	.

50-64

Lambda	Dev.ratio
0.001611113	63%

Variable	Selected Coefficients
Intercept	-3.97
Ct_np	-0.07
Age	-0.35
Sex	0.73
Pupils	0.54
EdArtpCO2	-0.72
Lactate	-3.03
Sodium	-1.11
Glucose	1.32
Platelet	0.97
WhiteBldCel	-0.07
Lymph	-0.83
Neutroph	-0.48
CRP	-0.03
Albumin	2.35
CT_DAI	-3.5
MidShift	-1.007
Sah	-1.95
Contusion	3.22
DeprSkull	-2.83
BasalCistern	-0.5
ExDurHaem	-1.9
Theatre	0.01
Wpeaks	0.48

65-85

Lambda	Dev.ratio
0.004050073	80%

Variable	Selected Coefficients
Intercept	-0.16
Ct_np	-0.80
Age	2.34
Sex	.
Pupils	1.36
EdArtpCO2	-2.39
Lactate	2.58
Haemoglo	-1.59
Glucose	-1.31
WhiteBldCel	-0.33
Lymph	3.35
Albumin	0.60
CT_DAI	1.41
MidShift	-1.04
Sah	-1.46
Contusion	-1.24
DeprSkull	0.83
BasalCistern	-0.03
ExDurHaem	0.85
Theatre	-0.60
Wpeaks	.

Figure 5.6: Figure showing the lambda, null deviance and coefficients selected by the elastic net model. At the top of the various tables we can see the age ranges they refer to. λ and deviance explained by the model are also specified at the top of each table. The variables selected are associated to their respective coefficients, and the dot in the coefficient tables would mean that the variable has not been selected for the model.

patients mortality, was extended to an adult cohort.
Despite the fact that adults and paediatric cohorts cannot be completely compared, due to the physiological differences discussed earlier in the section, it is however worth noticing some interesting parallels. Similarly to paediatric cohorts, scores have been developed in the literature to assess the severity of the patients clinical conditions and therefore the need of assessing patients clinical management. Example is the IMPACT score [137] where admission characteristics such as: age, motor score, pupils, hypoxia, hypotension, CT variables,glucose and haemoglobin are used to assess the patients condition at the time of hospitalization. Here the CT information are directly considered in the model differently from the paediatric case where, as discussed in Chapter 5, mainly the interest is in understanding if the CT scan needs to be performed or not. In our model, we introduced the new variable of brain-heart crosstalks, and studied it with respect to mortality outcome. The relationship of brain-heart crosstalks with respect to mortality is confirmed. The higher the number of crosstalks, the lower the probability of mortality.
We also added network measures, similarly to the paediatrics case. Also in the adult case, such metrics show similar behaviour with respect to mortality outcome. As for the children case, the brain-heart crosstalks detection analysis and the application of multiplex networks analysis represent a novelty in the field, to the best of our knowledge.
We presented therefore the outcome prediction modelling, dividing the cohort into age range subsets. This also shows an interesting relationship between brain-heart crosstalks and mortality.
The same behaviour is confirmed also when considering the network measures, related to mortality, and variations can be seen between different age ranges.

5.7 Related publications

Part of the work of this chapter has been accepted for poster presentation at the 2019 International Symposium on Intracranial pressure and Neuromonitoring, September 2019, KU Leuven (Belgium).

Chapter 6

NetRank: a multiplex network approach for profiling neurocognitive ageing

6.1 Introduction

As life expectancy increases, there is an increasing interest in understanding how the world population can be neurocognitively healthier [106] [127]. The interaction between lifestyle, demographics and clinical measure is considered crucial in undercovering the mechanisms underlying a healthy neurocognitive ageing process. Many theories have been formulated in previous studies, through experimental settings, which are looking for validation in bigger and different cohorts [127]. A key concept in the field, which has become quite popular in neuroscience in the last few years, is so called brain plasticity [81]. This refers to the capability of the brain to rewire and readjust its shape and functionalities, and studies have shown it to be a process which appears to happen in pathological events (such as strokes [77]) as well as in ageing [127].
A clear trend that can be seen in the ageing process, is the loss of cognitive functions such as learning, memory and executives. These are in fact subjected to a natural decline with age, as described in [24]. Such functions rely mainly on the medial temporal lobe and prefrontal cortex, that have been shown to be the ones mostly subjected to a loss in grey matter volumes, as a result of ageing. In addition to this, evidence shows how also other cognitive functions, related to such areas of the brain, present declining functionalities with ageing. In [63] authors focus on showing how cognitive ageing

is not only related to the loss of brain volume, but also to the adaptation of such loss, especially in the cortical areas. The authors therefore conclude that functional plasticity is responsible for the evolution of cognitive ageing [63].
A further interesting study, in this sense, was the one conducted by [27]. The research focuses on the difference in ageing between individuals, using the Positron Emission Tomography (PET) as an instrument for conducting the analysis. Researches conducted using PET and fMRI show, in fact, how PreFrontal Cortex (PFC) activity is usually less asymmetric in older people with respect to the younger ones. This phenomenon is known as Hemispheric Asymmetry Reduction in Old Adults, also known as HAROLD. As a consequence, the research question concerning loss of cognitive function, becomes mainly understanding the meaning of such a change. *Does such loss imply a compensation mechanism happening in older brains, or is it a reflection of a difficulty that older brains have in developing specialized neural mechanisms?* In [27] the authors compare PFC activity in younger adults and in high-low performing older adults through studies of recall and source memory. While only right PFC is activated in younger adults, in high performing older adults, both lateral regions of the PFC were activated [27]. The conclusion drawn by the authors, in [27], was therefore that in low performing older adults the activated network is similar to the one of the young adults, but the efficiency is lower. The use of both PFC lateral sides in high performing older adults was a counteractive action to the ageing natural decline process, that takes place in older brains [27].
This interesting research highlights exactly the mechanisms underlying the plasticity process that we were mentioning earlier in the section. As a further example of studies in the field, we can look at the research conducted by [40], where the goal is to understand the relationship between cognitive abilities and structural and functional changes in the brain.
A common feature emerging from neuroimaging studies is the identification of a reduction in the occipital activity, together with an increased activity in the frontal part. This represents a shift mechanism called PASA, which is identifiable in the posterior-anterior brain rewiring network, and that usually has been considered as a sort of functional compensation of older brains [40]. In [40] the study concentrated in testing young and older participants, when performing episodic retrieval and visual perceptual tasks. In this way the authors were able to detect age-related changes in brain activities, that were in common among individuals when performing the same tasks [40]. The conclusions drawn by the authors [40] was that the PASA pattern was found as present in the various

tasks performed. Another important finding was the fact that an increase in the frontal activity was positively correlated with performance, but negatively correlated with the age-related occipital decrease [40]. As a consequence of the PASA pattern identified, the effect of ageing was the one considered responsible for the reduction in deactivation of the posterior midline cortex, but at the same time also responsible in the case of the deactivations in the medial frontal cortex [40]. An aspect less investigated in the cognitive neuroscience field, so far, has been the role of brain flexibility, in the whole lifespan. The investigation of this aspect, could potentially be extremely helpful when trying to undercover what is the driver of a succesfull cognitive ageing process [127]. In the last few years a plethora of consortia have been created, to construct, and make publicly available for research, comprehensive and multimodal datasets, with the goal of studying several types of neurocognitive and neuropathological processes. An example of this is the Human Connectome Project (HCP), where data gathered using different neuroimaging modalities (EEG, MEG, fMRI, dMRI, physiological data, etc.) are combined with demographics, cognitive and lifestyle features [146]. The database is composed by different cohorts (healthy, young and older adults), collected by a wide range of research and medical centres. Another example is the UK Biobank initiative [138]. The project was created with the aim of preventing and better understanding a large number of diseases such as cancer, cardiovascular and other world wide diffused pathologies as dementia. The data was collected from 500.000 volunteers. It represents a unique database and, also in this case, imaging, lifestyle and cognitive information was collected in a unique effort of creating a resource for studies in the field [138]. Other interesting projects, born with the same intent of unifying imaging, lifestyle and demographics information, were started with the aim of studying neurodegenerative diseases. Among those the most notable can be identified in: Parkinson Progression Marker Initiative (PPMI) [98] and the Alzheimer Disease's Neuroimaging Initiative (ADNI) [104]. Both projects include imaging, genetic, lifestyle and cognitive information of patients with Parkinson and Alzheimer disease respectively. The intent was to provide the research community with open, public available, information on those wide spread neurodegenerative diseases. This would allow the development of multiomic and multi-modal models for these nowadays most common ageing pathologies.

6.2 Problem definition

Neurocognitive ageing is a process depending upon several factors. Its modelling needs, therefore, to be considered as a combination of information gathered from structural and functional brain features, as well as lifestyle and demographics factors. There is therefore the need of applying methodologies able to integrate different types of data, in a multi-modal fashion,. The main research questions driving our work and analysis were the following:

How do functional and structural features of the brain interact? What mostly predicts the outcome of the cognitive scores (i.e. what is mostly important to understand and predict the cognitive performance of an individual)?

If the functional features are, per se, not enough to describe a healthy neurocognitive ageing process, neither are the structural ones. A rich dataset, such as Cam-CAN, where structural, functional, cognitive and lifestyle features are jointly available, is therefore ideal to try to answer the above research questions. We will thoroughly describe the Cam-CAN project and the subset of the dataset we used in Section 6.3. To integrate the different types of data available and merge them in a unique framework, we used a multilayer network modelling. Such architecture can in fact satisfy the need of integration, without mining the interpretability and readability of the results so obtained. More specifically we proposed a multiplex network approach, in which the cross-modality integration and the study of common latent features, characterizing neurocognitive ageing, can be merged. As described in Chapter 2, a multiplex graph is a special type of multilayer network, with the property of having the same set of nodes across different layers, and having the interconnection between only the same corresponding nodes across layers.

6.3 The dataset

The Cam-CAN dataset is an epidemiological study structured in three main stages. In a preliminary stage, around 10.000 letters were sent through the GP as an invitation to participate to the study. After this preliminary step 3000 participants were selected to join the first stage [140]. This was composed by a home questionnaire where the participants responded to lifestyle and a core cognitive assessment.The second stage consisted in the subselection of 700 participants, who were identified considering only

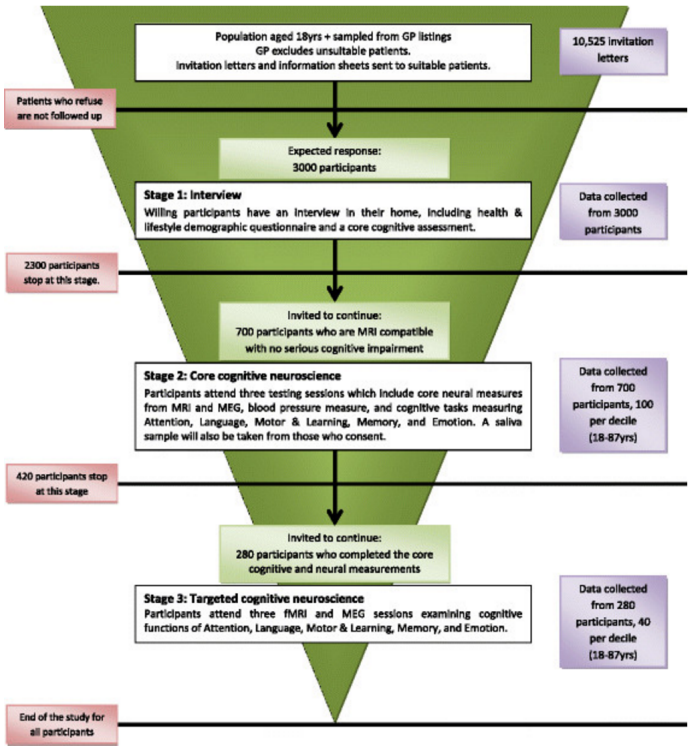

Figure 6.1: Figure representing the Cam-CAN pipeline and the three stages of the recruitment and data analysis process. As we can see invitation letters were sent through Cambridge GP to more than 10525 people. After this preliminary step a cohort of 3000 participants was selected to join the first stage of the study, the so called home interview phase. Afterwards stage 2 and 3 followed with 700 and 380 participants each. Such stages were composed by the collection of both MEG, MRI and fMRI images together with epidemiological measurements and cognitive neuroscience tests. The figure has been taken from [140].

those who had no severe core cognitive impairments and were suitable for MRI and MEG experiments. The sample included participants between 18 and 87 years old, and they completed tests for attention, language, motor and learning, memory and emotion tasks. A third stage was then performed in the study. In this one participants attended three fMRI and MEG sessions, where different cognitive functions were examined. The data sample was reduced from 700 to 480 [140] due to constraints on the number of participants that could take part to this stage. Figure 6.1 summarizes the Cam-CAN recruitment and study process.

In our study, we selected a subset of the dataset, coming from the second stage of the Cam-CAN study. We used a subset of 513 participants, considering those individuals having complete observations for one subset of variables relevant for the analysis. The

variables we considered for each individuals can be divided into three main sets:

1 **Brain Measures**:

- **Segregation (70 % threshold)**. This is used as a measure of brain network segregation in functional connectivity, and was investigated and obtained for the Cam-CAN cohort as described in [58]. Is a widely used functional measure in cognitive neuroscience. It has been largely studied in order to identify areas of the brain that are more active, or that tends to remain more separated in the brain, when the subject is performing a task or is in a resting state [136]. The measure was derived in the Cam-CAN cohort using the procedure described in [58].
- Mean volume of total **grey matter** for each participant and Regions of Interest (ROI) grey matter volumes per participant. The T1-MRI weighted images were pre-processed using the Statistical Parametric Mapping (SPM) [52] software and the mean total grey matter volume was obtained for the whole brain. Moreover the brain was parcelled using the Harvard Oxford Atlas (HOA) in 116 regions, and the volume of each area was calculated [140]. Since Region 112 and Region 115 (Left and Right Limbic Parahippocampal-Gyrus) had no measurement for all the patients, we discarded them from the analysis and we used only 114 regions in total.
- Mean volume total **white matter** for each participant. Also in this case the software used for the estimation of white matter volume is the SPM software [52].

2 **Cognitive tests scores**:

- **Benton** total score. This test is also called face recognition for unfamiliar faces, and is used for determining the capability of matching pictures of unfamiliar faces [140] [13].
- **Story recall delayed and immediate** (we will refer to it as St_d and St_i). This test can be made to assess memory performances. It consists in the capability of being able to repeat a story that has been told to the participant of the study. The story telling can happen in a delayed or immediate timing. For details see [140].

- **Ekman Hex**. This test evaluates the capability of recognising emotional faces, and we considered four categories of emotions: anger, fear, disappointing and surprise [140]. We considered the total number of correctly classified faces, regardless to the category to which they belonged to.
- **Cattell total score** obtained by each participant. The Cattell test is a pen-and-paper test and is used to assess fluid intelligence [140]. The definition of fluid intelligence is connected to the capability of an individual to be able to solve unknown problems. It was defined in 1971 by a british american psychologist, Raymond Cattell [30].
- **Addenbrookes Cognitive Examination ACE-R**: these tests aim to assess some elements of cognition. In particular the tests include assessment of memory scores (1-18), language scores (1-14) and other cognitive capabilities (for example visuospatial assessed in a range 1-26). A cumulative sum measure of the ACE-R tests performed was taken into account in our analysis and will be presented later in the chapter when describing the model.

3 **Demographic and lifestyle features**:

- **Age**: age of the participant at the time of data collection.
- **Hospital Anxiety and Depression scales HADS**: was originally developed in 1983 by Zigmond and Snaith [156]. It is a score initially used for the identification of depression and anxiety in patients and individuals in general. It is a pen and paper test, and the score can vary up to 21 for the definition of the grade of anxiety or depression of a person.
- **Drug_use Abuse Screening Test (DAST-20)**: is a questionnaire used for the identification of addiction to psychoactive drugs and it is also able to quantify the presence of problems related to drug misuse. It was originally developed in 1982 [131].
- **Alcohol**: the scale measuring the addiction to alcohol varies from -1 to 5. In particular the legend to answer the alcohol questionnaire is:
  - Past drinker: -1
  - Non drinker: 0
  - Occasional drinker: 1

    - Monthly: 2
    - Weekly one/two times: 3
    - Weekly three/four times: 4
    - Daily: 5
  - **Smoking**: for smoking habits the legend to answer the questionnaire is as follows:
    - Non current at least 100 and past smoker : -1
    - Never smoked: 0
    - Non current less than 100: 1
    - Current smoker, occasional and current at least 100 : 2
  - **Qualification**: the qualification scale legend is as follows:
    - None: 0
    - GCSE/O-Level: 1
    - A level: 2
    - Degree: 3
  - **Hours slept**: the number of hours slept was calculated considering the Pittsburgh Sleep Quality Index (PSQI) hours listed as being asleep by the participants [25]. The PSQI index is a questionnaire to perform an analysis of sleep quality and patterns in older adults, which has been widely used in clinical practice since 1989.

6.4 Methods: NetRank

We implemented a pipeline, that we called **NetRank**, in which a multiplex architecture was integrated in a community detection framework, allowing for the identification of overlapping communities across multiple layers. We will describe here its general structure. We will then refer to the Cam-CAN modelling in the later results section, where the **NetRank** procedure is used to characterize complex brain-behaviour relationships and their risks and modifiable factors. Consider a multi-dimensional dataset, in which the same group of individuals has several features available. In the case of the Cam-CAN study, each layer in the multiplex architecture will represent a different feature: age, grey matter, white matter, cognitive tests score and so on. Taking this as a

starting point, we then needed to define the graph adjacency matrix for each feature. We integrated this step in the **NetRank** procedure, that we will now describe. Consider a multiplex architecture, in which each layer models a feature type. In the Cam-CAN study, each node in the graph represents a participant, and the edges of the graph will be weighted according to the ranked similarity/distance between two participants. To create the adjacency matrix in **NetRank** we proceeded as follows (as summarized in Figure 6.2):

1 The original raw features vector, are replaced by their ranking values. To obtain the ranked vector, the original values are substituted by their respective order position considering the sorted features vector. As an example, consider the age vector of three individuals $V = [24, 35, 46]$; applying the ranking descending procedure to it, the vector will become: $V_{ranked} = [2, 1, 0]$. This means that to the maximum value 46 we will assign 0, to the second highest 35 we assign 1 and to the lowest value 24, of the original vector, we replace 2.

2 We then obtain the distance, similarity, matrix corresponding to the ranked features vector considered. We will therefore obtain a matrix where the number of rows and columns are the same, and given by the number of participants. The values $A_{i,j}$ in the matrix correspond to the absolute distance between the i_{th} and j_{th} element of the ranked features vector.

3 We apply again the ranking procedure to the whole distance matrix so obtained, and normalize it between 0 and the maximum value appearing in the ranking matrix. The matrix so obtained is, therefore, the adjacency matrix of the g_{th} layer of our multiplex architecture.

4 We apply the Louvain community detection method, in order to obtain communities for each layer separately. For details on the Louvain Method, refer to the background chapter (Chapter 2).

5 At this point we consider the global multiplexity matrix of the multiplex network so obtained. The global multiplexity index, introduced by [68], is a measure of the number of times that two nodes are clustered in the same community across different layers. If, for example, individual x and y are clustered together in the feature layer of structural MRI, functional MRI and cognitive score relative to the Cattell test, then the global community multiplexity index would be 3 (i.e. in

position i, j of the global multiplexity matrix there will be a 3 as value of global multiplexity index assigned to that pair of individuals). More formally, if L is the number of layers, g the generic layer, and N the number of nodes for each layer, then the global multiplexity index for participant i and j with $i = 0, ..., N$ is [68]:

$$gmi(i, j) = \sum_{g=1}^{L} \delta(c_i^g, c_j^g) \tag{6.1}$$

where $\delta(c_i^g, c_j^g)$ represents the delta Kroenecker function. This will increase by 1 if two individuals are found to be part of the same community across different layers of the graph [68]. In this way we can evaluate communities independently across the layers, and this will allow us to understand how strong the connections across the layers are [68].

6 The last step consists in the analysis of the global community multiplexity index matrix.

The **NetRank** procedure is summarised in Figure 6.2.

The ranking procedure: background and motivation for its application

The inspiration for the ranking procedure that we propose in our methodology, **NetRank**, comes from a standard approach which is widely used in non parametric statistics, where no assumption regarding the distribution of the data analysed is made [39] [3]. Ranking data is a particularly effective statistical approach to overcome two problem which often occur in statistical analysis: skewness and the presence of outliers in the dataset. When using ranks, in fact, the original data vector is transformed, such as each value is replaced by the value of its position in the ordered vector. Therefore if we have a n dimensional vector, its ranked transformation will be composed by n numbers between 1 and n. A number of largely used non parametric statistical tests, are based on the ranking transformation of the initial values. Examples are the well known Mann Whitney U test [97], or the Spearman Rank Correlation test [3]. In this last case for example, the Pearson Correlation coefficient of the variable is computed only after a rank transformation of the original vector, therefore accounting for the problem of skewness and outliers in the final correlation coefficient obtained. To the best of our knowledge this is the first application of such ranking procedure to networks and graphs analysis.

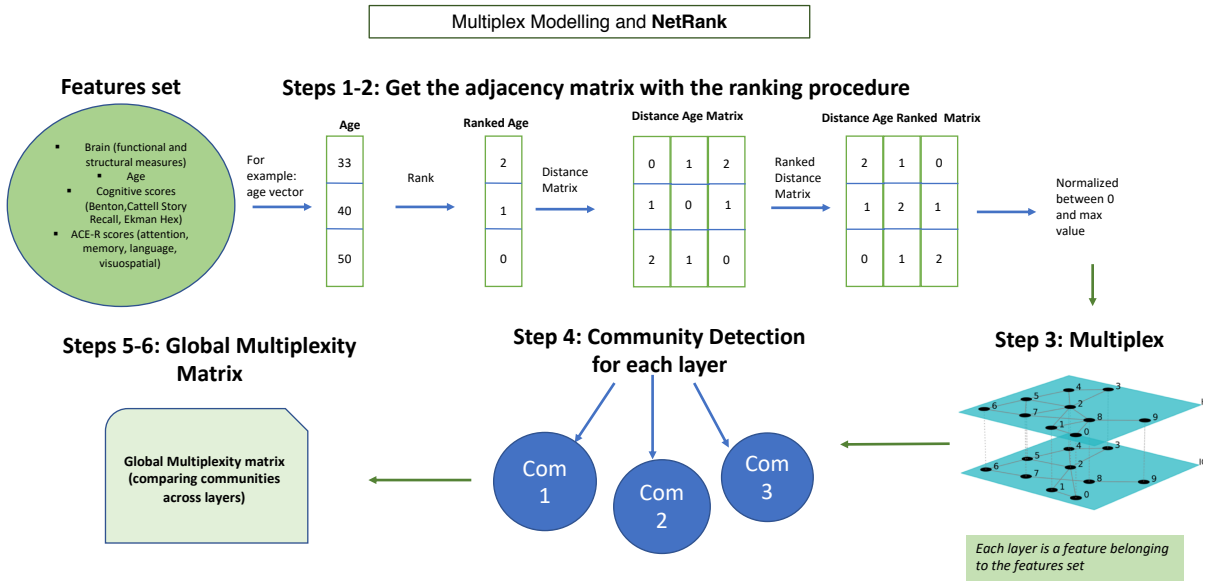

Figure 6.2: Figure showing the **NetRank** pipeline. The initial step consists in ranking the features vectors and distance matrix. The adjacency matrix so obtained, is used to build the multiplex model. In each layer the community detection method is then applied. From the communities so obtained the global mutliplexity matrix is computed and used to analyse the corresponding clusters.

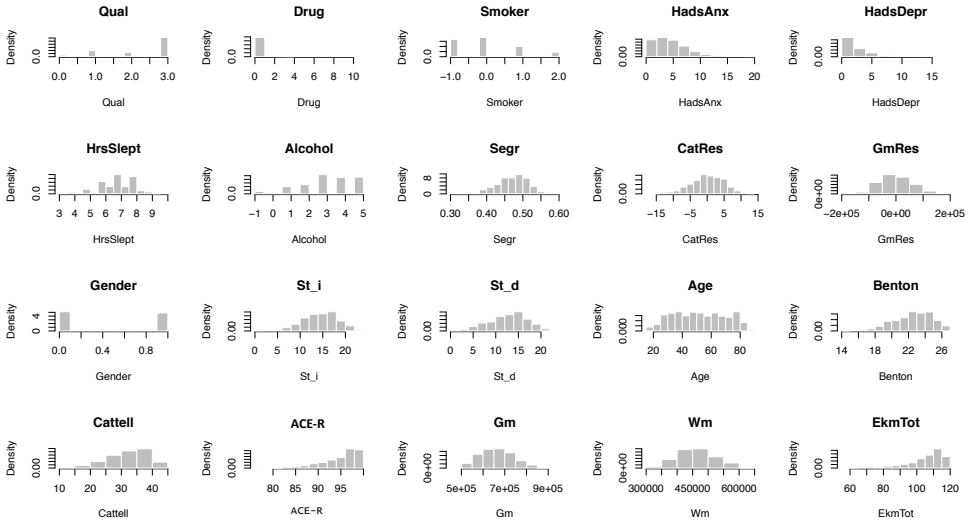

Figure 6.3: Features distribution in the Cam-CAN cohort considered. The dataset includes behavioural, cognitive tests and demographic variables.

6.5 Results

This section will be devoted to the presentation of the experiments performed. Initially, preliminary descriptive statistics will be shown. Subsequently we will introduce the application of the **NetRank** pipeline to the subset of 513 participants of the Cam-CAN cohort, used in our study.

6.5.1 Preliminary statistical analysis

In Table 6.1 we present the main descriptive statistics (mean, standard deviation, minimum and maximum value) of the features used in our experiments, and in Figure 6.3 we plot their distributions. The meaning of the features is described in Section 6.3. In Figure 6.4 we present the Pearson correlation coefficient matrix. The age range of the cohort analysed is between 18 and 88 years old. The gender distribution is almost uniform. In terms of qualification, instead, most of the cohort is highly qualified, and in fact the mean is 2.3.

In the correlation matrix 6.4, in Table 6.1 and in Figure 6.3 we present also two additional variables with resepect to Section 6.3: CatRes and GmRes. These are the vectors of Cattel scores and total mean grey matters volumes, linearly regressed out by age. We decided to use them, as this is a common practice in cognitive neuroscience

Table 6.1: Descriptive statistics for the subset of the Cam-CAN cohort considered in our experiments. CatRes and GmRes are the regression residuals of the Cattell test and the Grey Matter volume with respect to age. To compute residuals is a common practice in neuroscience and we used them in our multiplex analysis as well. Gm indicates the mean total volume of grey matter, and Wm the mean total volume of white matter. The unit of measure for Gm and Wm are mm^3

Feature	Mean	St. Dev.	Min	Max
Qualification	2.320	0.958	0	3
Drug	0.136	0.659	0	11
Smoker	0.041	0.946	-1	2
Hads Anx	4.984	3.277	0	20
Hads Depr	2.688	2.551	0	17
Hrs Slept	6.975	1.105	3	10
Alcohol	3.177	1.528	-1	5
Segregation	0.471	0.043	0.305	0.583
Gender	0.483	0.500	0	1
St_i	14.869	3.967	0	24
St_d	13.199	4.179	0	24
Age	52.595	17.937	18	88
Benton	23.058	2.302	14	27
Cattell	32.470	6.615	12	44
CatRes	0.023	4.963	-16.201	12.091
ACE-R	95.238	4.449	76	100
Gm (Tot)	662,484.800	76,861.770	486,986.200	940,123.800
GmRes	-245.776	61,120.070	$-165,221.400$	192,963.900
Wm (Tot)	461,832.300	58,799.130	314,381.500	625,187.300
Ekm	105.097	12.338	57	120

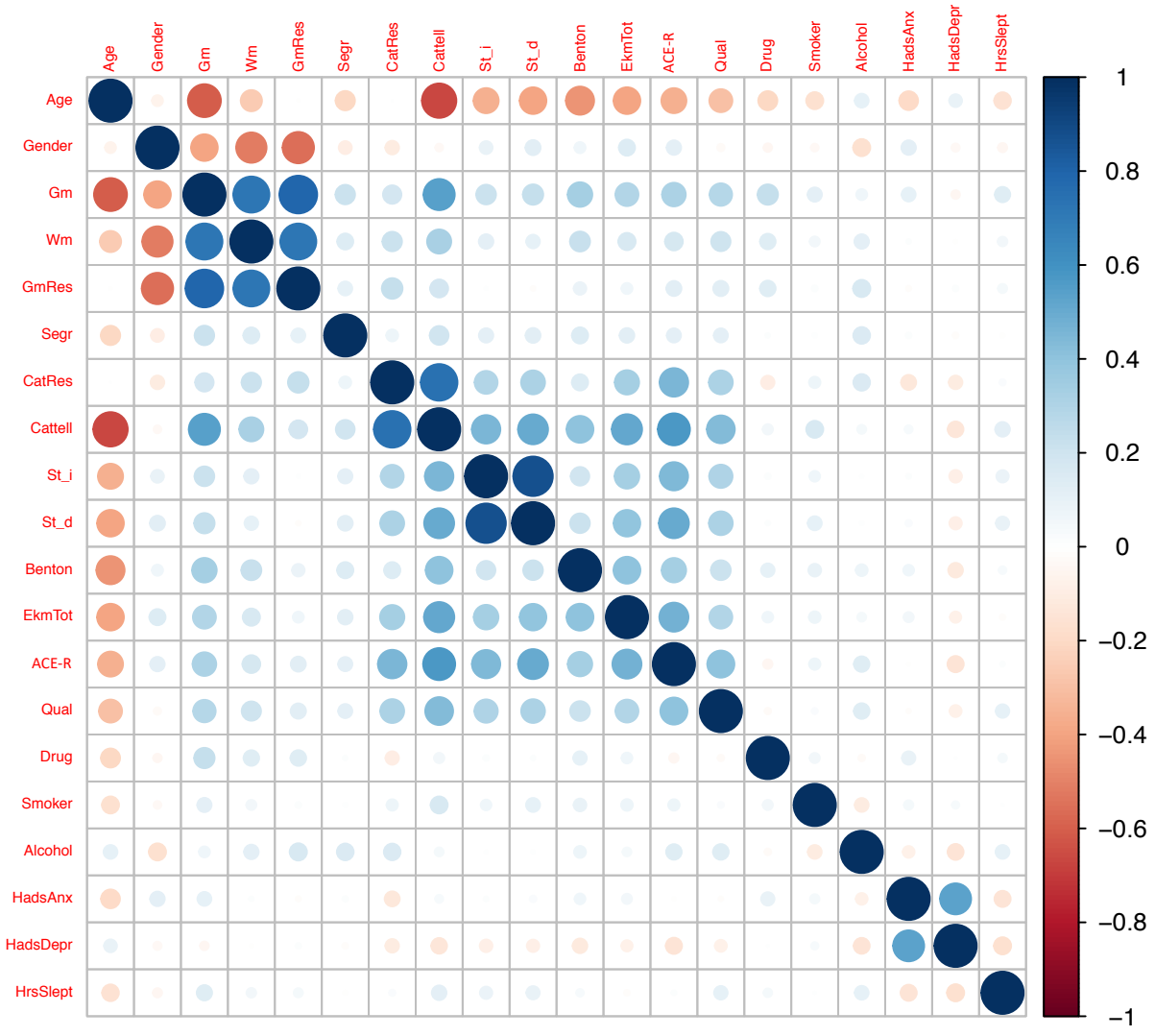

Figure 6.4: Pearson correlation coefficients matrix between the Cam-CAN features considered in our analysis. In the matrix we included clinical, demograhics, structural and functional information.

experiments [9] and in this way we could remove the potential confounding factor of age from the two measures of interest. Another common confounding factor in MRI studies, which is often regressed out, is gender, being on average women's head smaller than men. However since the focus of our research was related to neurocognitive ageing, we decided to remove only age.
From a first inspection of the correlation matrix in Figure 6.4, we can visually identify three clusters. Starting from the upper left part, the first cluster indicates a high correlation between structural variables, such as grey matter volumes, white matter volumes, gender and age. Secondly the other main cluster of interaction is formed in the central part of the matrix, which includes cognitive scores, up to the qualification feature. The rest of the matrix shows less obvious correlations, in particular regarding the part of lifestyle and demographics, but the overall visual structure of the correlation matrix seems to suggest the possible presence of communities inside the Cam-CAN cohort.
In order to better understand the relationship between all the variables, we also performed a series of linear regressions, predicting in turn one of the variables and using the remaining set as predictors. The results of the linear regression models are presented in Figure 6.5 and in Figure 6.6.

In Figure 6.7 we present a summary of the linear regressions as a network. Each node represents a layer of the multiplex. Given two nodes x and y an edge entering x exists, if y is a statistically significant predictor of x and viceversa. If both directions are true, then a bidirectional edge exists. Since the bidirectionality is true for all the nodes in the graph, then the resulting graph obtained is undirected. The Louvain Community detection method in this graph, returned three communities, composed as follows:

- **Community 1**: Cattell, story recall immediate, story recall delayed, Benton, Ekman Hex total, ACE-R, qualification, drug score
- **Community 2**: age, smoker, alcohol, Hads anxiety, Hads depression, hours slept, segregation
- **Community 3**: gender, grey matter, white matter

In Figure 6.8 we report the overall node degree of the graph. The node with the highest node degree is age, followed by the ACE-R and alcohol nodes. A few interesting points can therefore be noticed. Age represents the hub of the summary network. Moreover the structural features are clustered together with the gender variable. On the other

Predictors	Age			Gender			Gm			Wm			Cattell			St i			St d			Benton			Ekm Tot		
	Estimates	CI	p	Estimates	CI	p	Estimates	CI	p	Estimates	CI	p	Estimates	CI	p	Estimates	CI	p	Estimates	CI	p	Estimates	CI	p	Estimates	CI	p
(Intercept)	148.70	121.71 – 175.69	**<0.001**	1.49	0.40 – 2.58	**0.008**	277790.05	169449.60 – 386130.51	**<0.001**	10684.14	-94672.25 – 116040.53	0.842	-13.23	-24.74 – -1.72	**0.024**	3.54	-2.06 – 9.14	0.215	-8.48	-14.03 – -2.94	**0.003**	13.10	7.59 – 18.60	**<0.001**	15.36	-13.00 – 43.71	0.288
Qual	-0.40	-1.50 – 0.69	0.470	-0.01	-0.05 – 0.04	0.807	13.03	-4051.38 – 4077.45	0.995	1935.37	-1915.87 – 5786.62	0.324	0.71	0.29 – 1.12	**0.001**	0.12	-0.09 – 0.32	0.264	-0.01	-0.22 – 0.19	0.920	0.01	-0.20 – 0.22	0.918	0.45	-0.58 – 1.49	0.390
Drug	-1.36	-2.81 – 0.09	0.065	0.02	-0.03 – 0.07	0.464	8273.83	2946.87 – 13600.80	**0.002**	-427.43	-5527.14 – 4672.29	0.869	-0.45	-1.01 – 0.11	0.115	0.07	-0.20 – 0.34	0.629	-0.05	-0.32 – 0.22	0.723	0.07	-0.20 – 0.35	0.598	0.64	-0.73 – 2.02	0.357
Smoker	-0.48	-1.47 – 0.51	0.341	-0.03	-0.06 – 0.01	0.174	-413.11	-4074.59 – 3248.38	0.825	-403.69	-3876.55 – 3069.16	0.819	0.33	-0.05 – 0.71	0.085	-0.15	-0.33 – 0.04	0.119	0.17	-0.01 – 0.35	0.069	0.07	-0.11 – 0.26	0.447	-0.13	-1.07 – 0.80	0.778
Hads Anx	-0.76	-1.11 – -0.41	**<0.001**	0.02	0.01 – 0.04	**0.001**	996.18	-311.99 – 2304.35	0.135	-229.04	-1472.46 – 1014.37	0.718	-0.08	-0.22 – 0.05	0.226	0.00	-0.06 – 0.07	0.916	-0.01	-0.07 – 0.06	0.802	0.01	-0.05 – 0.08	0.696	-0.07	-0.40 – 0.27	0.684
Hads Depr	0.61	0.17 – 1.05	**0.007**	-0.02	-0.03 – -0.00	**0.028**	-219.17	-1873.93 – 1435.59	0.795	334.21	-1235.13 – 1903.56	0.676	-0.03	-0.20 – 0.14	0.725	-0.02	-0.11 – 0.06	0.579	0.03	-0.06 – 0.11	0.518	-0.06	-0.14 – 0.02	0.166	0.15	-0.28 – 0.57	0.496
Hrs Slept	-1.05	-1.91 – -0.18	**0.018**	0.00	-0.03 – 0.03	0.915	2210.64	-997.45 – 5418.72	0.176	-1433.07	-4478.89 – 1612.76	0.356	0.08	-0.26 – 0.41	0.657	-0.02	-0.18 – 0.14	0.809	0.09	-0.07 – 0.26	0.253	-0.05	-0.21 – 0.11	0.544	-0.82	-1.63 – 0.00	0.051
Alcohol	1.46	0.83 – 2.10	**<0.001**	-0.03	-0.06 – -0.01	**0.005**	355.17	-2052.34 – 2762.69	0.772	21.19	-2262.49 – 2304.87	0.985	0.04	-0.21 – 0.29	0.755	-0.04	-0.16 – 0.09	0.558	0.01	-0.12 – 0.13	0.923	0.12	-0.00 – 0.24	0.051	0.16	-0.46 – 0.77	0.617
Segr	-25.39	-47.35 – -3.42	**0.024**	-0.41	-1.22 – 0.39	0.314	38140.44	-43484.29 – 119765.16	0.359	-8594.97	-86076.95 – 68887.00	0.828	2.37	-6.13 – 10.88	0.584	0.33	-3.79 – 4.46	0.874	0.90	-3.21 – 5.01	0.668	1.64	-2.49 – 5.78	0.435	0.90	-19.98 – 21.78	0.933
Gender	-5.19	-7.56 – -2.83	**<0.001**				-26795.97	-35403.14 – -18188.80	**<0.001**	-24298.63	-32488.88 – -16108.39	**<0.001**	-0.80	-1.72 – 0.13	0.092	-0.08	-0.53 – 0.38	0.742	0.21	-0.23 – 0.66	0.347	0.45	-0.00 – 0.90	0.052	3.64	1.38 – 5.90	**0.002**
St i	-0.01	-0.48 – 0.47	0.979	-0.00	-0.02 – 0.01	0.742	-453.11	-2201.99 – 1295.77	0.611	760.44	-897.42 – 2418.30	0.368	0.04	-0.14 – 0.23	0.628				0.82	0.77 – 0.87	**<0.001**	0.00	-0.09 – 0.09	0.967	-0.16	-0.61 – 0.28	0.470
St d	-0.36	-0.83 – 0.12	0.140	0.01	-0.01 – 0.03	0.347	-477.97	-2231.92 – 1275.98	0.593	-321.60	-1985.43 – 1342.24	0.704	0.15	-0.03 – 0.33	0.103	0.82	0.77 – 0.87	**<0.001**				-0.05	-0.14 – 0.04	0.287	0.47	0.02 – 0.91	**0.040**
Benton	-1.06	-1.53 – -0.60	**<0.001**	0.02	-0.00 – 0.03	0.052	-138.97	-1881.92 – 1603.99	0.876	1864.79	219.81 – 3509.77	**0.026**	0.05	-0.14 – 0.23	0.621	0.00	-0.09 – 0.09	0.967	-0.05	-0.14 – 0.04	0.287				0.97	0.54 – 1.41	**<0.001**
Cattell	-0.95	-1.17 – -0.74	**<0.001**	-0.01	-0.02 – 0.00	0.092	764.16	-81.14 – 1609.47	0.076	239.24	-564.79 – 1043.27	0.559				0.01	-0.03 – 0.05	0.628	0.04	-0.01 – 0.08	0.103	0.01	-0.03 – 0.05	0.621	0.46	0.25 – 0.68	**<0.001**
Acer	0.41	0.13 – 0.69	**0.004**	0.02	0.01 – 0.03	**<0.001**	1426.98	384.50 – 2469.46	**0.007**	-225.49	-1221.27 – 770.28	0.657	0.34	0.23 – 0.44	**<0.001**	0.00	-0.05 – 0.06	0.856	0.09	0.03 – 0.14	**0.001**	0.05	-0.00 – 0.11	0.053	0.45	0.18 – 0.72	**0.001**
Gm	-0.00	-0.00 – -0.00	**<0.001**	-0.00	-0.00 – -0.00	**<0.001**			0.57	0.51 – 0.64	**<0.001**	0.00	-0.00	-0.00 – 0.00	0.076	-0.00	-0.00 – 0.00	0.611	-0.00	-0.00 – 0.00	0.593	-0.00	-0.00 – 0.00	0.876	0.00	-0.00 – 0.00	0.596
Wm	0.00	0.00 – 0.00	**<0.001**	-0.00	-0.00 – -0.00	**<0.001**	0.64	0.56 – 0.71	**<0.001**				0.00	-0.00 – 0.00	0.559	0.00	-0.00 – 0.00	0.368	-0.00	-0.00 – 0.00	0.704	0.00	0.00 – 0.00	**0.026**	0.00	-0.00 – 0.00	0.482
Ekm Tot	-0.01	-0.10 – 0.08	0.822	0.01	0.00 – 0.01	**0.002**	93.27	-252.16 – 438.71	0.596	117.37	-210.20 – 444.94	0.482	0.08	0.04 – 0.11	**<0.001**	-0.01	-0.02 – 0.01	0.470	0.02	0.00 – 0.04	**0.040**	0.04	0.02 – 0.06	**<0.001**			
Age				-0.01	-0.01 – -0.00	**<0.001**	-1741.10	-2029.46 – -1452.75	**<0.001**	825.77	524.52 – 1127.02	**<0.001**	-0.14	-0.17 – -0.11	**<0.001**	-0.00	-0.02 – 0.02	0.979	-0.01	-0.03 – 0.00	0.140	-0.04	-0.05 – -0.02	**<0.001**	-0.01	-0.09 – 0.07	0.822
Observations	513			513			513			513			513			513			513			513			513		
R^2 / adjusted	0.671 / 0.659			0.433 / 0.413			0.754 / 0.746			0.622 / 0.610			0.640 / 0.628			0.765 / 0.757			0.790 / 0.782			0.297 / 0.273			0.377 / 0.356		
R^2																											

Figure 6.5: Linear regression models for the Cam-CAN cohort. On top, in bold, we can see the predicted variables. The predictors are in the rows of the table, and the bold coefficients represent the ones that are statistically significant.

Predictors	Acer			Qual			Drug			Smoker			Alcohol			Hads Anx			Hads Depr			Hrs Slept			Segr		
	Estimates	CI	p	Estimates	CI	p	Estimates	CI	p	Estimates	CI	p	Estimates	CI	p	Estimates	CI	p	Estimates	CI	p	Estimates	CI	p	Estimates	CI	p
(Intercept)	68.87	61.78 – 75.96	**<0.001**	-4.16	-6.55 – -1.78	**0.001**	0.99	-0.84 – 2.81	0.288	0.17	-2.50 – 2.85	0.898	-8.81	-12.81 – -4.81	**<0.001**	6.95	-0.50 – 14.41	0.068	4.21	-1.70 – 10.13	0.163	11.38	8.50 – 14.26	**<0.001**	0.48	0.37 – 0.59	**<0.001**
Qual	0.63	0.29 – 0.97	**<0.001**				-0.04	-0.10 – 0.03	0.273	-0.05	-0.14 – 0.05	0.358	0.15	0.00 – 0.30	**0.045**	-0.07	-0.35 – 0.20	ACE-R).597	0.07	-0.15 – 0.28	0.554	0.07	-0.04 – 0.18	0.219	0.00	-0.00 – 0.00	0.997
Drug	-0.52	-0.97 – -0.07	**0.023**	-0.07	-0.18 – 0.05	0.273				0.05	-0.08 – 0.18	0.481	0.03	-0.16 – 0.23	0.741	0.20	-0.17 – 0.56	0.286	-0.09	-0.38 – 0.19	0.528	0.02	-0.13 – 0.16	0.826	-0.00	-0.01 – 0.00	0.383
Smoker	0.01	-0.30 – 0.32	0.938	-0.04	-0.12 – 0.04	0.358	0.02	-0.04 – 0.08	0.481				-0.14	-0.28 – -0.01	**0.034**	0.02	-0.23 – 0.26	0.902	0.06	-0.14 – 0.26	0.544	-0.01	-0.11 – 0.09	0.822	-0.00	-0.00 – 0.00	0.658
Hads Anx	-0.01	-0.12 – 0.10	0.871	-0.01	-0.04 – 0.02	0.597	0.01	-0.01 – 0.03	0.286	0.00	-0.03 – 0.03	0.902	0.05	-0.00 – 0.09	0.060				0.44	0.39 – 0.50	**<0.001**	-0.05	-0.08 – -0.01	**0.008**	-0.00	-0.00 – 0.00	0.503
Hads Depr	-0.09	-0.22 – 0.05	0.226	0.01	-0.03 – 0.05	0.554	-0.01	-0.04 – 0.02	0.528	0.01	-0.03 – 0.05	0.544	-0.10	-0.16 – -0.04	**0.002**	0.71	0.62 – 0.80	**<0.001**				-0.03	-0.07 – 0.02	0.262	0.00	-0.00 – 0.00	0.470
Hrs Slept	-0.27	-0.54 – -0.01	**0.046**	0.04	-0.03 – 0.11	0.219	0.01	-0.05 – 0.06	0.826	-0.01	-0.09 – 0.07	0.822	0.17	0.05 – 0.28	**0.005**	-0.29	-0.51 – -0.08	**0.008**	-0.10	-0.27 – 0.07	0.262				-0.00	-0.01 – 0.00	0.105
Alcohol	0.26	0.06 – 0.46	**0.012**	0.05	0.00 – 0.11	**0.045**	0.01	-0.03 – 0.05	0.741	-0.06	-0.12 – -0.00	**0.034**				0.16	-0.01 – 0.32	0.060	-0.20	-0.33 – -0.08	**0.002**	0.09	0.03 – 0.16	**0.005**	0.00	0.00 – 0.01	**<0.001**
Segr	-2.56	-9.43 – 4.31	0.464	0.00	-1.77 – 1.78	0.997	-0.60	-1.94 – 0.74	0.383	-0.44	-2.41 – 1.53	0.658	5.53	2.58 – 8.49	**<0.001**	-1.88	-7.38 – 3.62	0.503	1.60	-2.75 – 5.96	0.470	-1.85	-4.09 – 0.39	0.105			
Gender	1.33	0.59 – 2.07	**<0.001**	-0.02	-0.22 – 0.17	0.807	0.05	-0.09 – 0.20	0.464	-0.15	-0.36 – 0.07	0.174	-0.46	-0.79 – -0.14	**0.005**	1.05	0.46 – 1.65	**0.001**	-0.53	-1.01 – -0.06	**0.028**	0.01	-0.23 – 0.26	0.915	-0.00	-0.01 – 0.00	0.314
St i	0.01	-0.13 – 0.16	0.856	0.02	-0.02 – 0.06	0.264	0.01	-0.02 – 0.04	0.629	-0.03	-0.08 – 0.01	0.119	-0.02	-0.08 – 0.04	0.558	0.01	-0.11 – 0.12	0.916	-0.03	-0.12 – 0.07	0.579	-0.01	-0.05 – 0.04	0.809	0.00	-0.00 – 0.00	0.874
St d	0.24	0.10 – 0.39	**0.001**	-0.00	-0.04 – 0.04	0.920	-0.01	-0.03 – 0.02	0.723	0.04	-0.00 – 0.08	0.069	0.00	-0.06 – 0.07	0.923	-0.02	-0.13 – 0.10	0.802	0.03	-0.06 – 0.12	0.518	0.03	-0.02 – 0.08	0.253	0.00	-0.00 – 0.00	0.668
Age	0.04	0.01 – 0.07	**0.004**	-0.00	-0.01 – 0.00	0.470	-0.01	-0.01 – 0.00	0.065	-0.00	-0.01 – 0.00	0.341	0.03	0.02 – 0.04	**<0.001**	-0.05	-0.07 – -0.03	**<0.001**	0.02	0.01 – 0.04	**0.007**	-0.01	-0.02 – -0.00	**0.018**	-0.00	-0.00 – -0.00	**0.024**
Benton	0.14	-0.00 – 0.29	0.053	0.00	-0.04 – 0.04	0.918	0.01	-0.02 – 0.04	0.598	0.02	-0.03 – 0.06	0.447	0.06	-0.00 – 0.13	0.051	0.02	-0.09 – 0.14	0.696	-0.07	-0.16 – 0.03	0.166	-0.01	-0.06 – 0.03	0.544	0.00	-0.00 – 0.00	0.435
Cattell	0.22	0.15 – 0.29	**<0.001**	0.03	0.01 – 0.05	**0.001**	-0.01	-0.03 – 0.00	0.115	0.02	-0.00 – 0.04	0.085	0.00	-0.03 – 0.04	0.755	-0.04	-0.09 – 0.02	0.226	-0.01	-0.05 – 0.04	0.725	0.01	-0.02 – 0.03	0.657	0.00	-0.00 – 0.00	0.584
Gm	0.00	0.00 – 0.00	**0.007**	0.00	-0.00 – 0.00	0.995	0.00	0.00 – 0.00	**0.002**	-0.00	-0.00 – 0.00	0.825	0.00	-0.00 – 0.00	0.772	0.00	-0.00 – 0.00	0.135	-0.00	-0.00 – 0.00	0.795	0.00	-0.00 – 0.00	0.176	0.00	-0.00 – 0.00	0.359
Wm	-0.00	-0.00 – 0.00	0.657	0.00	-0.00 – 0.00	0.324	-0.00	-0.00 – 0.00	0.869	-0.00	-0.00 – 0.00	0.819	0.00	-0.00 – 0.00	0.985	-0.00	-0.00 – 0.00	0.718	0.00	-0.00 – 0.00	0.676	-0.00	-0.00 – 0.00	0.356	-0.00	-0.00 – 0.00	0.828
Ekm Tot	0.05	0.02 – 0.08	**0.001**	0.00	-0.00 – 0.01	0.390	0.00	-0.00 – 0.01	0.357	-0.00	-0.01 – 0.01	0.778	0.00	-0.01 – 0.02	0.617	-0.00	-0.03 – 0.02	0.684	0.01	-0.01 – 0.02	0.496	-0.01	-0.02 – 0.00	0.051	0.00	-0.00 – 0.00	0.933
Acer				0.04	0.02 – 0.06	**<0.001**	-0.02	-0.04 – -0.00	**0.023**	0.00	-0.02 – 0.03	0.938	0.05	0.01 – 0.09	**0.012**	-0.01	-0.08 – 0.06	0.871	-0.03	-0.09 – 0.02	0.226	-0.03	-0.06 – -0.00	**0.046**	-0.00	-0.00 – 0.00	0.464
Observations	513			513			513			513			513			513			513			513			513		
R^2 / adjusted	0.482 / 0.464			0.253 / 0.228			0.099 / 0.068			0.057 / 0.025			0.164 / 0.135			0.387 / 0.366			0.365 / 0.343			0.102 / 0.072			0.096 / 0.065		
R^2																											

Figure 6.6: Linear regression models for the Cam-CAN cohort. For description on the format of bold and variables presented refer to Figure 6.5

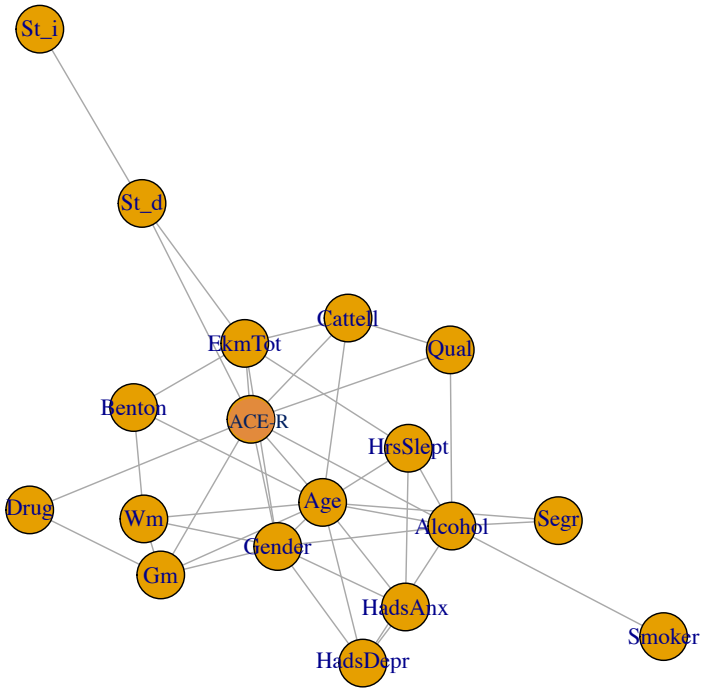

Figure 6.7: Graph summarizing all the layers of the multiplex in a single graph. Each node is a layer of the multiplex and edges exists accordingly to the linear regression performed, in the statistical exploratory analysis in the previous section.

hand the functional measure is instead clustered in community 2, where the majority of variables is represented by the lifestyle ones.

6.5.2 Integrating structural, functional and cognitive brain features using a multiplex approach

As we were mentioning earlier in this chapter, the graph and network modelling we used, was mainly guided by the research question of integrating, and understanding how and if there exists a relationship between structural, functional and cognitive features. Applying the **NetRank** pipeline we were therefore able to detect the presence of communities in the Cam-CAN cohort. Analysing the global multiplexity matrix, obtained following the **NetRank** steps, we tried to answer research questions such as:

What do individuals, sharing the same global community multiplexity values, have in common?

Furthermore: *Are cognitive and structural features guiding the communities characterizations of individuals?*

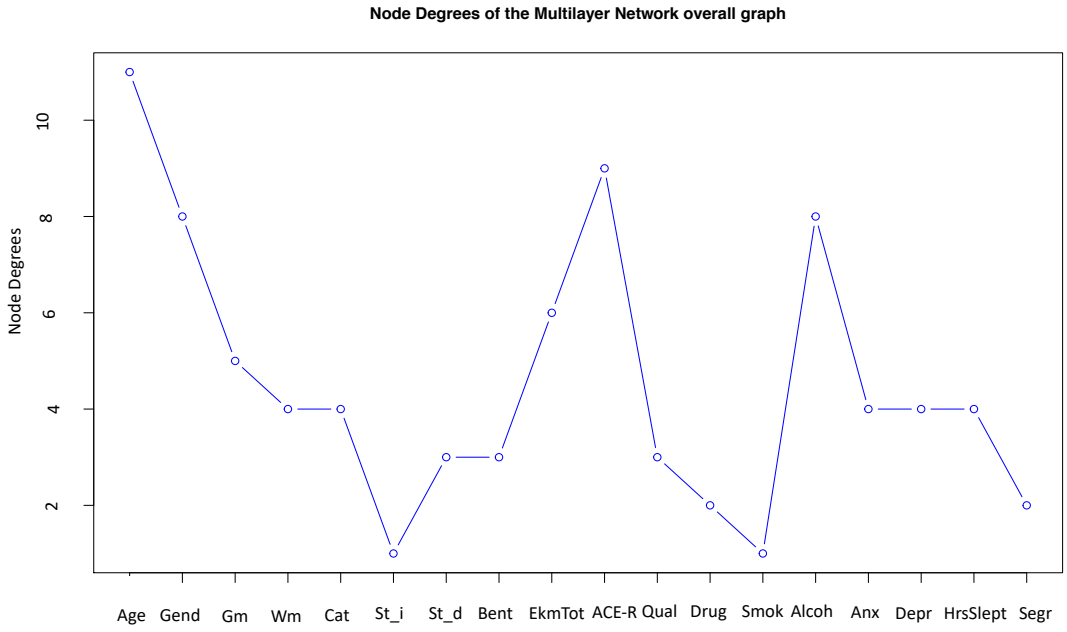

Figure 6.8: Overall node degree of the multilayer total network graph. On the x axis the various features, i.e. nodes of Figure 6.7 are depicted.

Or, alternatively: *Can we obtain more indications of communities structure, if we consider lifestyle features?*

To answer these research questions, we structured the analysis as follows. The original dataset was divided into two subsets:

1 **Structural and Cognitive subset**: this is composed by 10 features; the mean grey matter volume (corrected by age), mean white total matter volume, segregation measure, Ekman Hex, Cattell (corrected by age), Benton tests total scores,ACE-R scores, story recall immediate, story recall delayed and age.

2 **Lifestyle and Behavioural subset**: this is composed by the features of alcohol, smoking, drug use, hours slept, qualification, Hads anxiety and Hads depression scores.

We then applied the **NetRank** pipeline to the two cases in parallel, as shown in Figure 6.9. We believe that these two sets are representatives of the two set of complementary features that we wanted to investigate, and represent a good division of the available

set of features to perform the analysis on the interaction between the two aspects of the cohort analysed. We built, in fact, two multiplex architectures: one obtained with features from subset 1 and the other one with features from subset 2. To construct the adjacency matrix, we performed the first step of the **NetRank** procedure as described in Section 6.4 and Figure 6.2. Each feature represents a layer in one of the two multiplexes. Each node is a participant (so we will have a total of 513 nodes per graph), and the connection between nodes in a layer is weighted according to the ranked normalized distance matrix, as described in Section 6.4.

Considering the two multiplex architectures, we then ran the community detection algorithm for each layer individually. The number of communities in every layer was always 3, with the exception of age giving as a result only 2 clusters. We therefore obtained two separate global multiplexity matrices for the two cases, i.e. the global multiplexity corresponding to the structural and cognitive features and the global multiplexity corresponding to the lifestyle features (see Figure 6.9). A first aspect we analysed was the similarity between individuals sharing the same global community multiplexity index.

If two individuals share a high value of community multiplexity index, it means they are likely to be similar, as they appear multiple times in the same community across different layers. We therefore focused our analysis on those groups of individuals who share the maximum value for the global community multiplexity index in the two experiments. In particular we proceeded as follows:

1 We considered those subgroups of individuals having the highest global community multiplexity in the two experiments. Such maximum value corresponds to 7, in the case of the lifestyle features, and 10 in the case of the structural and cognitive measures

2 Among those sharing the same highest global multiplexity value, we obtained subclusters of individuals, who always appear in the same community across the layers

3 We therefore analysed the similarities of the participants in each subgroup using the set of complementary features.This was to understand if individuals having similar structural/cognitive brain features have also similar lifestyle behaviour, and the contrary.

We identified several number of subclusters in both experiments. Many of them with

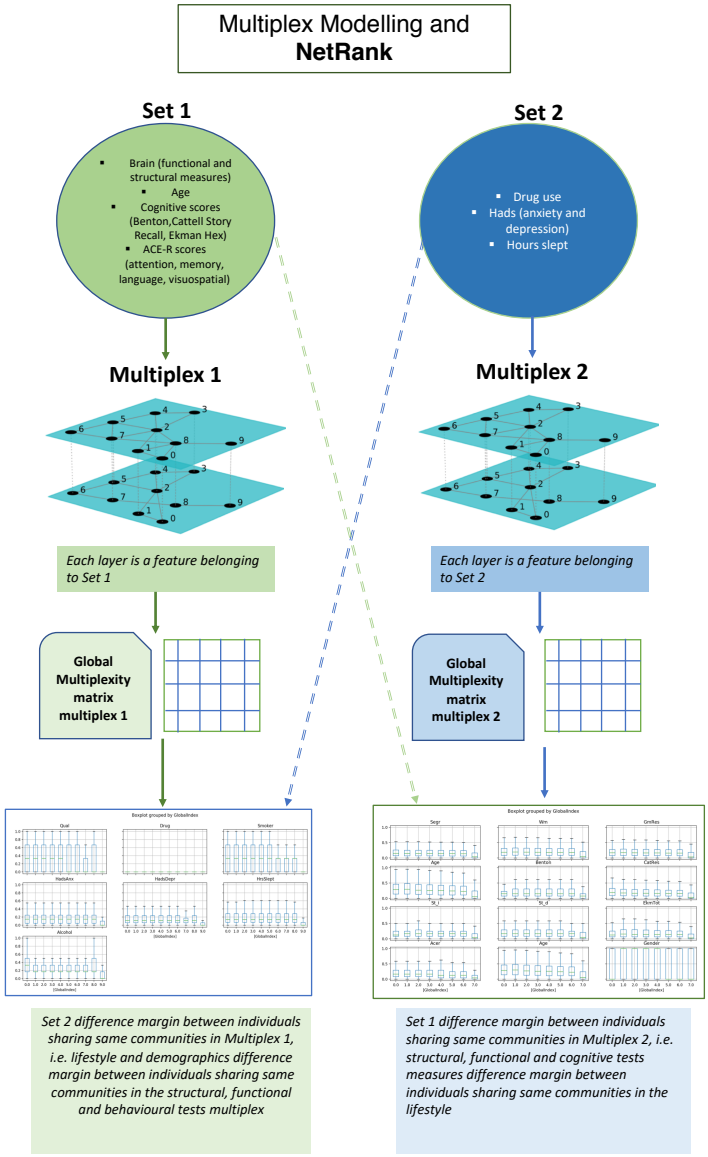

Figure 6.9: Figure describing the modelling performed with the **NetRank** pipeline, to compare multiplexes with lifestyle and structural and functional information. The two complementary sets of lifestyle, and non lifestyle, features are shown at the beginning and the arrows indicate the similarity tests when the communities are obtained from the global multiplexity matrix.

very few individuals (mostly composed by two elements). For this reason we decided to use only the three most numerous subgroups of the two sets of features. We now briefly describe such subgroups. In Table 6.2 we present the mean of the lifestyle features for the three lifestyle subgroups identified. In all the three cases qualification, drugs and smokers present the same value for all the individuals. Moreover the values of Hads scores are quite low, and similar values are obtained for the alcohol scores across the three subgroups. On the other hand in Table 6.3 we present the summary statistics for the structural subgroups. Here the age, as we can tell from the mean values, separates between older individuals (SubGroup3) and younger ones in the other two. The other values appear to be comparable.

Table 6.2: Summary statistics of the subgroups of lifestyle obtained for the highest value of global multiplexity community (equal to 7)

Lifestyle	**Qual**	**Drug**	**Smoker**	**HadsAnx**	**HadsDepr**	**HrsSlept**	**Alcohol**
SubGroup1	3	0	0	1.5	0.5	8.155	2.2
SubGroup2	3	0	0	1.625	0.875	5.750	2
SubGroup3	3	0	0	4.7	1.2	8.	2.7

Table 6.3: Summary statistics of the subgroups of structural,functional and cognitive features obtained for the highest value of global multiplexity index (10)

StructFunCog	**Segr**	**Cattell**	**Gm**	**St_i**	**St_d**	**Age**	**Benton**	**ACE-R**	**EkmTot**	**Wm**
SubGroup1	0.5	39.91	733998.9	18.7	17.25	39.9	25.25	98.91	114.7	511084.61
SubGroup2	0.44	39.7	735337.62	19	17.9	38	25	98	114	511511.61
SubGroup3	0.4213472	21.46	557707.4	9.85	7.53	73.38	20.07	87.23	79	385551.4

We therefore tried to answer one of our original research question: *can we say whether structural/functional variables bring more information than the lifestyle one? Alternatively, is the similarity going in the opposite direction?* We therefore decided to test the similarity of the individuals in the various groups according to the complementary features dataset. For example we considered individuals clustered together in Lifestyle Subgroup1 and computed the mean euclidean distance between such individuals, using structural features. The results are shown in Table 6.4. To enhance comparison the matrix values of structural and lifestyle features were normalized between 0 and 1. Individuals clustered according to lifestyle features appear to be quite similar also with respect to their corresponding structural/functional and cognitive variables. However participants grouped according to structural/functional/cognitive

features, appear to have a lower internal degree of similarity with respect to their lifestyle features. This is an interesting indication of how lifestyle could help in disentangling also structural and functional features similarity, enforcing the idea of the interaction between such characteristics and brain conformation. Future analysis needs to be done to validate clusters robustness and confidence on the results.

Table 6.4: Mean euclidean distance between subgroups members using the complementary features datasets

SubGroup	Distance Within Groups Using Complementary Features
SubGroupLifestyle1	0.12
SubGroupLifestyle2	0.16
SubGroupLifestyle3	0.13
SuGroupStructural1	0.22
SubGroupStructural2	0.27
StubGroupStructural3	0.34

6.5.3 Neurocognitive ageing profiles and brain regions

In the previous chapter we only used the average volume of grey matter as a major indication of structural properties. In this section, instead, we want to further investigate if different areas of the grey matter could play different roles in cognitive ageing. For this reason we articulated the analysis to add also an identification of brain regions (ROI) which are mostly correlated to the communities (i.e groups of individuals), identified across the different layers. For this we proceeded as follows:

- We considered the multiplex formed by the structural features, except for the total mean grey matter volume layer. The final goal of the current analysis was, in fact, to correlate identified communities to specific brain regions. For this reason, to avoid redundancies, we omitted the mean grey matter volume as a layer in the multiplex analysis. We therefore built the network using: mean white matter volume, Ekman scores, Cattell scores, Benton scores, ACE-R scores, functional measure of segregation and age.

- We proceeded with steps 1, 2 and 3 of the **NetRank** procedure, as described in Figure 6.4, to obtain the corresponding global multiplexity matrix.

- In the global multiplexity matrix, so obtained, we ran the Louvain community detection algorithm. This allowed us to separate the groups of participants into

three subgroups, according to their respective global multiplexity value, since we used this matrix as the adjacency matrix of our graph.

- We then considered the three groups so obtained, and their relative volume of the 114 segmented grey matter regions ROIs, in each community of participants. The three communities are composed, respectively, by 255, 231 and 27 individuals. We report the histograms of the various features for the three communities in Figure 6.10.

- For each of these three subsets of ROIs grey matter volumes, we considered the corresponding Pearson correlation coefficients matrices of the 114 ROIs. We used each of them as an adjacency matrix of a network, on which we ran the Louvain community detection algorithm. We then ranked these final communities of ROIs identified, according to the overall edges weights of each of them, using a network measure that we called Community Strength. This is defined as:

$$CommunityStrength = \frac{\sum_{i=1}^{n} \sum_{j=1}^{n} w_{i,j}}{E} \tag{6.2}$$

where $w_{i,j}$ is the weight between two given nodes i and j in a subcommunity of the network, n is the number of nodes (i.e. 114, number of ROIs) and $E = \frac{n(n+1)}{2}$ is the number of edges of a given network. In this way we could identify the grey matter brain regions, most tightly correlated, for the three groups of individuals. That is, the brain regions that mainly characterized the three groups of individuals clustered together by such procedure. In particular the value of the network strength considered is the mean value of the network weights.
For community 0 of the individuals, six subcommunities of ROIs, were identified. The highest scoring community network strength, has a score of 0.77, as shown in Figure 6.11.
In community 1, instead, 9 were the ROIS communities identified, with 0.88 as the highest scoring strength of the subnetworks.
In the last community of individuals, instead, the highest one had strength score of 0.83, and eight was the total number of subcommunities in this case. A summary of the various strengths is reported in Figure 6.11.
Each table is referring to one of the communities composed by individuals. Then each row of the table represents one of the ROIs communities identified and the relative network strength measure associated to it. The ROIs community with the

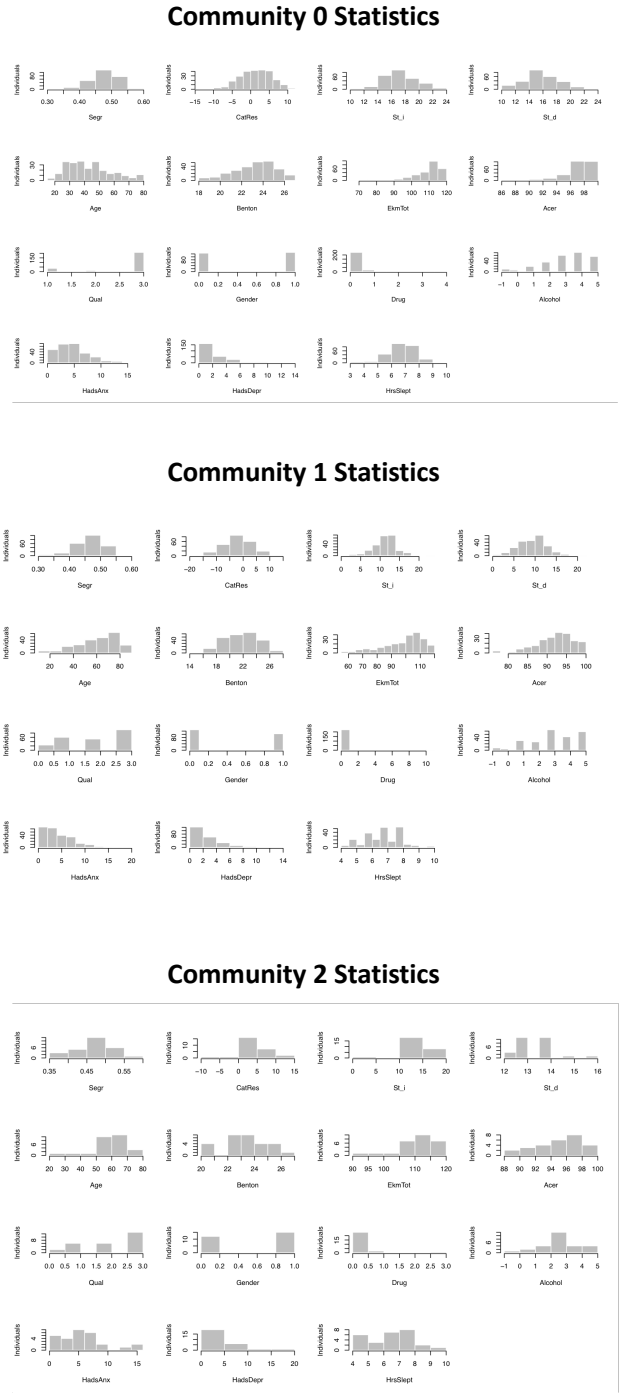

Figure 6.10: Histograms of the features of the three communities of individuals. Community 0 is composed by 255 individuals, community 1 by 231 individuals and community 2 by 27 individuals. Older individuals are mainly clustered in community 2. In each of them we considered the corresponding most correlated communities, which allowed us to identify the regions of grey matter that mostly characterized them.

Grey Matter ROIs Communities Strengths

Community 0 Individuals

Community ROI	Community Strenghts
1	0.68
2	0.77
3	0.71
4	0.70
5	0.72
6	0.56

Community 1 Individuals

Community ROIs	Community Strenghts
1	0.79
2	0.79
3	0.75
4	0.78
5	0.88
6	0.78
7	0.87
8	0.72
9	0.55

Community 2 Individuals

Community ROIs	Community Strenghts
1	0.76
2	0.66
3	NA (1 node only)
4	0.83
5	0.68
6	0.74
7	0.69
8	0.69

Figure 6.11: Summary of communities strengths for the grey matter ROIs. In yellow we highlighted the communities with the highest community network strength score. The value is included between 0 and 1 and all of the three top scorers present quite a high value

highest community network strength score is highlighted in yellow.

- Therefore, considering the highest network strengths communities of ROIS, we were able to identify the ROIs included in each community. The number of the most significant ROIs were less for the smallest community and higher for the ones having a higher number of individuals clustered inside. Summarizing: such regions are the brain regions mostly correlated and representatives of the three communities of individuals, previously obtained with the **NetRank** procedure. The regions identified are:
  - **Community 0**: R42:Opercular-Precentral, R43:Operculum-Insular, R44:Superior-Temporal-Gyrus-Planum-Polare, R45:Superior-Temporal-Gyrus-Heschls-Gyrus, R46:Superior-Temporal-Gyrus-Planum-Temporale-Transverse-Temporal-Gyrus, R90:Opercular-Precentral, R91:Parietal-Operculum-Insular,R92:Superior-Temporal-Gyrus-Planum-Polare, R93: Superior-Temporal-Gyrus-Heschls-Gyrus and R94: Superior-Temporal-Gyrus-Planum-Temporale-Transverse-Temporal-Gyrus

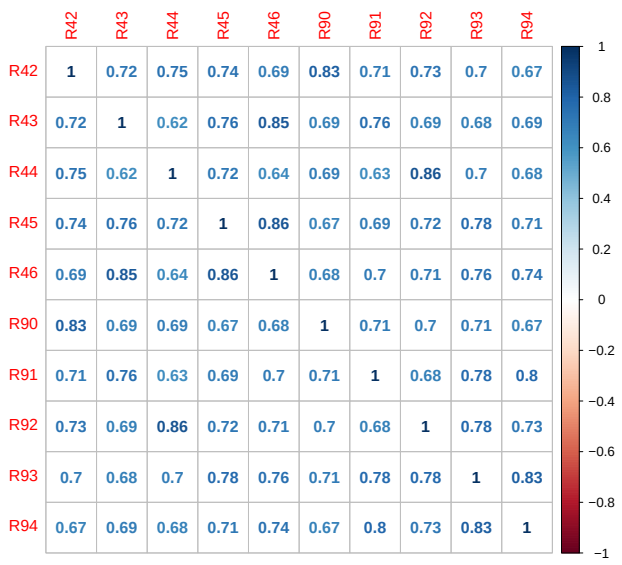

Figure 6.12: Pearson correlation coefficient of the representative ROIs, for the community 0 of individuals.

  - **Community 1**: R1: Middle-Frontal-Gyrus-Pole, R25: Medial-Frontal-Gyrus (Left), R27: Subcallosal-Gyrus (Left), R28:Anterior-ParaCingulate, R29:Anterior-Cingulate 24/33,R49:Middle-Frontal-Gyrus-Pole, R73:Medial-Frontal-Gyrus (Right), R75:Subcallosal-Gyrus (Right) and R76: Anterior-ParaCingulate (Right)
  - **Community 2**: R14: Inferior-Temporal-Gyrus-anterior (left,temporal), R53: Inferior-Frontal-Gyrus-triangularis (Right,frontal) and R62: Inferior-Temporal-Gyrus-anterior (right, temporal)

- We also show the Pearson correlation matrix of such subgroups of ROI regions, characterizing the three communities and presented in Figure 6.12, 6.13 and in Figure 6.14. As we can see, these identified regions are highly correlated among themselves, and can be considered as the ones that better represent each community of individuals. Interestingly enough all the three subgroups with the highest community strength score appear to be characterized by regions positively correlated among them. No clear pattern of correlations between the ROIs communities and lifestyle features was detected.

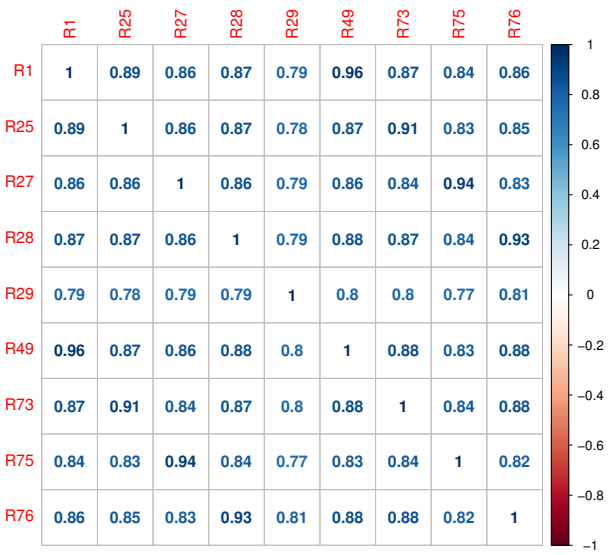

Figure 6.13: Pearson correlation coefficient of the representative ROIs, for community 1 of individuals

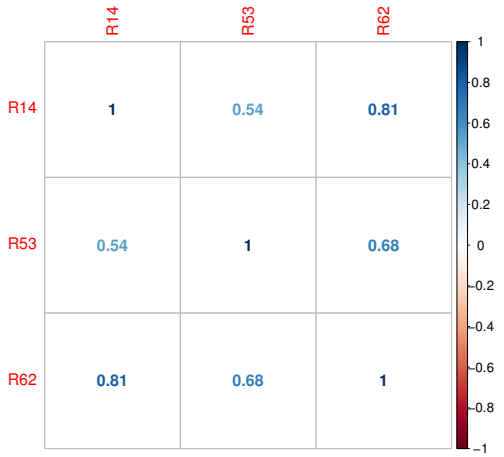

Figure 6.14: Pearson correlation coefficient of the representative ROIs for community 2 of the individuals

6.6 Summary

The study of healthy neurocognitive ageing is a central topic in psychology and neuroscience nowadays.
While genetics represents a factor, which is fixed, this is not true for lifestyle and other modifiable factors. Several studies show how correcting the lifestyle (avoid smoking, reducing alcohol consumptions and increase physical activity) can heavily reduce the risk of developing pathologies such as diabetes or heart coronary diseases [29]. An interesting study in the field is [80]. Here the authors analysed a cohort of more then 20.000 participants, from Norfolk, through 4 years, and aged between 45 to 79 [80] [28].
The results of the study were able to quantify thresholds in terms of number of alcohol units, fruit and vegetable consumption, and physical activity which were able to reduce the risk of mortality by 4 times [28]. Additionally it has been shown how modifying these behaviours, together with social and cognitive engagements, can meaningfully decrease also the risk of developing dementia and other neurocognitive diseases such as Alzheimer's [125] [126].
Therefore healthy neurocognitive ageing can be as well considerably affected by modifiable factors, such as physical activity and other lifestyles. Physical activity, for example, has been shown to have a beneficial effect in healthy cognitive ageing [10]. Further studies moreover show how other modifiable factors such as smoking [118] [115], alcohol [54], or dietary choices [133], can actually greatly contribute towards a healthy cognitive ageing process.
The Cam-CAN dataset represents a great opportunity to study the interaction among such factors. The cohexistence of lifestyle and modifiable factors, together with structural brain features, and cognitive variables, is, in fact, a great resource for researcher analysis and in depth understanding of the relationship between the two sets of information regarding the population studied.
To try to give an answer to such research questions, in our work we first decided to use a multilayer network approach, which could allow a study of the integration of lifestyle, cognitive and structural/functional brain features.
We constructed a pipeline of analysis called **NetRank**, in which the multilayer network modelling was also integrated by a community detection step.
We first performed an experiment which led to the construction of two different multilayer models: one constructed with the structural and functional brain features, and the

other one characterized by the lifestyle indicators.
In this way we could compute communities of individuals. From the results obtained we could see how groups of individuals, clustered according to features lifestyle, turned out to be more similar also in terms of structural and functional brain features. Such similarity between lifestyle didn't appear to be present, though, when considering individuals clustered according to the structural, functional and cognitive brain features. This could suggest how groups of individuals sharing similar lifestyles, could potentially be also characterized by similar structural and functional brain features, rather than the other way around. We then wanted to deeply study the role of different brain areas, and understand if there existed groups of brain regions mostly related to certain communities. For this reason we considered the communities obtained and then extracted the ROIs mostly characterizing such communities. Further work is needed for a better understanding of the identified ROIs.

6.7 Related publications

The present work has been accepted and presented as poster at the 2019 Organization for Human Brain Mapping Conference and Annual Meeting (OHBM), Rome, June 2019.

Chapter 7

Conclusion

In this dissertation we have investigated the application of multilayer networks for the modelling and the integration of different brain data types.
The availability of such multi-modal and diverse datasets, in the field of neuroscience, has in fact consequently determined the necessity of developing and applying algorithmic solutions. These are necessary to address the issue of integration, leaving results interpretable.
I will conclude the dissertation briefly summarising its contributions across the various chapters, before mentioning future developments and directions of the present work.

7.1 Contributions

- in **Chapter 3** I have introduced and studied the clinical question that guided our research for the ICP and HR interaction project. In this chapter, in fact, we present our own implementation of the crosstalks detection algorithm, that we applied to the ICP and HR time series of the two cohorts analysed.
  The detection and quantification of such events made it possible to proceed further with the modelling of the system. To the best of our knowledge is the first time that such clinical question is addressed in the literature. In the second part of the chapter, we present the multilayer modelling of such system. Each node in the graph represents a time stamp, and connections between two nodes are made according to the horizontal visibility graph definition, as given in Chapter 2.
  Again, to the best of our knowledge a multilayer network approach hasn't been applied so far to the analysis of ICP and HR systems. Summarizing the chapter

presents new tools for the identification of crosstalks, and a new modelling approach in terms of multilayer networks. Moreover the identification of the brain-heart crosstalks, represent a new clinical finding in the area, being the first time that this event has been studied and formalized in the literature.

- in **Chapter 4-5** we present a mortality prediction model for two cohorts of TBI patients: a paediatric and adult one. To the best of our knowledge is the first time that the interaction between brain-heart crosstalks and mortality is investigated. Moreover we extend such investigation, also to the networks measures obtained in Chapter 3. This is also a novelty in terms of computational modelling applied to the field. The clinical and biological findings of this chapter are of great interest too. The interaction and relationship between mortality and brain-heart crosstalks, in fact, sheds light on the possibility of a new parameter to be evaluated in TBI patients, for determining mortality probability. The work regarding TBI and HR that we present can be considered of interesting clinical impact. Confirming the results obtained in a bigger cohort, in fact, the brain-heart crosstalks could actually be included in a model for predicting and monitoring TBI patients, acquiring such events as possible indicators of the patients condition.

- in **Chapter 6** a new pipeline approach for the analysis of communities in multiplex network is proposed. In the pipeline, that we called **NetRank**, the ranking approach for constructing adjacency matrix of the corresponding graphs is introduced, to the best of our knowledge, for the first time. The analysis sheds light on the importance of lifestyle behaviour also towards a better understanding of structural, functional and cognitive measures of the population under investigation. All aspects which contribute heavily towards a better understanding of the neurocognitive ageing process. The computational tool proposed is exportable also to other field of investigations, where the integration between different data types is necessary.

7.2 Future work

The research described in the present dissertation may lay the ground to further explorations which can be conducted.
I will briefly summarize possible future developments of the research hereby presented.

Moreover I will also briefly sketch an additional research areas I am currently interested and involved in, which has not been included in the dissertation, still connected to the neuroscience field.

- Being the first time that the brain-heart crosstalks have been investigated and related to mortality, this leaves multiple possibilities in terms of future development of the current work. Further steps should include analysis of the predictive impact of this new parameter in a multivariate model, including other known, significant, predictors of outcome, like cerebral autoregulation and the initial presentation of the patient as assessed by IMPACT models. Should the cross-talk prove to contribute independent information to the outcome model, its use in real time quantification of the patient state severity, alongside with other physiological monitoring derived parameters, will become crucial. Advanced brain monitoring applications like ICM+ allow easy addition of the new metric into the battery of secondary parameters already available at the bedside, and further explorations into the usefulness of this index in a clinical environment. There is also much room for an extended investigation with regards to the modelling of the ICP-HR system using the multiplex approach. Further network measures could be obtained, studied and related to patients parameters.

- A new python interface of the code developed and presented in this thesis, is currently under implementation. This code will be released in the new ICM+ [132] Python plugin interface. In this way the brain-heart crosstalk variable will be included directly in the analysis of patients hospitalised for a TBI.

- The Cam-CAN dataset analysis, presents multiple aspects which could be further investigated. The role of the different brain areas, as well as the identification of further similarity within the clusters identified can be of importance and interest for future research.
  Cam-CAN also presents other types of data, which have not been integrated in the analysis discussed here (such as MEG information) and could therefore be included to expand the current work even more.
  Moreover in recent years, further similar projects of healthy cohorts of patients, have been released and it could be interesting to make a comparison between Cam-CAN and the available cohorts. Another interesting variable which we are currently investigating, to add to the analysis presented here, is genetics.

- During my PhD I have also worked on deep learning models and applications (as previously mentioned in the Introduction), and a future line of my research interests will lead towards the application of such methodologies to medical imaging. The area of deep learning (DL) and neuroimaging has seen in fact a wide expansion in the last few years, and various research projects have been devoted to the use of DL techniques for many different tasks.For example the brain ageing prediction using structural MRI, has seen a wide diffusion in many different applications from Alzheimer disease prediction [134], to segmentation tasks [2]. Is a field of research which looks promising and its applicability in the clinical area can bring to important improvements for the medical community.

Appendix 1

Table 7.1: Table showing the number of peaks, the number of peaks normalised, and the number of observations for each patient in the adult cohort subset of the CENTER-TBI dataset. Ct is the number of crosstalks, Obs are the number of observations per patients, and ct_{np} is the number of brain-heart crosstalks normalized.

Ct	Obs	ct_{np}
32	87905	0.10063
29	44833	0.09119
171	86736	0.53774
47	120979	0.14780
7	59843	0.02201
44	22098	0.13836
8	43540	0.02516
5	51667	0.01572
68	96048	0.21384
39	51626	0.12264
8	50329	0.02516
61	54045	0.19182
68	49315	0.21384
125	72321	0.39308
73	46652	0.22956
31	61020	0.09748
102	44679	0.32075

Ct	Obs	ct_{np}
110	44064	0.34591
3	1120	0.00943
12	5539	0.03774
71	37300	0.22327
3	31054	0.00943
86	52395	0.27044
11	60172	0.03459
85	120937	0.26730
14	30265	0.04403
58	60726	0.18239
11	32171	0.03459
16	17685	0.05031
4	22474	0.01258
12	44231	0.03774
89	51421	0.27987
45	66171	0.14151
11	43359	0.03459
6	54190	0.01887
35	48700	0.11006
29	116667	0.09119
16	34662	0.05031
135	65133	0.42453
54	38017	0.16981
132	50427	0.41509
57	58191	0.17925
2	111859	0.00629
4	35603	0.01258

Ct	Obs	ct_{np}
1	15834	0.00314
29	41473	0.09119
2	4567	0.00629
5	25300	0.01572
17	43083	0.05346
41	44204	0.12893
113	83505	0.35535
11	50368	0.03459
5	49210	0.01572
23	76315	0.07233
2	49879	0.00629
61	60282	0.19182
64	105270	0.20126
16	3210	0.05031
52	221155	0.16352
1	52319	0.00314
55	51354	0.17296
35	11738	0.11006
49	31474	0.15409
33	90845	0.10377
174	54343	0.54717
11	23708	0.03459
5	22781	0.01572
7	24936	0.02201
16	86084	0.05031
91	42392	0.28616
148	129677	0.46541

Ct	Obs	ct_{np}
29	50636	0.09119
71	129392	0.22327
120	72973	0.37736
27	58947	0.08491
51	31197	0.16038
36	35645	0.11321
86	40623	0.27044
3	8727	0.00943
282	77340	0.88679
283	53983	0.88994
19	11824	0.05975
24	13220	0.07547
51	32222	0.16038
10	30255	0.03145
1	4178	0.00314
10	38381	0.03145
68	41254	0.21384
2	23233	0.00629
65	53974	0.20440
46	10653	0.14465
318	80521	1.00000
27	17331	0.08491
91	18517	0.28616
59	76494	0.18553
155	42930	0.48742
287	89661	0.90252
7	50313	0.02201

Ct	Obs	ct_{np}
49	104080	0.15409
84	42212	0.26415
7	23832	0.02201
158	241919	0.49686
12	14470	0.03774
53	35314	0.16667
46	110350	0.14465
41	34469	0.12893
12	35258	0.03774
59	38435	0.18553
112	129812	0.35220
20	60612	0.06289
314	262919	0.98742
35	56740	0.11006
20	53047	0.06289
64	47023	0.20126
5	25961	0.01572
53	140275	0.16667
17	48304	0.05346
64	116738	0.20126
1	38794	0.00314
20	137816	0.06289
25	57178	0.07862
16	76909	0.05031
10	61345	0.03145
11	17131	0.03459
161	99902	0.50629

Ct	Obs	ct_{np}
94	16861	0.29560
5	52730	0.01572
44	101233	0.13836
11	22450	0.03459
6	42703	0.01887
30	51876	0.09434
97	41149	0.30503
1	8726	0.00314
32	60733	0.10063
39	20551	0.12264
23	62941	0.07233
125	56107	0.39308
116	79988	0.36478
19	95910	0.05975
1	4207	0.00314
18	13468	0.05660
91	144484	0.28616
38	15595	0.11950
3	39785	0.00943
45	67429	0.14151
219	106357	0.68868
192	69822	0.60377
12	57571	0.03774
26	50698	0.08176
62	162443	0.19497
1	50627	0.00314
34	13577	0.10692

Ct	Obs	ct_{np}
53	22540	0.16667
117	62729	0.36792
109	42863	0.34277
6	60363	0.01887
28	70261	0.08805
15	18083	0.04717
5	44094	0.01572
45	17733	0.14151
9	43200	0.02830
3	10126	0.00943
36	56381	0.11321
18	26941	0.05660
122	93602	0.38365
45	23403	0.14151
13	33858	0.04088
21	38085	0.06604
11	18385	0.03459
23	42424	0.07233
1	54514	0.00314
27	126680	0.08491
86	132733	0.27044
2	45697	0.00629
11	104453	0.03459
17	22920	0.05346
54	37841	0.16981
214	50096	0.67296
48	55667	0.15094

Ct	Obs	ct_{np}
5	60939	0.01572
1	69355	0.00314
39	105993	0.12264
65	62742	0.20440
22	24917	0.06918
8	67442	0.02516
30	50625	0.09434
57	25150	0.17925
19	148679	0.05975
33	20028	0.10377
81	40803	0.25472
26	201911	0.08176
14	64774	0.04403
30	103434	0.09434
97	51882	0.30503
24	22792	0.07547
60	102870	0.18868
8	52395	0.02516
1	44148	0.00314
1	24666	0.00314
66	32446	0.20755
32	41791	0.10063
3	13305	0.00943
59	58049	0.18553
167	32246	0.52516
54	29293	0.16981
39	47725	0.12264

Ct	Obs	ct_{np}
62	50340	0.19497
24	25631	0.07547
88	106870	0.27673
1	41801	0.00314
75	87111	0.23585
43	30429	0.13522
67	140169	0.21069
26	35501	0.08176
18	88351	0.05660
101	121654	0.31761
1	93	0.00314
1	12817	0.00314
114	78970	0.35849
213	118186	0.66981
42	103325	0.13208

Appendix 2

Table 7.2: Table showing the network measures for the CENTER-TBI cohort dataset. Each line is a patient. Individuals with less than 10 brain-heart crosstalks were assigned 0.5 in each column.

Mi_{nct}	Mi_{ct}	ω_{nct}	ω_{ct}
0.50823	0.58256	0.74677	0.75209
0.67607	0.54436	0.75050	0.75263
0.69838	0.72020	0.77040	0.77071
0.66693	0.64616	0.74127	0.74853
0.50000	0.50000	0.50000	0.50000
0.67461	0.71717	0.73395	0.74188
0.50000	0.50000	0.50000	0.50000
0.50000	0.50000	0.50000	0.50000
0.47477	0.61512	0.75473	0.73999
0.63255	0.57998	0.73881	0.73173
0.50000	0.50000	0.50000	0.50000
0.59329	0.52817	0.73373	0.74498
0.69232	0.58051	0.75524	0.72624
0.50662	0.60486	0.73976	0.74295
0.56162	0.61406	0.74859	0.74146
0.59270	0.58768	0.75126	0.74078
0.71793	0.69676	0.74795	0.74673
0.60724	0.56868	0.76329	0.72344

Mi_{nct}	Mi_{ct}	ω_{nct}	ω_{ct}
0.50000	0.50000	0.50000	0.50000
0.60319	0.58211	0.73317	0.73668
0.72865	0.62178	0.75208	0.76490
0.50000	0.50000	0.50000	0.50000
0.56858	0.55923	0.73038	0.71794
0.52517	0.48315	0.76168	0.74036
0.58114	0.59548	0.75230	0.73846
0.56168	0.56186	0.74377	0.73110
0.55776	0.50735	0.71857	0.72624
0.50646	0.45755	0.74535	0.74642
0.42402	0.41746	0.76961	0.76557
0.50000	0.50000	0.50000	0.50000
0.62557	0.57550	0.74459	0.73839
0.55353	0.49331	0.75125	0.73046
0.54953	0.47550	0.75511	0.74252
0.57513	0.52626	0.73842	0.73166
0.50000	0.50000	0.50000	0.50000
0.50778	0.46571	0.73470	0.75374
0.54535	0.57412	0.74501	0.73550
0.57312	0.52410	0.70936	0.72257
0.51257	0.58460	0.71716	0.71615
0.50487	0.55067	0.73224	0.72678
0.61760	0.57528	0.74420	0.77249
0.59854	0.67002	0.74809	0.75668
0.50000	0.50000	0.50000	0.50000
0.50000	0.50000	0.50000	0.50000
0.50000	0.50000	0.50000	0.50000

Mi_{nct}	Mi_{ct}	ω_{nct}	ω_{ct}
0.54629	0.57202	0.73597	0.74208
0.50000	0.50000	0.50000	0.50000
0.50000	0.50000	0.50000	0.50000
0.56078	0.52588	0.74743	0.74783
0.52218	0.55346	0.76737	0.73643
0.47660	0.50356	0.75468	0.76534
0.56379	0.53670	0.74570	0.74861
0.50000	0.50000	0.50000	0.50000
0.54417	0.59664	0.74659	0.74813
0.50000	0.50000	0.50000	0.50000
0.58270	0.65655	0.74397	0.73020
0.57531	0.62339	0.74540	0.74210
0.68167	0.63562	0.75386	0.75037
0.60388	0.62661	0.73228	0.72577
0.53390	0.51438	0.75262	0.74441
0.50000	0.50000	0.50000	0.50000
0.66127	0.83677	0.76828	0.78009
0.64091	0.53416	0.74806	0.74019
0.64319	0.67363	0.74762	0.74705
0.62775	0.57388	0.75316	0.75816
0.67844	0.66438	0.76731	0.76724
0.53714	0.51894	0.72976	0.73803
0.50000	0.50000	0.50000	0.50000
0.50000	0.50000	0.50000	0.50000
0.55930	0.47443	0.74613	0.75338
0.53715	0.58191	0.73883	0.73695
0.58269	0.58267	0.73409	0.74778

Mi_{nct}	Mi_{ct}	ω_{nct}	ω_{ct}
0.65064	0.62333	0.74577	0.75189
0.54430	0.51391	0.71399	0.71370
0.52065	0.56707	0.72966	0.73828
0.57989	0.55370	0.72690	0.74026
0.67402	0.50365	0.75614	0.75048
0.55195	0.53431	0.73683	0.73879
0.59538	0.69765	0.73425	0.75064
0.67797	0.71475	0.74883	0.75987
0.50000	0.50000	0.50000	0.50000
0.68854	0.70661	0.77137	0.77807
0.63524	0.65771	0.73879	0.73124
0.60373	0.61464	0.76209	0.74850
0.69409	0.49932	0.73318	0.73185
0.64053	0.66827	0.75103	0.75021
0.47794	0.51967	0.78553	0.73010
0.50000	0.50000	0.50000	0.50000
0.51840	0.48520	0.72610	0.72220
0.33905	0.47943	0.82301	0.82080
0.50000	0.50000	0.50000	0.50000
0.52282	0.53862	0.74255	0.72729
0.54858	0.52765	0.70991	0.71283
0.65311	0.70808	0.74607	0.73919
0.64287	0.61158	0.73825	0.73563
0.57064	0.61920	0.73080	0.74402
0.67235	0.52652	0.74937	0.73708
0.59289	0.60802	0.74966	0.73944
0.59373	0.57788	0.72598	0.72528

Mi_{nct}	Mi_{ct}	ω_{nct}	ω_{ct}
0.50000	0.50000	0.50000	0.50000
0.47410	0.45988	0.74854	0.75104
0.53595	0.61715	0.75394	0.75886
0.50000	0.50000	0.50000	0.50000
0.56547	0.66991	0.79659	0.76221
0.58047	0.68459	0.75520	0.76535
0.54862	0.66437	0.77348	0.74851
0.50194	0.48041	0.72506	0.72192
0.60133	0.46096	0.74207	0.75329
0.55624	0.49295	0.73769	0.73358
0.56738	0.63077	0.75512	0.75617
0.57912	0.57578	0.74332	0.73172
0.62818	0.57008	0.75785	0.77947
0.50859	0.60023	0.75188	0.74583
0.55046	0.50960	0.72942	0.73582
0.58121	0.52802	0.73152	0.73627
0.58979	0.61596	0.73910	0.73411
0.50000	0.50000	0.50000	0.50000
0.66383	0.67576	0.76307	0.74921
0.60275	0.59101	0.75418	0.73524
0.49368	0.56284	0.71351	0.71879
0.50000	0.50000	0.50000	0.50000
0.46957	0.52453	0.73969	0.74113
0.47924	0.53525	0.74162	0.73166
0.48676	0.53413	0.76068	0.77070
0.57051	0.50507	0.74684	0.75018
0.55685	0.49377	0.74987	0.75038

Mi_{nct}	Mi_{ct}	ω_{nct}	ω_{ct}
0.56526	0.57013	0.73245	0.73338
0.63034	0.61415	0.73485	0.73245
0.50000	0.50000	0.50000	0.50000
0.48767	0.50204	0.73060	0.75084
0.63668	0.58965	0.78702	0.76112
0.50000	0.50000	0.50000	0.50000
0.58978	0.58673	0.72945	0.74043
0.56873	0.60782	0.73061	0.73727
0.50000	0.50000	0.50000	0.50000
0.53475	0.51824	0.74171	0.74136
0.45939	0.51450	0.71506	0.71223
0.53762	0.47321	0.73928	0.73951
0.64558	0.61737	0.74092	0.74188
0.61996	0.69534	0.74241	0.75104
0.52081	0.51418	0.72514	0.73468
0.50000	0.50000	0.50000	0.50000
0.64732	0.63011	0.74640	0.75770
0.63713	0.52537	0.73796	0.74443
0.51456	0.58477	0.72454	0.73534
0.50000	0.50000	0.50000	0.50000
0.64406	0.65800	0.73210	0.75179
0.51357	0.50310	0.73710	0.75838
0.59141	0.48043	0.72056	0.71883
0.49225	0.54748	0.73399	0.71512
0.49521	0.53394	0.71036	0.71631
0.51326	0.44564	0.73608	0.78085
0.56306	0.50423	0.75509	0.73830

Mi_{nct}	Mi_{ct}	ω_{nct}	ω_{ct}
0.50000	0.50000	0.50000	0.50000
0.49341	0.48693	0.71516	0.71410
0.53472	0.57219	0.73603	0.74513
0.74231	0.64914	0.75461	0.75330
0.54488	0.51297	0.72817	0.72998
0.50000	0.50000	0.50000	0.50000
0.57955	0.54986	0.73783	0.74910
0.56465	0.53981	0.74224	0.74343
0.50000	0.50000	0.50000	0.50000
0.60992	0.58385	0.71741	0.72406
0.50000	0.50000	0.50000	0.50000
0.50000	0.50000	0.50000	0.50000
0.55236	0.55592	0.74600	0.72677
0.57708	0.56153	0.74821	0.76567
0.55804	0.51928	0.77328	0.75463
0.59541	0.61102	0.73864	0.74618
0.43461	0.50840	0.74322	0.74408
0.54424	0.52519	0.73873	0.73857
0.60099	0.47044	0.72872	0.73189
0.62392	0.59213	0.74784	0.75046
0.50000	0.50000	0.50000	0.50000
0.56080	0.46969	0.74737	0.76043
0.57626	0.57203	0.74305	0.73935
0.50000	0.50000	0.50000	0.50000
0.50000	0.50000	0.50000	0.50000
0.56790	0.58470	0.74831	0.74960
0.70730	0.59267	0.75627	0.74813

Mi_{nct}	Mi_{ct}	ω_{nct}	ω_{ct}
0.73044	0.69460	0.75202	0.75331
0.62264	0.56650	0.72791	0.72778
0.62089	0.64644	0.75073	0.72849
0.50000	0.50000	0.50000	0.50000
0.50000	0.50000	0.50000	0.50000
0.51009	0.45621	0.72395	0.74234
0.70306	0.62257	0.77299	0.75265
0.59521	0.57052	0.74214	0.73685
0.50000	0.50000	0.50000	0.50000
0.70434	0.72240	0.74522	0.75580
0.61600	0.59855	0.75804	0.74653
0.54338	0.60230	0.74181	0.75488
0.52695	0.57987	0.73425	0.72621
0.50808	0.51712	0.72683	0.71991
0.53873	0.51026	0.73999	0.74212
0.46281	0.47290	0.77037	0.74146
0.58123	0.62366	0.73905	0.73742
0.53872	0.55388	0.73915	0.73778
0.54262	0.53582	0.72562	0.73108
0.64023	0.60463	0.73938	0.72748
0.50000	0.50000	0.50000	0.50000
0.50000	0.50000	0.50000	0.50000
0.50000	0.50000	0.50000	0.50000
0.60398	0.67616	0.75998	0.77501
0.89657	0.64166	0.77333	0.74996
0.50000	0.50000	0.50000	0.50000
0.51485	0.42776	0.71745	0.74325

Mi_{nct}	Mi_{ct}	ω_{nct}	ω_{ct}
0.63798	0.64894	0.73643	0.72573
0.62493	0.69326	0.76004	0.77368
0.49003	0.44196	0.75245	0.72269
0.58294	0.56199	0.74491	0.75968
0.68047	0.57348	0.74095	0.74690
0.54984	0.56217	0.75189	0.76082
0.51627	0.53878	0.73290	0.72443
0.50000	0.50000	0.50000	0.50000
0.55760	0.52315	0.73776	0.74515
0.74422	0.73744	0.77882	0.77886
0.49710	0.47020	0.73573	0.73054
0.56479	0.57501	0.73297	0.73194
0.52757	0.59393	0.73340	0.73476
0.59367	0.45398	0.72726	0.73196
0.50000	0.50000	0.50000	0.50000
0.50000	0.50000	0.50000	0.50000
0.61100	0.52088	0.72644	0.73229
0.50652	0.53915	0.70885	0.71738
0.51094	0.45428	0.72263	0.72855

Bibliography

[1] Ahmadlou, M., Adeli, H., and Adeli, A. (2010). New diagnostic eeg markers of the alzheimer's disease using visibility graph. *Journal of neural transmission*, 117(9):1099--1109.

[2] Akkus, Z., Galimzianova, A., Hoogi, A., Rubin, D. L., and Erickson, B. J. (2017). Deep learning for brain mri segmentation: state of the art and future directions. *Journal of digital imaging*, 30(4):449--459.

[3] Alvo, M. and Philip, L. (2014). *Statistical methods for ranking data*. Springer.

[4] Angione, C. and Lió, P. (2015). Predictive analytics of environmental adaptability in multi-omic network models. *Scientific reports*, 5:15147.

[5] Asgari, S., Adams, H., Kasprowicz, M., Czosnyka, M., Smielewski, P., and Ercole, A. (2019). Feasibility of hidden markov models for the description of time-varying physiologic state after severe traumatic brain injury. *Critical care medicine*, 47(11):e880--e885.

[6] Azzini, I., Dell'Anna, R., Ciocchetta, F., Demichelis, F., Sboner, A., Blanzieri, E., and Malossini, A. (2004). Simple methods for peak detection in time series microarray data. *Proc. CAMDA'04 (Critical Assessment of Microarray Data)*.

[7] Banerjee, A., Dolado, J. J., Galbraith, J. W., Hendry, D., et al. (1993). Co-integration, error correction, and the econometric analysis of non-stationary data. *OUP Catalogue*.

[8] Barabási, A.-L. et al. (2016). *Network science*. Cambridge university press.

[9] Barnes, J., Ridgway, G. R., Bartlett, J., Henley, S. M., Lehmann, M., Hobbs, N., Clarkson, M. J., MacManus, D. G., Ourselin, S., and Fox, N. C. (2010). Head

size, age and gender adjustment in mri studies: a necessary nuisance? *Neuroimage*, 53(4):1244--1255.

[10] Barnes, J. N. (2015). Exercise, cognitive function, and aging. *Advances in physiology education*, 39(2):55--62.

[11] Battiston, F., Nicosia, V., and Latora, V. (2014). Structural measures for multiplex networks. *Physical Review E*, 89(3):032804.

[12] Bell, E. T. (1934). Exponential polynomials. *Annals of Mathematics*, pages 258--277.

[13] Benton, A. L., Sivan, A. B., deS Hamsher, K., and Varney, N. R. (1994). *Contributions to neuropsychological assessment: A clinical manual*. Oxford University Press, USA.

[14] Bianconi, G. (2013). Statistical mechanics of multiplex networks: Entropy and overlap. *Physical Review E*, 87(6):062806.

[15] Blondel, V. D., Guillaume, J.-L., Lambiotte, R., and Lefebvre, E. (2008). Fast unfolding of communities in large networks. *Journal of statistical mechanics: theory and experiment*, 2008(10):P10008.

[16] Boccaletti, S., Bianconi, G., Criado, R., Del Genio, C. I., Gómez-Gardenes, J., Romance, M., Sendina-Nadal, I., Wang, Z., and Zanin, M. (2014). The structure and dynamics of multilayer networks. *Physics Reports*, 544(1):1--122.

[17] Boccaletti, S., Latora, V., Moreno, Y., Chavez, M., and Hwang, D.-U. (2006). Complex networks: Structure and dynamics. *Physics reports*, 424(4):175--308.

[18] Bollobás, B. (2013). *Modern graph theory*, volume 184. Springer Science & Business Media.

[19] Bonett, D. G. (2019). Point-biserial correlation: Interval estimation, hypothesis testing, meta-analysis, and sample size determination. *British Journal of Mathematical and Statistical Psychology*.

[20] Box, G. E. and Pierce, D. A. (1970). Distribution of residual autocorrelations in autoregressive-integrated moving average time series models. *Journal of the American statistical Association*, 65(332):1509--1526.

[21] Branting, L. K. (2012). Context-sensitive detection of local community structure. *Social Network Analysis and Mining*, 2(3):279--289.

[22] Brenner, S. (1974). The genetics of caenorhabditis elegans. *Genetics*, 77(1):71--94.

[23] Bullmore, E. and Sporns, O. (2009). Complex brain networks: graph theoretical analysis of structural and functional systems. *Nature reviews neuroscience*, 10(3):186.

[24] Burke, S. N. and Barnes, C. A. (2006). Neural plasticity in the ageing brain. *Nature Reviews Neuroscience*, 7(1):30--40.

[25] Buysse, D. J., Reynolds III, C. F., Monk, T. H., Berman, S. R., and Kupfer, D. J. (1989). The pittsburgh sleep quality index: a new instrument for psychiatric practice and research. *Psychiatry research*, 28(2):193--213.

[26] Cabella, B., Donnelly, J., Cardim, D., Liu, X., Cabeleira, M., Smielewski, P., Haubrich, C., Hutchinson, P. J., Kim, D.-J., and Czosnyka, M. (2017). An association between icp-derived data and outcome in tbi patients: the role of sample size. *Neurocritical care*, 27(1):103--107.

[27] Cabeza, R., Anderson, N. D., Locantore, J. K., and McIntosh, A. R. (2002). Aging gracefully: compensatory brain activity in high-performing older adults. *Neuroimage*, 17(3):1394--1402.

[28] Cadar, D. (2018). Cognitive ageing. *Geriatrics Health, DOI: 10.5772 intechopen.79119*, pages 1--49.

[29] Cadar, D., Pikhart, H., Mishra, G., Stephen, A., Kuh, D., and Richards, M. (2012). The role of lifestyle behaviors on 20-year cognitive decline. *Journal of aging research*, 2012.

[30] Cattell, R. B. (1971). Abilities: Their structure, growth, and action, *Houghton Mifflin*.

[31] Chen, J. and Yuan, B. (2006). Detecting functional modules in the yeast protein--protein interaction network. *Bioinformatics*, 22(18):2283--2290.

[32] Chen, J., Zaïane, O., and Goebel, R. (2009). Local community identification in social networks. In *2009 International Conference on Advances in Social Network Analysis and Mining*, pages 237--242. IEEE.

[33] Cheung, K.-H., Lim, E., Samwald, M., Chen, H., Marenco, L., Holford, M. E., Morse, T. M., Mutalik, P., Shepherd, G. M., and Miller, P. L. (2009). Approaches to neuroscience data integration. *Briefings in bioinformatics*, 10(4):345--353.

[34] Chong, S.-L., Liu, N., Barbier, S., and Ong, M. E. H. (2015). Predictive modeling in pediatric traumatic brain injury using machine learning. *BMC medical research methodology*, 15(1):22.

[35] Collaborators, M. C. T. (2008). Predicting outcome after traumatic brain injury: practical prognostic models based on large cohort of international patients. *Bmj*, 336(7641):425--429.

[36] Cooke, R., McNicholl, B., and Byrnes, D. (1995). Use of the injury severity score in head injury. *Injury*, 26(6):399--400.

[37] Cozzo, E., Kivelä, M., De Domenico, M., Solé-Ribalta, A., Arenas, A., Gómez, S., Porter, M. A., and Moreno, Y. (2015). Structure of triadic relations in multiplex networks. *New Journal of Physics*, 17(7):073029.

[38] Czosnyka, M. and Pickard, J. D. (2004). Monitoring and interpretation of intracranial pressure. *Journal of Neurology, Neurosurgery & Psychiatry*, 75(6):813--821.

[39] D'Abrera, H. and Lehmann, E. (1975). *Nonparametrics: statistical methods based on ranks*. Holden-Day.

[40] Davis, S. W., Dennis, N. A., Daselaar, S. M., Fleck, M. S., and Cabeza, R. (2008). Que pasa? the posterior--anterior shift in aging. *Cerebral cortex*, 18(5):1201--1209.

[41] De Domenico, M., Granell, C., Porter, M. A., and Arenas, A. (2016). The physics of spreading processes in multilayer networks. *Nature Physics*, 12:901–906.

[42] De Domenico, M., Nicosia, V., Arenas, A., and Latora, V. (2015). Structural reducibility of multilayer networks. *Nature communications*, 6:6864.

[43] De Domenico, M., Solé-Ribalta, A., Cozzo, E., Kivelä, M., Moreno, Y., Porter, M. A., Gómez, S., and Arenas, A. (2013). Mathematical formulation of multilayer networks. *Physical Review X*, 3(4):041022.

[44] Dijkland, S. A., Foks, K. A., Polinder, S., Dippel, D. W., Maas, A. I., Lingsma, H. F., and Steyerberg, E. W. (2020). Prognosis in moderate and severe traumatic brain injury: a systematic review of contemporary models and validation studies. *Journal of neurotrauma*, 37(1):1--13.

[45] Dimitri, G. M., Agrawal, S., Young, A., Donnelly, J., Liu, X., Smielewski, P., Hutchinson, P., Czosnyka, M., Lio, P., and Haubrich, C. (2018). Simultaneous transients of intracranial pressure and heart rate in traumatic brain injury: Methods of analysis. In *Intracranial Pressure & Neuromonitoring XVI*, pages 147--151. Springer.

[46] Donges, J. F., Zou, Y., Marwan, N., and Kurths, J. (2009). Complex networks in climate dynamics. *The European Physical Journal Special Topics*, 174(1):157--179.

[47] Easter, J. S., Bakes, K., Dhaliwal, J., Miller, M., Caruso, E., and Haukoos, J. S. (2014). Comparison of pecarn, catch, and chalice rules for children with minor head injury: a prospective cohort study. *Annals of emergency medicine*, 64(2):145--152.

[48] Faes, L., Greco, A., Lanata, A., Barbieri, R., Scilingo, E. P., and Valenza, G. (2017). Causal brain-heart information transfer during visual emotional elicitation in healthy subjects: Preliminary evaluations and future perspectives. In *2017 39th Annual International Conference of the IEEE Engineering in Medicine and Biology Society (EMBC)*, pages 1559--1562. IEEE.

[49] Figaji, A. A. (2017). Anatomical and physiological differences between children and adults relevant to traumatic brain injury and the implications for clinical assessment and care. *Frontiers in neurology*, 8:685.

[50] Forman, G. and Cohen, I. (2004). Learning from little: Comparison of classifiers given little training. In *European Conference on Principles of Data Mining and Knowledge Discovery*, pages 161--172. Springer.

[51] Friedman, J., Hastie, T., and Tibshirani, R. (2010). Regularization paths for generalized linear models via coordinate descent. *Journal of statistical software*, 33(1):1.

[52] Friston, K. J. (2003). Statistical parametric mapping. In *Neuroscience databases*, pages 237--250. Springer.

[53] Galloway, N. R., Tong, K. A., Ashwal, S., Oyoyo, U., and Obenaus, A. (2008). Diffusion-weighted imaging improves outcome prediction in pediatric traumatic brain injury. *Journal of neurotrauma*, 25(10):1153--1162.

[54] Ganguli, M., Vander Bilt, J., Saxton, J., Shen, C., and Dodge, H. (2005). Alcohol consumption and cognitive function in late life: a longitudinal community study. *Neurology*, 65(8):1210--1217.

[55] Gao, L., Smielewski, P., Czosnyka, M., and Ercole, A. (2016). Cerebrovascular signal complexity six hours after intensive care unit admission correlates with outcome after severe traumatic brain injury. *Journal of neurotrauma*, 33(22):2011--2018.

[56] Gao, L., Smielewski, P., Czosnyka, M., and Ercole, A. (2017). Early asymmetric cardio-cerebral causality and outcome after severe traumatic brain injury. *Journal of neurotrauma*, 34(19):2743--2752.

[57] Garg, K., Sharma, R., Gupta, D., Sinha, S., Satyarthee, G. D., Agarwal, D., Kale, S. S., Sharma, B. S., and Mahapatra, A. K. (2017). Outcome predictors in pediatric head trauma: A study of clinicoradiological factors. *Journal of pediatric neurosciences*, 12(2):149.

[58] Geerligs, L., Rubinov, M., Henson, R. N., et al. (2015). State and trait components of functional connectivity: individual differences vary with mental state. *Journal of Neuroscience*, 35(41):13949--13961.

[59] Giva, M. and newman, M. E. (2002). Community structure in social and biological networks. *Proceeding of the national academy of sciences*, 99(12):78217826.

[60] Giza, C. C., Mink, R. B., and Madikians, A. (2007). Pediatric traumatic brain injury: not just little adults. *Current opinion in critical care*, 13(2):143--152.

[61] Granger, C. W. (1969). Investigating causal relations by econometric models and cross-spectral methods. *Econometrica: Journal of the Econometric Society*, pages 424--438.

[62] Granovetter, M. S. (1977). The strength of weak ties. In *Social networks*, pages 347--367. Elsevier.

[63] Greenwood, P. (2007). Functional plasticity in cognitive aging: review and hypothesis. *Neuropsychology*, 21(6):657.

[64] Hastie, T. and Qian, J. (2014). Glmnet vignette. *Retrieved June*, 9(2016):1--30.

[65] Healy, P., Hunt, G., Kilroy, S., Lynn, T., Morrison, J. P., and Venkatagiri, S. (2015). Evaluation of peak detection algorithms for social media event detection. In *2015 10th International Workshop on Semantic and Social Media Adaptation and Personalization (SMAP)*, pages 1--9. IEEE.

[66] Herrgård, M. J., Swainston, N., Dobson, P., Dunn, W. B., Arga, K. Y., Arvas, M., Blüthgen, N., Borger, S., Costenoble, R., Heinemann, M., et al. (2008). A consensus yeast metabolic network reconstruction obtained from a community approach to systems biology. *Nature biotechnology*, 26(10):1155.

[67] Hoerl, A. E. and Kennard, R. W. (1970). Ridge regression: Biased estimation for nonorthogonal problems. *Technometrics*, 12(1):55--67.

[68] Hristova, D., Rutherford, A., Anson, J., Luengo-Oroz, M., and Mascolo, C. (2016). The international postal network and other global flows as proxies for national wellbeing. *PloS one*, 11(6):e0155976.

[69] Hu, X., Miller, C., Vespa, P., and Bergsneider, M. (2008). Adaptive computation of approximate entropy and its application in integrative analysis of irregularity of heart rate variability and intracranial pressure signals. *Medical engineering & physics*, 30(5):631--639.

[70] Hu, X., Nenov, V., Bergsneider, M., Glenn, T. C., Vespa, P., and Martin, N. (2007a). Estimation of hidden state variables of the intracranial system using constrained nonlinear kalman filters. *IEEE transactions on biomedical engineering*, 54(4):597--610.

[71] Hu, X., Nenov, V., Vespa, P., and Bergsneider, M. (2007b). Characterization of interdependency between intracranial pressure and heart variability signals: A causal spectral measure and a generalized synchronization measure. *IEEE transactions on biomedical engineering*, 54(8):1407--1417.

[72] Hu, X., Xu, P., Scalzo, F., Vespa, P., and Bergsneider, M. (2009). Morphological clustering and analysis of continuous intracranial pressure. *IEEE Transactions on Biomedical Engineering*, 56(3):696--705.

[73] Hukkelhoven, C. W., Steyerberg, E. W., Habbema, J. D. F., Farace, E., Marmarou, A., Murray, G. D., Marshall, L. F., and Maas, A. I. (2005). Predicting outcome after traumatic brain injury: development and validation of a prognostic score based on admission characteristics. *Journal of neurotrauma*, 22(10):1025--1039.

[74] Iacovacci, J. and Lacasa, L. (2016). Sequential visibility-graph motifs. *Physical Review E*, 93(4):042309.

[75] Interdonato, R., Tagarelli, A., Ienco, D., Sallaberry, A., and Poncelet, P. (2017). Local community detection in multilayer networks. *Data Mining and Knowledge Discovery*, 31(5):1444--1479.

[76] Jeong, H., Mason, S. P., Barabási, A.-L., and Oltvai, Z. N. (2001). Lethality and centrality in protein networks. *Nature*, 411(6833):41.

[77] Johansson, B. B. (2000). Brain plasticity and stroke rehabilitation: the willis lecture. *Stroke*, 31(1):223--230.

[78] Kayhanian, S., Young, A. M., Ewen, R. L., Piper, R. J., Guilfoyle, M. R., Donnelly, J., Fernandes, H. M., Garnett, M., Smielewski, P., Czosnyka, M., et al. (2019). Thresholds for identifying pathological intracranial pressure in paediatric traumatic brain injury. *Scientific reports*, 9(1):3537.

[79] Kernighan, B. W. and Lin, S. (1970). An efficient heuristic procedure for partitioning graphs. *Bell system technical journal*, 49(2):291--307.

[80] Khaw, K.-T., Wareham, N., Bingham, S., Welch, A., Luben, R., and Day, N. (2008). Combined impact of health behaviours and mortality in men and women: the epic-norfolk prospective population study. *PLoS medicine*, 5(1):e12.

[81] Kolb, B. and Whishaw, I. Q. (1998). Brain plasticity and behavior. *Annual review of psychology*, 49(1):43--64.

[82] Lacasa, L., Luque, B., Ballesteros, F., Luque, J., and Nuno, J. C. (2008). From time series to complex networks: The visibility graph. *Proceedings of the National Academy of Sciences*, 105(13):4972--4975.

[83] Lacasa, L., Nicosia, V., and Latora, V. (2014). Network structure of multivariate time series. *Scientific reports*, 5:15508--15508.

[84] Lacasa, L., Nunez, A., Roldán, É., Parrondo, J. M., and Luque, B. (2012). Time series irreversibility: a visibility graph approach. *The European Physical Journal B*, 85(6):217.

[85] Langfelder, P. and Horvath, S. (2008). Wgcna: an r package for weighted correlation network analysis. *BMC bioinformatics*, 9(1):559.

[86] Larcher, V., Craig, F., Bhogal, K., Wilkinson, D., Brierley, J., et al. (2015). Making decisions to limit treatment in life-limiting and life-threatening conditions in children: a framework for practice. *Archives of disease in childhood*, 100(Suppl 2):s1--s23.

[87] Latora, V., Nicosia, V., and Russo, G. (2017). *Complex networks: principles, methods and applications*. Cambridge University Press.

[88] Lee, J. D., Sun, D. L., Sun, Y., Taylor, J. E., et al. (2016). Exact post-selection inference, with application to the lasso. *The Annals of Statistics*, 44(3):907--927.

[89] Lewis, K., Kaufman, J., Gonzalez, M., Wimmer, A., and Christakis, N. (2008). Tastes, ties, and time: A new social network dataset using facebook. com. *Social networks*, 30(4):330--342.

[90] Li, Y., He, K., Bindel, D., and Hopcroft, J. E. (2015). Uncovering the small community structure in large networks: A local spectral approach. In *Proceedings of the 24th international conference on world wide web*, pages 658--668. International World Wide Web Conferences Steering Committee.

[91] Loe, C. W. and Jensen, H. J. (2015). Comparison of communities detection algorithms for multiplex. *Physica A: Statistical Mechanics and its Applications*, 431:29--45.

[92] Long, Y. (2013). Visibility graph network analysis of gold price time series. *Physica A: Statistical Mechanics and its Applications*, 392(16):3374--3384.

[93] Luque, B., Lacasa, L., Ballesteros, F., and Luque, J. (2009). Horizontal visibility graphs: Exact results for random time series. *Physical Review E*, 80(4):046103.

[94] Maas, A. I., Menon, D. K., Adelson, P. D., Andelic, N., Bell, M. J., Belli, A., Bragge, P., Brazinova, A., Büki, A., Chesnut, R. M., et al. (2017). Traumatic brain

injury: integrated approaches to improve prevention, clinical care, and research. *The Lancet Neurology*, 16(12):987--1048.

[95] Maas, A. I., Menon, D. K., Steyerberg, E. W., Citerio, G., Lecky, F., Manley, G. T., Hill, S., Legrand, V., and Sorgner, A. (2014). Collaborative european neurotrauma effectiveness research in traumatic brain injury (center-tbi) a prospective longitudinal observational study. *Neurosurgery*, 76(1):67--80.

[96] Maas, A. I., Murray, G. D., Roozenbeek, B., Lingsma, H. F., Butcher, I., McHugh, G. S., Weir, J., Lu, J., Steyerberg, E. W., on Prognosis Analysis of Clinical Trials in Traumatic Brain Injury (IMPACT) Study Group, I. M., et al. (2013). Advancing care for traumatic brain injury: findings from the impact studies and perspectives on future research. *The Lancet Neurology*, 12(12):1200--1210.

[97] Mann, H. B. and Whitney, D. R. (1947). On a test of whether one of two random variables is stochastically larger than the other. *The annals of mathematical statistics*, pages 50--60.

[98] Marek, K., Jennings, D., Lasch, S., Siderowf, A., Tanner, C., Simuni, T., Coffey, C., Kieburtz, K., Flagg, E., Chowdhury, S., et al. (2011). The parkinson progression marker initiative (ppmi). *Progress in neurobiology*, 95(4):629--635.

[99] Marwan, N., Donges, J. F., Zou, Y., Donner, R. V., and Kurths, J. (2009). Complex network approach for recurrence analysis of time series. *Physics Letters A*, 373(46):4246--4254.

[100] Massucci, F. A. and Docampo, D. (2019). Measuring the academic reputation through citation networks via pagerank. *Journal of Informetrics*, 13(1):185--201.

[101] Motyka, P., Grund, M., Forschack, N., Al, E., Villringer, A., and Gaebler, M. (2019). Interactions between cardiac activity and conscious somatosensory perception. *Psychophysiology*, 56(10):e13424.

[102] Mucha, P. J., Richardson, T., Macon, K., Porter, M., and Onnela, J.-P. (2010a). Community structure in time-dependent, multiscale, and multiplex networks. *Science Reports*, pages 876--878.

[103] Mucha, P. J., Richardson, T., Macon, K., Porter, M. A., and Onnela, J.-P. (2010b). Community structure in time-dependent, multiscale, and multiplex networks. *science*, 328(5980):876--878.

[104] Mueller, S. G., Weiner, M. W., Thal, L. J., Petersen, R. C., Jack, C. R., Jagust, W., Trojanowski, J. Q., Toga, A. W., and Beckett, L. (2005). Ways toward an early diagnosis in alzheimer's disease: the alzheimer's disease neuroimaging initiative (adni). *Alzheimer's & Dementia*, 1(1):55--66.

[105] Mushkudiani, N. A., Hukkelhoven, C. W., Hernández, A. V., Murray, G. D., Choi, S. C., Maas, A. I., and Steyerberg, E. W. (2008). A systematic review finds methodological improvements necessary for prognostic models in determining traumatic brain injury outcomes. *Journal of clinical epidemiology*, 61(4):331--343.

[106] Nations, U. (2002). *World population ageing, 1950-2050*. UN.

[107] Nepusz, T., Yu, H., and Paccanaro, A. (2012). Detecting overlapping protein complexes in protein-protein interaction networks. *Nature methods*, 9(5):471.

[108] Newman, M. (2018a). *Networks*. Oxford university press.

[109] Newman, M. (2018b). *Networks*. Oxford university press.

[110] Newman, M. E. (2004). Fast algorithm for detecting community structure in networks. *Physical review E*, 69(6):066133.

[111] Newman, M. E. (2006). Modularity and community structure in networks. *Proceedings of the national academy of sciences*, 103(23):8577--8582.

[112] Newman, M. E. and Girvan, M. (2004). Finding and evaluating community structure in networks. *Physical review E*, 69(2):026113.

[113] Nuñez, A. M., Luque, B., Gomez, J. P., and Lacasa, L. (2012). *Visibility algorithms: A short review, INTECH Open Access Publisher*.

[114] on Medical Aspects of Automotive Safety, C. (1971). Rating the severity of tissue damage. i. the abbreviated scale. *Jama*, 215(2):277--280.

[115] Ott, A., Slooter, A., Hofman, A., van Harskamp, F., Witteman, J., Van Broeckhoven, C., Van Duijn, C., and Breteler, M. (1998). Smoking and risk of dementia and alzheimer's disease in a population-based cohort study: the rotterdam study. *The Lancet*, 351(9119):1840--1843.

[116] Palshikar, G. et al. (2009). Simple algorithms for peak detection in time-series. In *Proc. 1st Int. Conf. Advanced Data Analysis, Business Analytics and Intelligence*, pages 1--13.

[117] Perel, P., Edwards, P., Wentz, R., and Roberts, I. (2006). Systematic review of prognostic models in traumatic brain injury. *BMC medical informatics and decision making*, 6(1):38.

[118] Peters, R., Poulter, R., Warner, J., Beckett, N., Burch, L., and Bulpitt, C. (2008). Smoking, dementia and cognitive decline in the elderly, a systematic review. *BMC geriatrics*, 8(1):36.

[119] Ravasz, E., Somera, A. L., Mongru, D. A., Oltvai, Z. N., and Barabási, A.-L. (2002). Hierarchical organization of modularity in metabolic networks. *science*, 297(5586):1551--1555.

[120] Saeys, Y., Inza, I., and Larrañaga, P. (2007). A review of feature selection techniques in bioinformatics. *bioinformatics*, 23(19):2507--2517.

[121] Said, S. E. and Dickey, D. A. (1984). Testing for unit roots in autoregressive-moving average models of unknown order. *Biometrika*, 71(3):599--607.

[122] Sala-Llonch, R., Bartrés-Faz, D., and Junqué, C. (2015). Reorganization of brain networks in aging: a review of functional connectivity studies. *Frontiers in psychology*, 6:663.

[123] Sannino, S., Lacasa, L., Marinazzo, D., et al. (2017). Visibility graphs for fmri data: multiplex temporal graphs and their modulations across resting state networks. *bioRxiv*, page 106443.

[124] Satulovsky, J. E. (2010). Detecting peaks in two-dimensional signals. US Patent App. 12/463,566.

[125] Scarmeas, N., Luchsinger, J. A., Schupf, N., Brickman, A. M., Cosentino, S., Tang, M. X., and Stern, Y. (2009). Physical activity, diet, and risk of alzheimer disease. *Jama*, 302(6):627--637.

[126] Serrano-Pozo, A. and Growdon, J. H. (2019). Is alzheimer's disease risk modifiable? *Journal of Alzheimer's Disease*, 67(3):795--819.

[127] Shafto, M. A., Tyler, L. K., Dixon, M., Taylor, J. R., Rowe, J. B., Cusack, R., Calder, A. J., Marslen-Wilson, W. D., Duncan, J., Dalgleish, T., et al. (2014). The cambridge centre for ageing and neuroscience (cam-can) study protocol: a cross-sectional, lifespan, multidisciplinary examination of healthy cognitive ageing. *BMC neurology*, 14(1):1.

[128] Shakir, A., Aksoy, D., Mlynash, M., Harris, O. A., Albers, G. W., and Hirsch, K. G. (2016). Prognostic value of quantitative diffusion-weighted mri in patients with traumatic brain injury. *Journal of Neuroimaging*, 26(1):103--108.

[129] Silvani, A., Calandra-Buonaura, G., Dampney, R. A., and Cortelli, P. (2016). Brain--heart interactions: physiology and clinical implications. *Philosophical Transactions of the Royal Society A: Mathematical, Physical and Engineering Sciences*, 374(2067):20150181.

[130] Simon, N., Friedman, J., Hastie, T., and Tibshirani, R. (2011). Regularization paths for cox's proportional hazards model via coordinate descent. *Journal of statistical software*, 39(5):1.

[131] Skinner, H. A. (1982). Guide for using the drug abuse screening test (dast). *Toronto: Centre for Addiction and Mental Health*.

[132] Smielewski, P., Czosnyka, M., Steiner, L., Belestri, M., Piechnik, S., and Pickard, J. (2005). Icm+: software for on-line analysis of bedside monitoring data after severe head trauma. In *Intracranial pressure and brain monitoring XII*, pages 43--49. Springer.

[133] Solfrizzi, V., Panza, F., and Capurso, A. (2003). The role of diet in cognitive decline. *Journal of neural transmission*, 110(1):95--110.

[134] Spasov, S., Passamonti, L., Duggento, A., Liò, P., Toschi, N., Initiative, A. D. N., et al. (2019). A parameter-efficient deep learning approach to predict conversion from mild cognitive impairment to alzheimer's disease. *Neuroimage*, 189:276--287.

[135] Sporns, O. (2010). *Networks of the Brain*. MIT press.

[136] Sporns, O., Chialvo, D. R., Kaiser, M., and Hilgetag, C. C. (2004). Organization, development and function of complex brain networks. *Trends in cognitive sciences*, 8(9):418--425.

[137] Steyerberg, E. W., Mushkudiani, N., Perel, P., Butcher, I., Lu, J., McHugh, G. S., Murray, G. D., Marmarou, A., Roberts, I., Habbema, J. D. F., et al. (2008). Predicting outcome after traumatic brain injury: development and international validation of prognostic scores based on admission characteristics. *PLoS medicine*, 5(8):e165.

[138] Sudlow, C., Gallacher, J., Allen, N., Beral, V., Burton, P., Danesh, J., Downey, P., Elliott, P., Green, J., Landray, M., et al. (2015). Uk biobank: an open access resource for identifying the causes of a wide range of complex diseases of middle and old age. *PLoS medicine*, 12(3):e1001779.

[139] Takens, F. (1981). Detecting strange attractors in turbulence. In *Dynamical systems and turbulence, Warwick 1980*, pages 366--381. Springer.

[140] Taylor, J. R., Williams, N., Cusack, R., Auer, T., Shafto, M. A., Dixon, M., Tyler, L. K., Henson, R. N., et al. (2017). The cambridge centre for ageing and neuroscience (cam-can) data repository: structural and functional mri, meg, and cognitive data from a cross-sectional adult lifespan sample. *Neuroimage*, 144:262--269.

[141] Teasdale, G. and Jennett, B. (1974). Assessment of coma and impaired consciousness: a practical scale. *The Lancet*, 304(7872):81--84.

[142] Tibshirani, R. (1996). Regression shrinkage and selection via the lasso. *Journal of the Royal Statistical Society: Series B (Methodological)*, 58(1):267--288.

[143] Traud, A. L., Mucha, P. J., and Porter, M. A. (2012). Social structure of facebook networks. *Physica A: Statistical Mechanics and its Applications*, 391(16):4165--4180.

[144] Tymko, M. M., Donnelly, J., Smielewski, P., Zeiler, F. A., Sykora, M., Haubrich, C., Nasr, N., and Czosnyka, M. (2019). Changes in cardiac autonomic activity during intracranial pressure plateau waves in patients with traumatic brain injury. *Clinical autonomic research*, 29(1):123--126.

[145] Valenza, G., Toschi, N., and Barbieri, R. (2016). Uncovering brain--heart information through advanced signal and image processing.

[146] Van Essen, D. C., Smith, S. M., Barch, D. M., Behrens, T. E., Yacoub, E., Ugurbil, K., Consortium, W.-M. H., et al. (2013). The wu-minn human connectome project: an overview. *Neuroimage*, 80:62--79.

[147] Varshney, L. R., Chen, B. L., Paniagua, E., Hall, D. H., and Chklovskii, D. B. (2011). Structural properties of the caenorhabditis elegans neuronal network. *PLoS computational biology*, 7(2):e1001066.

[148] Wang, K., Tarczy-Hornoch, P., Shaker, R., Mork, P., and Brinkley, J. F. (2005). Biomediator data integration: beyond genomics to neuroscience data. In *AMIA Annual Symposium Proceedings*, volume 2005, page 779. American Medical Informatics Association.

[149] White, J. G., Southgate, E., Thomson, J. N., and Brenner, S. (1986). The structure of the nervous system of the nematode caenorhabditis elegans. *Philos Trans R Soc Lond B Biol Sci*, 314(1165):1--340.

[150] Young, A. M., Adams, H., Donnelly, J., Guilfoyle, M. R., Fernandes, H., Garnett, M. R., Czosnyka, M., Smielewski, P., Plummer, M., Agrawal, S., et al. (2017). glycemia is related to impaired cerebrovascular autoregulation after severe pediatric traumatic brain injury: a retrospective observational study. *Frontiers in pediatrics*, 5:205.

[151] Young, A. M., Donnelly, J., Czosnyka, M., Jalloh, I., Liu, X., Aries, M. J., Fernandes, H. M., Garnett, M. R., Smielewski, P., Hutchinson, P. J., et al. (2016). Continuous multimodality monitoring in children after traumatic brain injury—preliminary experience. *PLoS one*, 11(3):e0148817.

[152] Yu, M., Hillebrand, A., Gouw, A. A., and Stam, C. J. (2017). Horizontal visibility graph transfer entropy (hvg-te): A novel metric to characterize directed connectivity in large-scale brain networks. *NeuroImage*, 156:249--264.

[153] Zeiler, F. A., Donnelly, J., Smielewski, P., Menon, D. K., Hutchinson, P. J., and Czosnyka, M. (2018). Critical thresholds of intracranial pressure-derived continuous cerebrovascular reactivity indices for outcome prediction in noncraniectomized patients with traumatic brain injury. *Journal of neurotrauma*, 35(10):1107--1115.

[154] Zhang, J. and Small, M. (2006). Complex network from pseudoperiodic time series: Topology versus dynamics. *Physical review letters*, 96(23):238701.

[155] Zhu, G., Li, Y., and Wen, P. P. (2014). Analysis and classification of sleep stages based on difference visibility graphs from a single-channel eeg signal. *IEEE journal of biomedical and health informatics*, 18(6):1813--1821.

[156] Zigmond, A. S. and Snaith, R. P. (1983). The hospital anxiety and depression scale. *Acta psychiatrica scandinavica*, 67(6):361--370.